Spring 1-1-2014

Enhancement of Li+ ion Tranport in High Energy Solid State Li-ion Batteries

Jae Ha Woo
University of Colorado at Boulder, gigaflare@hanmail.net

Enhancement of Li^+ ion Tranport in High Energy Solid State Li-ion Batteries

by

Jae Ha Woo

B.S., Yonsei University, 2006

M.S., University of Colorado, Boulder, 2012

A thesis submitted to the

Faculty of the Graduate School of the

University of Colorado in partial fulfillment

of the requirements for the degree of

Doctor of Philosophy

Department of Mechanical Engineering

2014

This thesis entitled:
Enhancement of Li^+ ion Tranport in High Energy Solid State Li-ion Batteries
written by Jae Ha Woo
has been approved for the Department of Mechanical Engineering

_____

Prof. Se-Hee Lee

_____

Prof. Steven M. George

Date _____

The final copy of this thesis has been examined by the signatories, and we find that both the content and the form meet acceptable presentation standards of scholarly work in the above mentioned discipline.

Woo, Jae Ha (Ph. D., Mechanical Engineering)

Enhancement of Li^+ ion Tranport in High Energy Solid State Li-ion Batteries

Thesis directed by Prof. Se-Hee Lee

Li-ion battery (LIB) is one of the major candidates for the future form of the energy storage system. However, the ignitability of organic liquid electrolyte is the primary obstacle for the large scale-up of LIB systems. Solid state Li-ion batteries (SSLIBs) with nonflammable solid state electrolytes (SSEs) are expected to be one of the solutions. Nevertheless, SSLIBs suffer from fast degradation and low power density because of limitations at interfaces in SSLIBs. This dissertation demonstrates efforts to address interfacial limitations in SSLIBs. Al_2O_3 atomic layer deposition (ALD) on a high voltage cathode material successfully reduces the resistive layer growth at active material/SSE interfaces during battery cycling. In addition, thermal treatment of Al_2O_3 ALD layer around active material particles utilizes Al_2O_3 ALD layer as Li^+ ion pathway providing additional access to Li^+ ion intercalation sites on active material which will induce an increase in energy. Employing gradients of SSE portion in working electrodes and the combination of enhanced electrodes are described in the latter part of this dissertation as continuing studies toward the commericialization of SSLIBs with stable cycling and high energy/power density. This dissertation provides effective strategies to overcome interfacial issues in SSLIBs, aiming for the goal to outperform current LIBs.

Dedication

To my parents and my sister who always encourage me.

Acknowledgements

I am really grateful to my advisor, Prof. Se-Hee Lee for his guidance, valuable advice, and support throughout my years in University of Colorado. Pursuing this degree would not have been successful without his help. Next, I would like to thank Prof. Steven M. George for guidance related to Al_2O_3 atomic layer deposition (ALD) study and for being my committee member. I also want to thank other committee members Prof. Yung-Cheng Lee, Prof. Ronggui Yang, and Dr. Chunmei Ban for their insight and comments given to improve this dissertation. I am thankful to Prof. Kyu Hwan Oh in Seoul National University for his generous help and guidance with transmission electron miscroscopy (TEM) analysis.

Thanks to my lab mates Dr. Daniela Molina Piper, Justin M. Whitely, and Tyler Evans for thier help and meaningful discussion. I am also thankful to former lab mates Dr. James E. Trevey, Dr. Thomas A. Yersak, and Dr. Seoung-Bum Son who helped to develop the foundation of my research.

I appreciate valuable help from Dr. Andrew S. Cavanagh and Jonathan J. Travis. Their excellent work regarding Al_2O_3 ALD samples enabled me to do many parts of my research. Also, I would like to thank collegues in Seoul National University, Seul Cham Kim and Yong Seok Choi for their amazing work with TEM study.

I would specially like to thank Prof. Jaekook Kim in Chonnam National University for his advice and encouragement. Thank you to my parents who always support me and my sister who is always a good companion in an academic track.

Finally, the author is grateful for financial support from National Science Foundation.

Contents

Tables

Figures

Chapter 1

Introduction

There are growing demands for sustainable and eco-friendly energy sources because of concerns for fossil fuels and the rising interest in environmental issues.[1] Li ion batteries (LIBs) which are widely used in many portable electronic devices are one of the major candidates for the future form of the energy storage system and are partially replacing the conventional internal combustion system of vehicles.[1,2] The development of reliable LIB configuration to obtain stable cycling performance with high energy/power density is indispensable for LIBs to prevail against other non-fossil fuels. One of concerns is organic liquid electrolyte employed for LIBs used in many electronic devices and electric vehicles (EVs).[3,4] The ignitability of organic electrolytes used for conventional LIBs is the primary obstacle for the large scale-up of the battery systems which is required for the application in electric vehicle (EV) and energy storage systems.[3,4] Consequently, solid state Li-ion batteries (SSLIBs) which use nonflammable solid state electrolytes (SSEs) are expected to be one of the solutions for this concern.[5]

In spite of their high safety, SSLIBs have not been practical subsititutes for current LIBs because of their poor performance such as faster degradation and low power densities.[4,6] There have been studies which reveal that the major cause of relatively poor performances from solid

state batteries can be attributed to the interfaces between active material and SSE in working electrodes.[4,6] There are limitations which lie at interfaces between different solid materials (ex. active materials, SSE, conductive additive). They are (1) highly resistive layers reported in previous works which are formed at interfaces during cycling[4,6] and (2) less number of Li^+ ion transport paths which comes from limited numbers of solid-solid contacts of particles compared to the numbers of interfaces in coventional LIBs which are soaked with liquid electrolyte. Many former studies show the limitation (1) (the interfacial resistive layer growth at the active material/SSE interface during charge-discharge process) by the electrochemical impedance spectroscopy (EIS) and transmission electron microscopy (TEM) studies.[6-10] In addition, the limitation (2) (the restricted pathways for Li^+ ions in SSLIBs) will limit transport of Li^+ ions which is essential for the battery cycling.

There have been many efforts to address the limitation (1) such as the exploitation of oxide coating by wet chemistry on active materials in working electrodes.[4,6-10] It is shown in these works that interfacial resistance at active material/SSE interface is greatly reduced by introducing a passivating oxide layer. As a result, increases in discharge capacities and enhanced current rate capabilities are observed from batteries which use the coatings of various oxide layers on active material pariticles in working electrodes.[4,7-10] The factors addressed for the role of the oxide layer are the alleviation of resistive layer growth at the interface[6-8] and the possibility of the increase in the electrochemically active area at the interface.[7,10] Although these reports commonly state the improvement of cycling performance, further enhancement is required for stable cycling and energy/power density. These works show less than 60 cycles and considerable decrease in capacities at high current densities (> 1 mA cm^{-2}) even with active materials coated with oxide layers.

The limitation (2) (the restricted pathways for Li^+ ions in SSLIBs) becomes more prominent in high energy SSLIBs. Typical studies done for SSLIBs are based on pellet-type testing cells fabricated from a powder compression method.[3,4,6-18] However, these works performed with this type of battery are limited by using the small portion of active material in their electrodes resulted in energy density less than 100 Wh kg^{-1} (practical LIB is ~ 150 Wh kg^{-1}).[2] A large portion of this laboratory scale SSLIB was occupied by SSE and conductive additive to compensate the limitation (2) mentioned above. Figure 1.1 shows an example of a pellet-type testing cell which has three components: a cathode, a SSE layer (a separator), and an anode. A LIB system with higher energy density & power density than current LIBs is essential for the substitution of fossil fuel-based energy systems. Therefore, overcoming limitations (1) and (2) to enhance Li^+ ion transport at various interfaces is crucial for LIB to replace other energy storage systems. With the trend toward the adoption of LIB system in large-scale systems (ex. EV), it would be essential to study SSLIBs with higher energy/power density.

This dissertation demonstrates our efforts to address interfacial limitations (1) and (2) mentioned in the 2nd paragraph to realize a SSLIB with a practical energy/power density. The transport of Li^+ ions is one of major limiting factors in SSLIBs with higher energy density than laboratory-scale testing cells. To address this issue, we explored four aspects of SSLIB system. First, the exploitation of a new coating method other than previous wet chemical methods (ex.

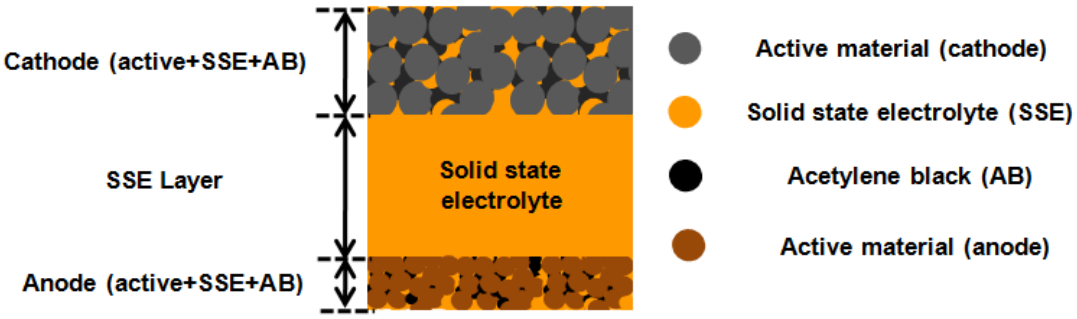

Figure 1.1: Schematic representation of a pellet-type SSLIB from powder compression method.

sol-gel method, spray coating) was carried out to overcome the insufficient surface coverage on active material particles that will induce an undesirable side reaction with SSE.[19] The insulating property of oxide coating layer on active materials and a limited number of effective active material/SSE contacts become noticeable when oxide coatings on active materials are used in solid state batteries at high current rates.[4,10,11] Utilization of oxide coating layers around active material particles as a Li^+ ion pathway enabled to achieve the increase of electrochemically active sites on electrode material particles.

Second, solid state electrolyte (SSE) with high ionic conductivity becomes an important component in SSLIBs to obtain high power density. Sulfide SSEs are known to have good feasibility to be pelletized with cold press method and to create good solid-solid contacts with active materials in pellet-type testing cells.[20,21] Among sulfide SSEs, $Li_{4-x}Ge_{1-x}P_xS_4$[22] and $77.5Li_2S–22.5P_2S_5$ (mol %)[23] were reported to have ionic conductivities of the order of 10^{-3} S cm^{-1} at room temperature. Therefore, $Li_{3.15}Ge_{0.15}P_{0.85}S_4$ and $77.5Li_2S–22.5P_2S_5$ (mol %) were adopted in our early works. In 2011, a Li superionic conductor $Li_{10}GeP_2S_{12}$ which has the highest conductivity among SSEs (1.2×10^{-2} S cm^{-1}) was proposed by Kamaya *et al*.[24] In addtion, Ong *et al.* adopted the substitution of Ge in $Li_{10}GeP_2S_{12}$ to other materials (Si, Sn) because of the scarceness and the cost issue of Ge.[25] According to their first principles calculations, $Li_{10}SiP_2S_{12}$, which has the same crystal structure as $Li_{10}GeP_2S_{12}$, is expected to have similar intrinsic properties such as high Li^+ conductivity. We chose $Li_{10}SiP_2S_{12}$ as our SSE and successfully synthesized them which showed good performances when used in our solid state batteries shown in the latter part of this dissertation.

Third, considerable weight percentage of SSLIB occupied by SSE and conductive additive as mentioned in the 4th paragraph is a drawback in obtaining high energy density.

Optimized design for the layout of active material, SSE particles, and conductive additive in electrodes is required for SSLIBs to achieve high volumetric and gravimetric energy density by minimizing the portion of unnecessary passive components. Employing gradient of SSE portion in working electrodes of SSLIBs will be shown in this dissertation as a strategy for an optimized design of a high energy SSLIB. It is shown that a gradient of SSE portion affects the polarization of voltage profiles which is an important factor related with the energy of a SSLIB.

Furthermore, attempts to employ advanced electrodes in our SSLIBs are shown in the latter part of this disseration. $LiNi_{1/3}Co_{1/3}Mn_{1/3}O_2$ (L333) which is known to have larger capacity, less cost, and more environment-friendliness than commonly used $LiCoO_2$[26-28] is adopted in our advanced cathode composites to obtain more energy density from our SSLIBs. Along with L333, Si which has natural abundance and much larger capacity compared to commercially used graphite[29] is selected as an active material in our anode composites for SSLIBs. In addition, embedding of Si particles in cyclized polyacrylonitrile (cPAN) fiber framework with cPAN coating is achieved by electrospinning.[30] This hierarchical framework provides minimal volume expansion and effective electronic/ionic transports which are essential for high energy Si-based anodes.

References

1. M. Armand and J.-M. Tarascon, *Nature*, **451**, 652 (2008).

2. J.-M. Tarascon and M. Armand, *Nature*, **414**, 359 (2001).

3. F. Mizuno, A. Hayashi, K. Tadanaga, T. Minami, and M. Tatsumisago, *J. Power Sources*, **124**, 170 (2003).

4. N. Ohta, K. Takada, L. Zhang,R.Ma, M. Osada, and T. Sasaki, *Adv. Mater*., **18**, 2226 (2006).

5. J. W. Fergus, *J. Power Sources*, **195,** 4554 (2010).

6. A. Sakuda, A. Hayashi, and M. Tatsumisago, *Chem. Mater.*, **22**, 949 (2010).

7. A. Sakuda, H. Kitaura, A. Hayashi, K. Tadanaga, and M. Tatsumisago, *J. Electrochem. Soc*., **156**, A27 (2009).

8. A. Sakuda, H. Kitaura, A. Hayashi, K. Tadanaga, and M. Tatsumisago, *J. Power Sources*, **189,** 527 (2009).

9. A. Sakuda, A. Hayashi, and M. Tatsumisago, *J. Power Sources*, **195**, 599 (2010).

10. H. Kitaura, A. Hayashi, K. Tadanaga, and M. Tatsumisago, *Solid State Ionics*, **192**, 304 (2011).

11. H. Kitaura, A. Hayashi, K. Tadanaga, and M. Tatsumisago, *Electrochimica Acta*, **55**, 8821 (2010).

12. N. Machida, J. Kashiwagi, M. Naito, and T. Shigematsu, *Solid State Ionics*, **225**, 354 (2012).

13. T. Takeuchi, H. Kageyama, K. Nakanishi, M. Tabuchi, H. Sakaebe, T. Ohta, H. Senoh, T. Sakai, and K. Tatsumi, *J. Electrochem. Soc*., **157**, A1196 (2010).

14. M. Nagao, Y. Imade, H. Narisawa, T. Kobayashi, R. Watanabe, T. Yokoi, T. Tatsumi, and R. Kanno, *J. Power Sources*, **222**, 237 (2013).

15. S. Noh, J. Kim, M. Eom, and D. Shin, *Ceramics International*, **39**, 8453 (2013).

16. S. Boulineau, J.-M. Tarascon, J.-B. Leriche, and V. Viallet, *Solid State Ionics*, **242**, 45 (2013).

17. T. Ohtomo, A. Hayashi, M. Tatsumisago,and K. Kawamoto, *J. Solid State Electrochem*, **17**, 2551 (2013).

18. T. Matsuyama, A. Sakuda, A. Hayashi, Y. Togawa, S. Mori, and M. Tatsumisago, *J. Solid State Electrochem.*, **17**, 2697 (2013).

19. I. D. Scott, Y. S. Jung, A. S. Cavanagh,Y. Yan, A. C. Dillon, S. M. George, and S.-H. Lee, *Nano Lett*., **11**, 414 (2011).

20. T. Minami, A. Hayashi, and M. Tatsumisago, *Solid State Ionics***, 177,** 2715 (2006).

21. K. Takada, T. Inada, A. Kajiyama, H. Sasaki, S. Kondo, M. Watanabe, M. Murayama, and Ryoji Kanno, *Solid State Ionics*, **158**, 269 (2003).

22. R. Kanno and M. Maruyama, *J. Electrochem. Soc*., **148**, A742 (2001).

23. J. Trevey, J. S. Jang, Y. S. Jung, C. R. Stoldt, and S.-H. Lee, *Electrochem. Commun.*, **11,** 1830 (2009).

24. N. Kamaya, K. Homma, Y. Yamakawa, M. Hirayama, R. Kanno, M. Yonemura, T. Kamiyama, Y. Kato, S. Hama, K. Kawamoto, and A. Mitsui, *Nat. mater*., **10,** 682 (2011).

25. S.P. Ong, Y. Mo, W.D. Richards, L. Miara, H.S. Lee, and G. Ceder, *Energy Environ. Sci.*,**6,** 148 (2012).

26. T. Ohzuku and Y. Makimura, *Chem. Lett*., **1**, 642 (2001).

27. K.M. Shaju, G.V. Subba Rao, and B.V.R. Chowdari, *Electrochim. Acta*, **48**, 145 (2002).

28. I. Belharouak, Y.K. Sun, J. Liu, and K. Amine, *J. Power Sources*, **123**, 247 (2003).

29. U. Kasavajjula , C. S. Wang , and A. J. Appleby, *J. Power Sources*, **163** , 1003 (2007).

30. D. M. Piper, J. H. Woo, S.-B. Son, S. C. Kim, K. H. Oh, and S.-H. Lee, *Adv. Mater*., **26**, 3520 (2014).

Chapter 2

Background

2.1 Basic concepts of Li-ion batteries (LIBs)

Components of a battery are two electrodes and ionically conductive material (electrolyte).[1] According to the chemical reaction which occurs at each electrode, different chemical potentials appear at each electrode. Spontaneous movement of electrons occur from the electrode which has more negative potential (anode) to the electrode which has more positive potential (cathode) when two electrodes are connected by an external device. Along with the flow of electrons, ions move through the electrolyte to maintain the charge balance. Electrical energy is obtained by the external device through these charge movements. When a larger voltage is applied in the opposite way, electrons are tranported from the cathode to the anode and the battery is recharged.

Lithium-ion batteries (LIBs) are operated with the exchange of Li^+ ions between the positive and negative electrodes.[2] Li^+ ions shuttle back and forth between these two electrodes, causing the Li insertion and extraction with a reduction and an oxidation (redox) of host structures in electrodes enabled by the movement of electrons through an external circuit. This "rocking-chair" design occurred in 1991 by Sony Corporation.[3] A schematic illustration of the working principles a LIB is shown in Figure 2.1.[2]

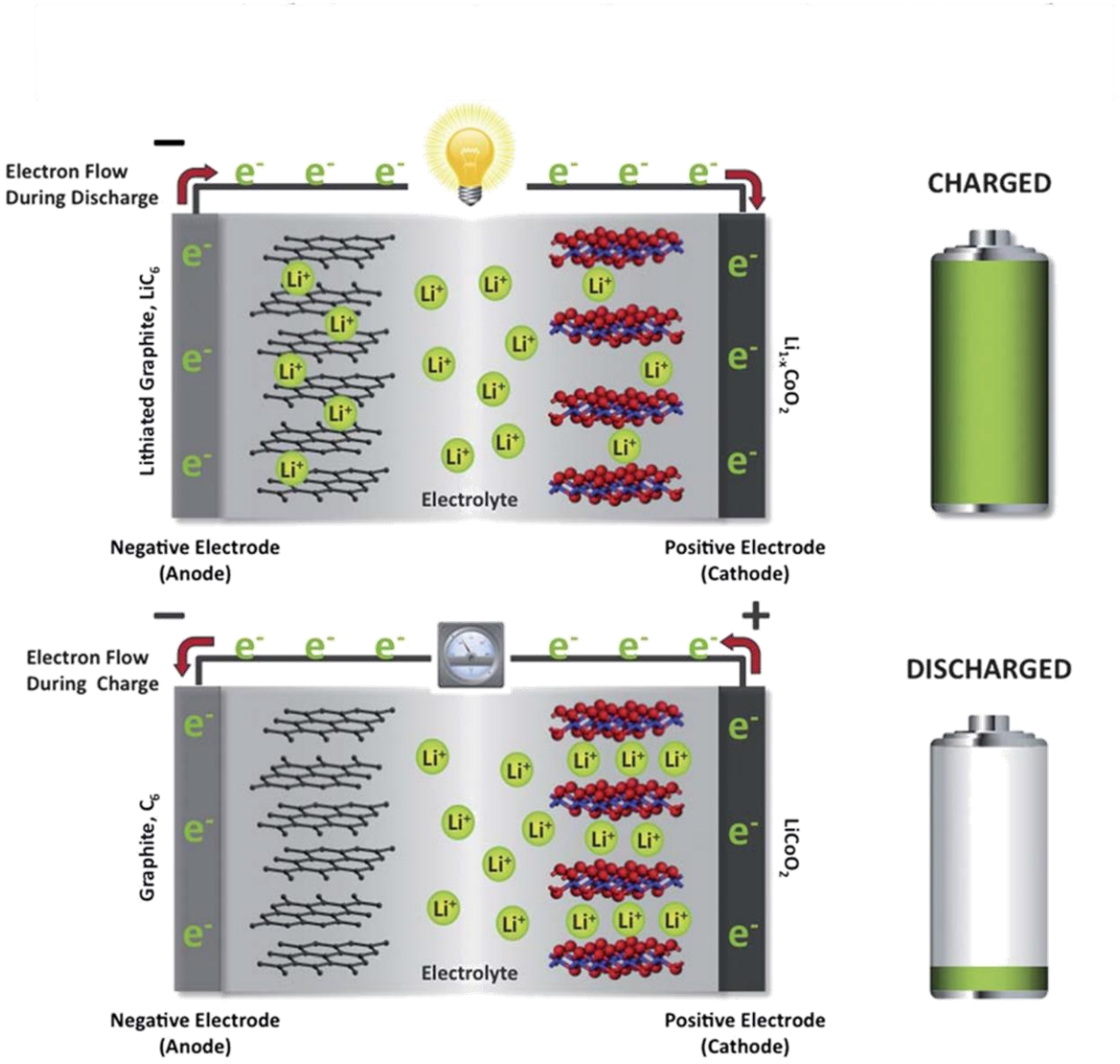

Figure 2.1: A schematic illustration of the working principles of a Li-ion battery.[2]

Lithium is known to be the third lightest element and to have the highest oxidation potential among all known elements (3 V above the standard hydrogen potential).[2] Therefore, lithium is favorable for the mobile ion species for batteries. LIBs have high energy densities and high power densities compared to other rechargeable batteries. Gravimeteric energy/power densities of various rechargeable batteries are compared in Figure 2.2.[4]

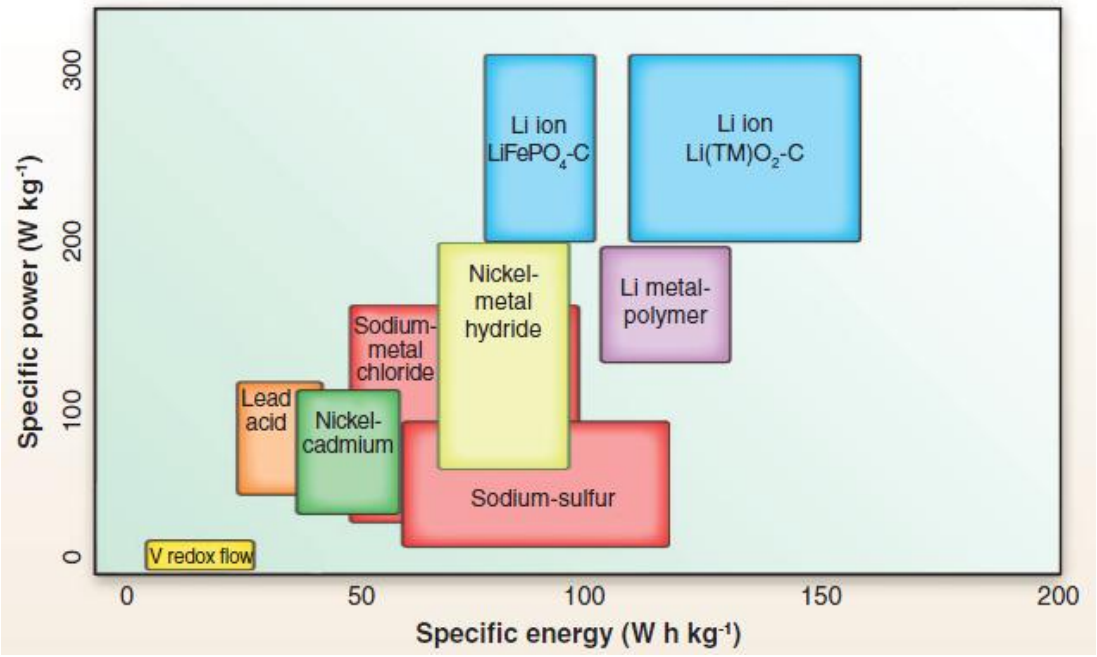

Figure 2.2: Gravimetric power and energy densities for different rechargeable batteries.[4]

Conventional cathode materials used in LIBs are layered $LiCoO_2$ (~ 140 mAh g^{-1}), spinel $LiMn_2O_4$ (100 ~ 140 mAh g^{-1}), and olivine $LiFePO_4$ (~ 170 mAh g^{-1}).[5-7] Using a graphite LiC_6 (372 mAh g^{-1})[8] as an anode material along with cathode materials stated above, current LIBs are popular energy systems for various applications (ex. portable electronics, electrified transportations) with a practical energy density of ~150 Wh kg^{-1} (based on mass of battery pack).[2,9] Because of strong prospect to fulfill the future needs for electric vehicles (EVs), LIBs are used in current EVs (Chevy Volts, Nissan Leaf) using a blend of layered $LiMO_2$ (M = Ni, Co, Mn) and spinel $LiMn_2O_4$ as the cathode along with a carbon material as the anode. However, a higher energy density is still needed to meet the performance requirement of EVs with a distance range over 300 miles. Even though state-of-the-art LIBs outperform other battery systems as mentioned above, they still have much lower energy densities compared to fossil

fuel-based energy systems as shown in Figure 2.3.[2] Therefore, many studies are ongoing to establish new electrochemical couples to achieve an energy density which is several times greater than that of current LIBs. Employment of advanced anode and cathode materials is expected to double the practical energy density of current LIBs (~ 300 Wh kg^{-1}) .

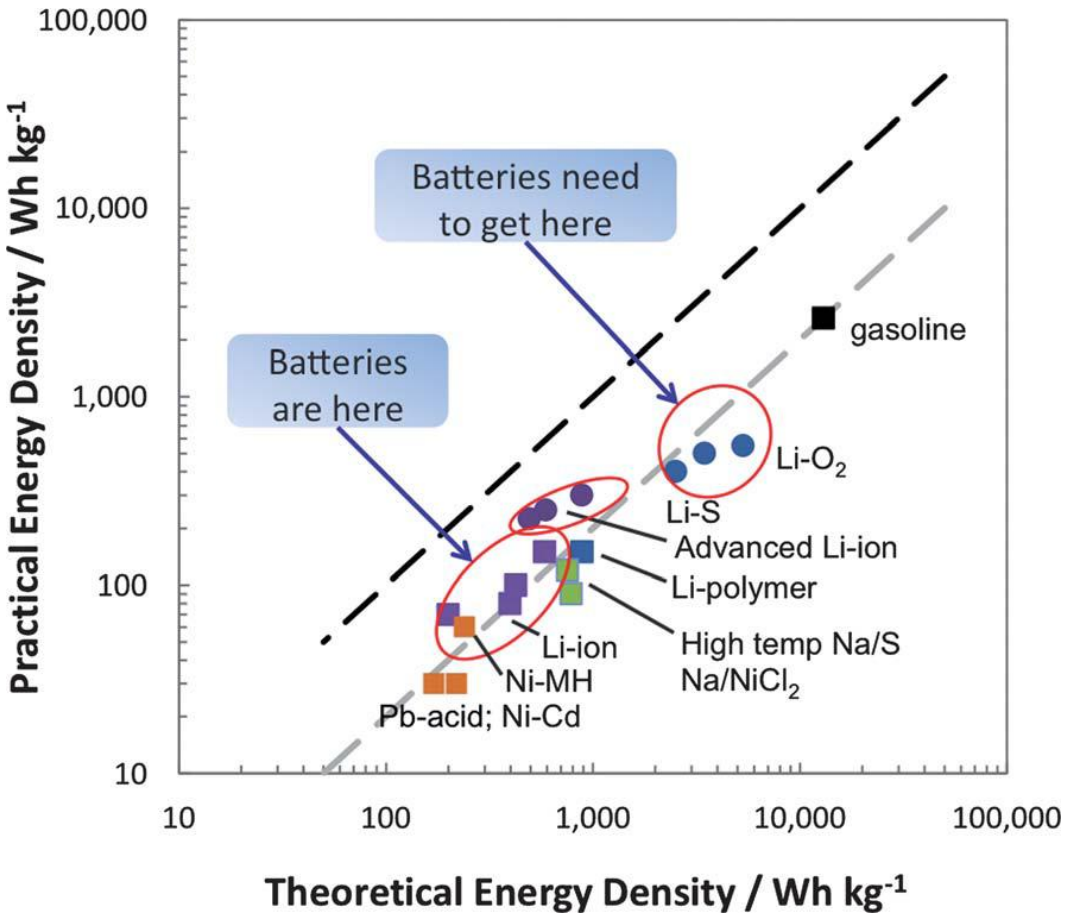

Figure 2.3: A plot of the theoretical specific energy (based on the masses of active electrode-electrolyte materials) of various rechargeable battery systems vs. their practical specific energies (based on mass of battery pack).[2]

2.2 Electrode materials

2.2.1 Layered transition metal oxides

The group of materials that has the chemical formula of $LiMO_2$ (M = Ni, Co, Cr, V) is called layered transition metal oxides. The crystal structure is a layered rock salt structure which consists of MO_2 layers, alternating Li^+ ions and M^{3+} ions which occupy (111) planes. A layered O-Li-O-M-O sequence appears along the c axis as shown in Figure 2.4.[10] Among those materials, $LiCoO_2$ is the most famous cathode material which is used in LIBs.[10-12] It has a theoretical capcity of ~ 140 mAh g^{-1} and a high voltage of ~ 4 V.[6] However, more advanced postive electrode materials are being searched because of the toxicity and high cost of $LiCoO_2$. $LiCoO_2$ belongs to the space group $R\bar{3}m$ having Li^+ ions and Co^{3+} ions at octahedral interstitial sites. Li^+ ions can intercalate into or out of gaps between CoO_2 layers. Typically, $LiCoO_2$ is delithiated until $\chi = 0.5$ in $Li_\chi CoO_2$ because of the appearance of a new phase.[13]

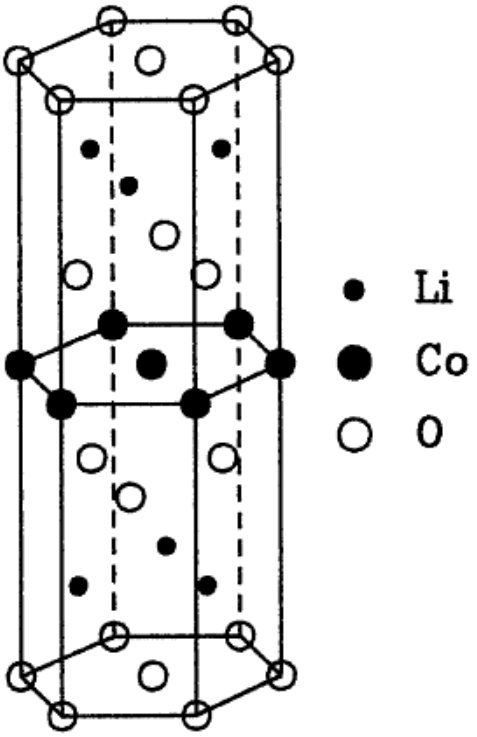

Figure 2.4: Schematic description of layered $LiCoO_2$ structure.[10]

2.2.2 Li alloys

Graphite has been generally employed as an anode material for current LIBs because of its stable cycling and its cheap price.[14] However, it can accomodate only one Li atom per C_6, thereby having limited capacity of 372 mAh g^{-1}.[8] Because of its capacity limit, graphite is not an adequate material for the next generation LIBs for future application (ex. EVs) as mentioned in Section 2.1. Therefore, many efforts have been made to develop superior anode materials with high capacity which can fulfill the needs for a high energy density.

Si has been drawing attention as the anode material for high energy density LIBs because it has the highest theoretical capacity ($Li_{22}Si_5$, 4200 mAh g^{-1}).[15-17] It can accommodate more than four Li atoms providing more than 10 times the capacity of graphite. Similarly, Sn is known as attractive anode material which can be alloyed with more than four atoms of Li, achieving theoretical capacity of 992 mAh g^{-1} which is three times that of graphite.[18,19] However, these metals have densely packed structure and exhibit large volumetric expansions during lithiation and delithiation process.[2] Si goes through ~ 400% volume expansion when it is fully lithiated.[20] Sn also experience a large volume expansion during Li alloying process.[21,22] As a result, large expansions leads to pulverization of electrode particle, losing electrical contact to suffer capacity fade during cycling. The mechanical failure of these metal anodes are known to be the major obstacle of commercializaing high energy metal anodes.

2.3 Solid state electrolytes (SSEs)

Inflammability of organic liquid electrolyte used in conventional LIBs aroused the safety concerns.[23] Solid state electrolytes (SSEs) offer better safety over liquid electrolyte by its nonflammable property.[24] Ions in solid are normally not able to migrate because the rigid

framework has to be maintained by the constituent cations and anions. Nevertheless, there are solids called as "solid state electrolyte" which allows only a single ion species to migrate with low activation energy, resulting in high ionic conductivities.[25] Therfore, SSEs in LIBs are generally single ionic condutors which only allows Li^+ ions to have an appreciable mobility, while the anions and other cations constitute the skeletal structure. Having one mobile ion species removes the anionc concentration gradient in the electrolyte, suppressing unwanted side reactions or decomposition of SSE.

2.3.1 Thio-LiSICON

Formation of a three dimension (3D) rigid skeletal structure for mobile alkali ions to migrate through interstitial sites was the motivation for developing a lithium superionic conductor (LISICON). LISICON SSEs have the chemical formula of $Li_xM_2M^*_3O_{12}$ (M, M* = metals which constitute network cations, octahedrally and tetrahedrally coordinated to O^{2-} ions).[26] Li^+ ion conductivity in SSEs is affected by the size of bottlenecks between interstitial alkali-ions and by the bonding energy between Li^+ ions and the network ions. Therefore, high Li^+ ion conductivity can be obtained by enlarging the size of bottlenecks and adopting highly polarizable anions to be strongly bonded to a robust network to affect intersitial ions less.

Thio-LISICON SSEs developed under the same principle of LISICON SSEs, adopting larger and more polarizable sulfur as the anion rather than oxygen.[27] Thio-LISICON has the general formula $Li_{4-x}Ge_{1-x}P_xS_4$ with the skeletal structure of the γ-Li_3PO_4 type. This sulfide based SSEs show high ionic conductivity at the order of 10^{-3} S cm^{-1} (room temperature) and they are promising electrolytes for solid state Li-ion batteries (SSLIBs). Li_2-P_2S_5 system is the special

example of Thio-LISICON SSEs which doesn't include metal elements. With high ionic conductivity, it exhibited stable cycling performance in solid state Li batteries (SSLBs).[28]

Amorphous Thio-LISICON SSE, Li_2-P_2S_5 SSE were synthesized by ball milling (Chapter 3) in this dissertation. It is known that crystallized Li_2-P_2S_5 SSE exhibits a higher ionic conductivity than its amorphous counterpart.[25] Therefore, heat treatments of $Li_{4-x}Ge_{1-x}P_xS_4$ SSEs for crystallization were performed to increase the ionic conductivity (Chapter 4, 5).

2.3.2 $Li_{10}MP_2S_{12}$ SSE (M = Ge, Si)

Although Thio-LISICONs showed good properties in SSLBs, their ionic conductivities are still below 10^{-2} S cm^{-1} which is lower than conductivities of organic liquid electrolytes. A novel Li superionic conductor $Li_{10}GeP_2S_{12}$ was proposed by Kamaya *et al.*[29] $Li_{10}GeP_2S_{12}$ SSE showed the highest ionic conductivity among SSEs reported (1.2 x 10^{-2} S cm^{-1}) which is even comparable to that of liquid electrolytes. The authors attributed the high conductivity of $Li_{10}GeP_2S_{12}$ to the fast 1D diffusion of Li^+ ions in its crystal structural framework which consists of $(Ge_{0.5}P_{0.5})S_4$ tetrahedra, PS_4 tetrahedra, LiS_6 octahedra, and LiS_4 tetrahedra. However, Mo *et al.* claimed that $Li_{10}GeP_2S_{12}$ has a 3D ionic diffusion network which is composed of 1D diffusion channels along *c* direction and the interchannel diffusion in the *ab* plane, using first principles modeling.[30]

The high cost of germanium in $Li_{10}GeP_2S_{12}$ SSE limits the scale-up application of the material. Ong *et al.* sought the material which has the same structural framework, substituting germanium with other metals.[31] As a result, $Li_{10}SiP_2S_{12}$ is expected to have similar phase stability, electrochemical stability, and Li^+ conductivity as $Li_{10}GeP_2S_{12}$ according to their first principle modeling. Low cost of Si make $Li_{10}SiP_2S_{12}$ SSE beneficial for mass production.

References

1. M. Armand and J.-M. Tarascon, *Nature*, **451**, 652 (2008).

2. M. M. Thackeray, C. Wolverton, and E. D. Isaacs, *Energy Environ.Sci.*, **5**, 7854 (2012).

3. T. Nagaura and K. Tozawa, Lithium ion rechargeable battery. *Prog. Batteries Solar Cells* **9,** 209 (1990).

4. B. Dunn, H. Kamath, and J.-M. Tarascon, *Science*, **334**, 928 (2011).

5. A. Sakuda, H. Kitaura, A. Hayashi, K. Tadanaga, and M. Tatsumisago, *J. Power Sources*, **189**, 527 (2009).

6. H. Kitaura, A. Hayashi, K. Tadanaga, and M. Tatsumisago, *Electrochim. Acta*, **55,** 8821 (2010).

7. Y. Liu, S. Gorgutsa, C. Santato, and M. Skorobogatiy, *J. Electrochem. Soc*., **159**, A349 (2012).

8. J. R. Dahn , T. Zheng , Y. Liu , and J. S. Xue , *Science*, ***270*** , 590 (1995) .

9. J.-M. Tarascon and M. Armand, *Nature*, **414**, 359 (2001).

10. J. N. Reimers and J. R. Dahn, *J. Electrochem. Soc*. **139**, 2091 (1992).

11. K. Mizushima, P. C. Jones, P. J. Wiseman, and J. B. Goodenough, *Mat. Res. Bull.*, **15**, 783 (1980)**.**

12. T. Ohzuku and A. Ueda, *J. Electrochem. Soc*. **141**, 2972 (1994).

13. G. G. Amatucci, J. M. Tarascon, and L. C. Klein, *J. Electrochem. Soc*., **143**, 1114 (1996).

14. W. J. Weydanz, M. Wohlfahrt-Mehrens, and R. A. Huggins, *J. Power Sources*, **81**, 237 (1999).

15. Y. Wang and J. Dahn , *J. Electrochem. Soc.*, **153** , A2314 (2006).

16. T. D. Hatchard and, J. R. Dahn , *J. Electrochem. Soc.*, **151**, A838 (2004).

17. Y. M. Kang, S. B. Suh, and Y. S. Kim, *Inorg. Chem.*, **48** , 11631 (2009).

18. Y. Idota, T. Kubota, A. Matsufuji, Y. Maekawa, and T. Miyasaka, *Science*, **276**, 1395 (1997).

19. M. Winter and J. O. Besenhard, *Electrochim. Acta*, **45**, 31 (1999).

20. J. L. Goldman, B. R. Long, A. A. Gewirth, and R. G. Nuzzo, *Adv.Funct. Mater*. **21**, 2412 (2011).

21. S. Grugeon, S. Laruelle, R. Herrera-Urbina, L. Dupont, P. Poizot, and J.M. Tarascon, *J. Electrochem. Soc*., **148**, A285 (2001).

22. E. Shembel, R. Apostolova, V. Nagirny, I. Kirsanova, Ph. Grebenkin, and P. Lytvyn, *J. Solid State Electrochem.*, **9**, 96 (2005).

23. F. Mizuno, A. Hayashi, K. Tadanaga, T. Minami, and M. Tatsumisago, *J. Power Sources*, **124**, 170 (2003).

24. J. W. Fergus, *J. Power Sources*, **195,** 4554 (2010).

25. G. Adachi, N. Imanaka, and H. Aono, *Adv. Mater.*, **8**, 127 (1996).

26. H. Hong, *Mat. Res. Bull.*, **13**, 117 (1978)**.**

27. R. Kanno and M. Murayama, *J. Electrochem. Soc.*, **148**, A742 (2001).

28. A. Hayashi, S. Hama, T. Minami, and M. Tatsumisago, *Electrochem. Commun.*, **5**, 111 (2003).

29. N. Kamaya, K. Homma, Y. Yamakawa, M. Hirayama, R. Kanno, M. Yonemura, T. Kamiyama, Y. Kato, S. Hama, K. Kawamoto, and A. Mitsui, *Nat. mater*., **10,** 682 (2011).

30. Y. Mo, S. P. Ong, and G. Ceder, *Chem. Mater.*, **24**, 15 (2012).

31. S.P. Ong, Y. Mo, W.D. Richards, L. Miara, H.S. Lee, and G. Ceder, *Energy Environ. Sci.*,**6,** 148 (2012).

Chapter 3

Methods

3.1 Ball milling

Ball milling which is normally done by the interaction between balls and precursor in a sealed container has been drawing attention as an attractive method to synthesize solid state electrolytes (SSEs) because of its lower cost and less required time compared to melt and quench methods which is previously used in the past to produce SSEs.[1] Fine amorphous powders are obtained at room temperature by employing ball milling methods for SSE synthesis. As a result, SSEs with high ionic condutivities are achieved as well as good solid-solid contacts between electrode material and SSE in solid state batteries.[2,3]

We adopted planetary ball milling method to synthesize our SSEs used in this dissertation. This process is performed by a rotation of sealed containers in a planetary motion under a controlled rotating speed. The sealed containers include precursors and balls. The impact between balls and precursors induces deformation of the materials, new surfaces, dislocations, and other defects.[4] The diffusion process can be accelerated by a high defect density created during planetary ball milling.[5] Metastable materials with high chemical reactivity can be generated by this method, enabling subsequent thermal treatment to form a variety of nanostructures as resultant materials.[6] In addition, it was found that heat treatment (HT) on

amorphous SSEs beyond their glass transition temperature can achieve highly conducting crystalline SSEs.[7] Therefore, HT on SSEs was used in this dissertation to increase Li^+ ionic conductivity.

3.2 Pellet-type testing batteries fabrication

This section will introduce the fabrication process of solid state batteries used in this dissertation. All cell fabrications were conducted in a dry Ar gas environment. Composite materials used for electrodes in solid state batteries were prepared like below. Active material, SSE, and a conductive additive were mixed at certain weight ratios by hand using a mortar and a pestle. The active material and SSE powders were gently ground together for a certain amount of time. Conductive additive powders were added to the mixture and hand-mixed to generate solid state composites as electrode materials.

Pellet-type solid state batteries were constructed by a sequential cold pressing of powders. As mentioned in Chapter 1, sulfide SSEs used for our solid batteries have good feasibility to be pelletized with cold press method and to create good solid-solid contacts.[8,9] 200 mg of SSE powders were cold pressed at 1 metric ton. Electrode composite materials were evenly spread on one side of SSE layer and cold pressed at 5 meteric tons. Li metal foil or other electrode compsite can be cold-pressed on the other side of SSE layer. Figure 3.1 shows an example of our pellet-type testing battery configuration. Side of the pellet battery is electronically insultated by polyaryletheretherketone. Titanium (Ti) metal cylinders are used as current collectors for both cathode and anode. The resultant battery pellet has 13 mm diameter and ~ 1 mm thickness.

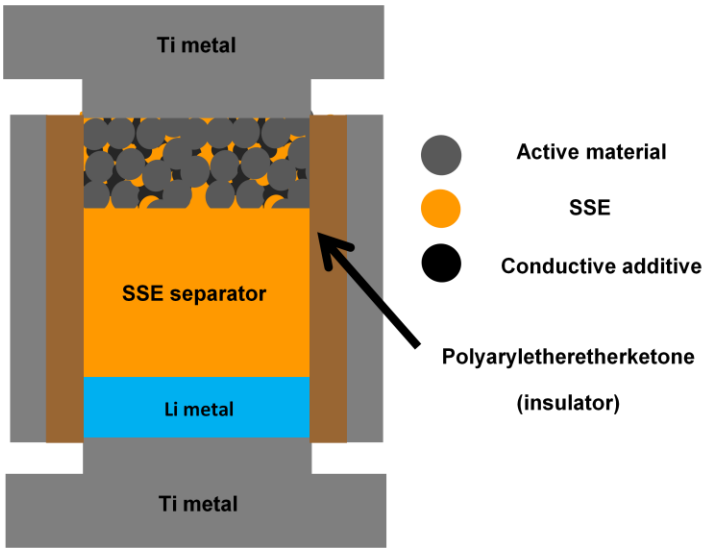

Figure 3.1: An example of our pellet-type testing cell configuration.

3.3 Electrochemical impedance spectroscopy

Basic concepts of electrochemical impedance spectroscopty (EIS) which is used in upcoming chapters will be explained.[10] A current will be induced to flow through an electrochemical battery when a voltage is applied to the battery. The sinusoidal current will be induced from a sinusoidal voltage ($\Delta E \sin\omega t$), with a value of $\Delta i \sin(\omega t+\varphi)$, of which harmonics of this current (2ω, 3ω,...etc.) will also go through the battery. This relationship between the applied voltage and the current is called as the impedance, which is similar to the relationship between resistance-current in a dc circuit. The impedance (Z) is a vector which consists of a magnitude ($\Delta E/\Delta i$) and phase (φ). Therefore, EIS profiles can be shown by plots of the real (Z´) and imaginary (Z") components. Figure 3.2 shows several examples of circuits and their EIS profiles.

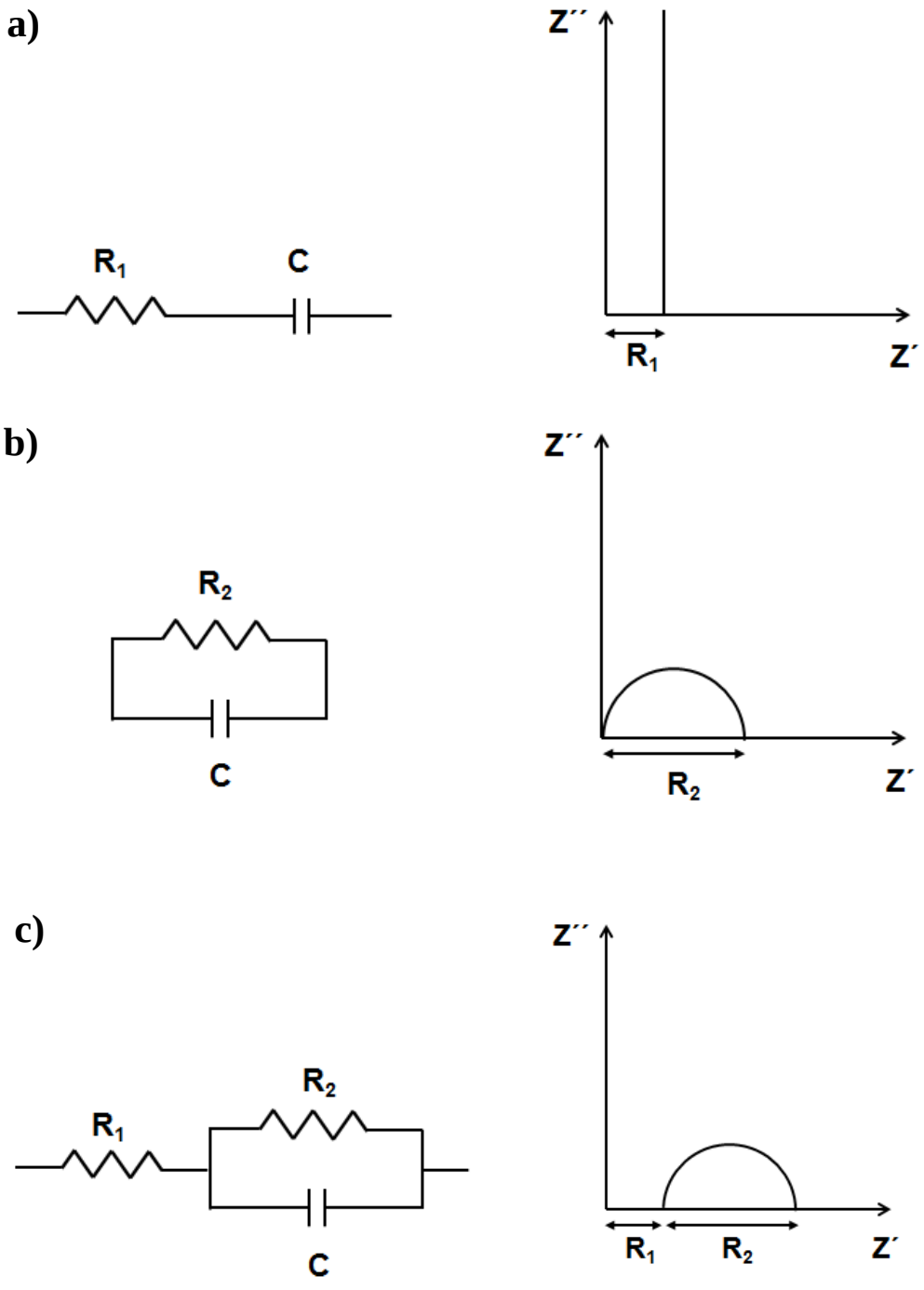

Figure 3.2: Examples of circuits and their EIS profiles. a) series resistance, capacitance. b) parallel resistance, capacitance. c) reisistance, pararllel resistance, capacitance.

3.4 Constant current constant voltage

Constant current constant voltage (CCCV) method is used to cycle our pellet-type solid state batteries in this dissertation. Either observing the varing voltage from an applied constant current or observing the changing current from a constant voltage was performed by our battery testing device (Arbin BT2000). The typical battery tesing protocol used in this study is the mixed process of galvanostatic process which is applying a fixed current[11] and potentiostatic process which is applying a fixed voltage.[12] An example of CCCV used for solid batteries is shown in Figure 3.3. Throughout this dissertation, charge process and discharge process correspond to the delithiation and the lithiation of cathode materials. Initially, a battery is charged with a constant current until its voltage reaches the upper limit of the voltage range. The battery maintains its voltage at the upper limit for a certain amount of time (a voltage hold) with decreasing currents

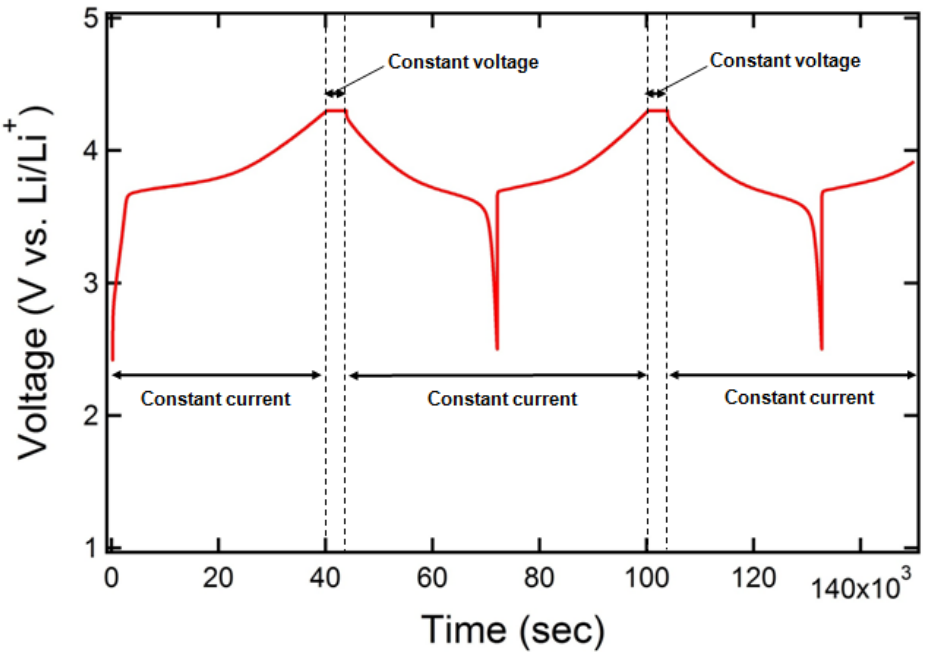

Figure 3.3: An example of a typical constant current constant voltage testing process.

during this process. Lastly, a fixed current with the opposite direction to the direction of the current during the charge process is applied to discharge the battery down to lower limit of the voltage range. Reaching to the lower limit of the voltage range completes one full cycle.

3.5 Atomic layer deposition

We employed a novel coating method, which is called as atomic layer deposition (ALD) to engineer surfaces of our elecrode materials. This section is based upon a review paper which is good text for readers to understand ALD in depth.[13] ALD has been a promising technique for thin film deposition used in a variety of applications. It produces a conformal, pinhole-free film with a precise thickness control of Å ngstrom level. This coating method uses sequential, self-limiting surface reactions to obtain films with atomic layer thickness. ALD is mostly composed of two surface reactions. It is possible for these reactions to proceed in a sequential manner to coat layers with atomic level control if each of reactions is self-limiting. Finite number of surface species which can be coated from reactions comes from the limited number of surface sites.

Al_2O_3 ALD is used for various studies in this dissertation. Two self-limiting reactions which constitute one cycle of Al_2O_3 ALD are like below.[14-16] The asterisks denote the surface

$$AlOH^* + Al(CH_3)_3 \rightarrow AlO–Al(CH_3)^*_2 + CH_4 \qquad (1)$$

$$AlO–Al(CH_3)^*_2 + H_2O \rightarrow AlO–Al–OH^* + CH_4 \qquad (2)$$

species. 1.1 ~ 1.2 Å thick Al_2O_3 layer is deposited per ALD cycle.[15,16] The schematic depiction of Al_2O_3 ALD on $LiCoO_2$ is shown in Figure 3.4.

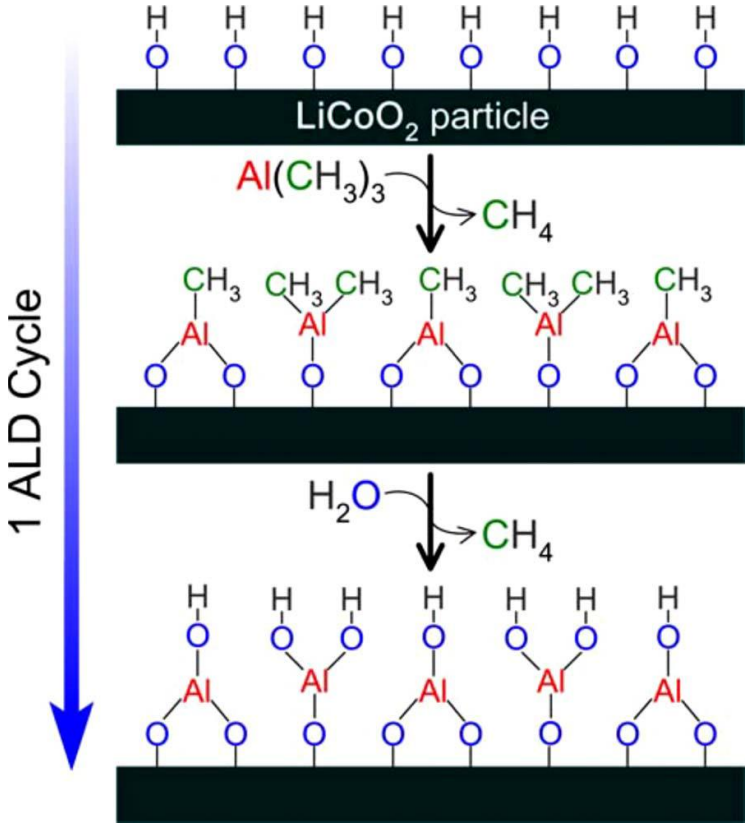

Figure 3.4: The schematic depiction of Al_2O_3 ALD on $LiCoO_2$.[17]

3.6 Electrospinning

This section includes a brief introduction of electrospinning which was used to synthesize Si-embedded polyacrylonitrile (PAN) fiber frameworks in Chapter 7. It is based upon a book by A.L. Andrady which is a good reference for readers to understand electrospinning in depth.[18] Electrospinning is one of the most popular methods to fabricate nanofibers. The process is feasible to be scaled up and is applied to produce commercialized products (ex. air filter media). Fibers with diameters of 50 ~ 900 nm can be easily synthesized by electrospinning.

Figure 3.5 exhibits the schematic depiction of a simple electrospinning set-up to produce nanofibers. The set-up consists of below components.

(1) A viscous polymer solution

(2) An electrode which is in contact with the polymer solution

(3) A high voltage DC generator which is connected to the electrode

(4) A nanofiber collector which is grounded

The quality of nanofibers is affected by several parameters from electrospinning set-up. The list of these parmeters is shown below.

(1) Polymer solution (ex. viscosity)

(2) Tip as an electrode

(3) Gap distance between tip and collector

(4) Gas components in environment

(5) Collector

(6) Feed rate of the polymer solution

(7) Applied potential

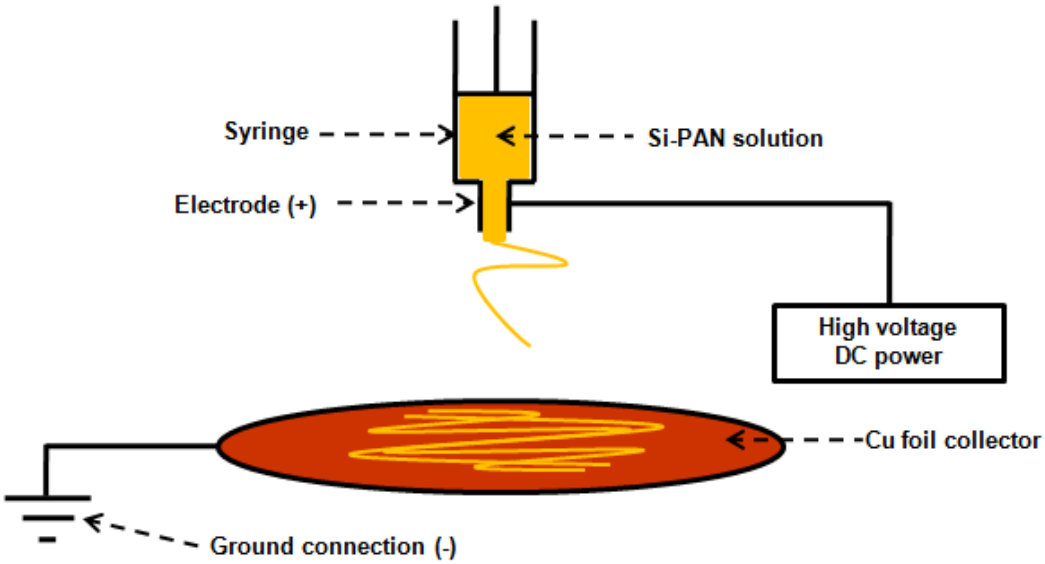

Figure 3.5: The schematic depiction of a simple electrospinning set-up.

References

1. A. Hayashi, S. Hama, H. Morimoto, M. Tatusmisago, and T. Minami, *J. Am. Ceram. Soc*., **84**, 477 (2001).

2. A. Hayashi, S. Hama, F. Mizuno, K. Tadanaga, T. Minami, and M. Tatsumisago, *Solid State Ionics*, **175**, 683 (2004).

3. A. Hayashi, S. Hama, T. Minami, and M. Tatsumisago, *Electrochem. Commun.*, **5**, 111 (2003).

4. C. C. Koch, *J. Non-Cryst. Solids*, **117**, 670 (1990).

5. E. H. Zhou, C. Suryanarayana,and F. H. Fores, *Mater. Lett*., **23**, 27 (1995).

6. Y. Chen, C. P. Li, H. Chen, and Y. J. Chen, *Science and Technology of Advanced Materials*, **7**, 839 (2006).

7. G. Adachi, N. Imanaka, H. Aono, *Adv. Mater.*, **8**, 127 (1996).

8. T. Minami, A. Hayashi, and M. Tatsumisago, *Solid State Ionics***, 177,** 2715 (2006).

9. K. Takada, T. Inada, A. Kajiyama, H. Sasaki, S. Kondo, M. Watanabe, M. Murayama, and Ryoji Kanno, *Solid State Ionics*, **158**, 269 (2003).

10. A. J. Bard and L. R. Faulkner, *ELECTROCHEMICAL METHODS: Fundamentals and Applications, 2nd ed.*, p. 370, John Wiley & Sons, New York (2001).

11. A. J. Bard and L. R. Faulkner, *ELECTROCHEMICAL METHODS: Fundamentals and Applications, 2nd ed.*, p. 305, John Wiley & Sons, New York (2001).

12. A. J. Bard and L. R. Faulkner, *ELECTROCHEMICAL METHODS: Fundamentals and Applications, 2nd ed.*, p. 632, John Wiley & Sons, New York (2001).

13. S. M. George, *Chem. Rev.*, **110**, 111 (2010).

14. A. C. Dillon, A. W. Ott, J. D. Way, and S. M. George, *Surf. Sci.*, **322**, 230 (1995).

15. M. D. Groner, F. H. Fabreguette, J. W. Elam, and S. M. George, *Chem. Mater.*, **16**, 639 (2004).

16. A. W. Ott, J. W. Klaus, J. M. Johnson, and S. M. George, *Thin Solid Films*, **292**, 135 (1997).

17. Y. S. Jung, A. S. Cavanagh, A. C. Dillon, M. D. Groner, S. M. George, and S.-H. Lee, *J. Electrochem. Soc*., **157**, A75 (2010).

18. A. L. Andrady, *Science and Technology of Polymer Nanofibers*, John Wiley & Sons, New York (2008).

Chapter 4

Nanoscale Interface Modification of $LiCoO_2$ by Al_2O_3 Atomic Layer Deposition for Solid State Li Batteries

Lithium-ion batteries (LIBs) are widely utilized in portable electronics and are one of the major contestants for the hybrid electric-vehicle (HEV) and electric-vehicle (EV) market because of their high energy density.[1] Despite their broad exploitation in the energy storage field, certain issues such as flammability and vulnerability in high temperature environments related to the use of organic liquid electrolytes in commercialized LIBs are primary concerns which prevent a large scale-up of LIBs for HEVs and EVs today.[2,3] As a result, there is a growing interest in solid-state lithium batteries (SSLBs) employing a solid state electrolyte (SSE) which is safer and more durable than LIBs with a liquid electrolyte.[4] However, inferior cycle performance resulting from the continous development of interfacial resistance layer between cathode and electrolyte materials in SSLBs is one of the major drawbacks which needs to be overcome for the successful commercialization of secondary SSLBs.[3,5]

$LiCoO_2$ is the most widespread cathode material for commercial LIBs.[5] It is typically utilized at voltages up to 4.2 V (vs. Li/Li^+) to prevent a significant capacity fade.[6] Enabling stable cycling in a higher voltage region above 4.2 V (vs. Li/Li^+) would result in an increase of available capacity. However, it is well known that the interfacial resistance between $LiCoO_2$ and

SSE increases significantly and leads to the rapid capacity fade when the battery is cycled at a high voltage over 4.2 V (vs. Li/Li^+).[6] Surface modification of $LiCoO_2$ by oxide coating has been proven to be effective for (i) lowering interfacial resistance between $LiCoO_2$ and SSE, (ii) reducing cobalt dissolution of $LiCoO_2$ into an electrolyte, and (iii) repression of mutual diffusion between $LiCoO_2$ and electrolyte.[5-7] Therefore, a good capacity retention is achieved by oxide coatings on $LiCoO_2$ even with a high upper limit voltage over 4.2 V (vs. Li/Li^+).[6,7] In most cases, however, heat treatments of oxide-coated $LiCoO_2$ at high temperatures were needed.[6-11] It was shown that an enhancement in the electrical conductivity for oxide-coated $LiCoO_2$ occurred by ionic diffusion between an oxide coating layer and $LiCoO_2$ after such heat treatments.[8,9] Also, an improvement of Li ion diffusion in Al_2O_3-coated $LiCoO_2$ after the heat treatments was achieved by forming the layer with a high Li ion conductivity near $LiCoO_2$.[10,11]

Typically, wet chemical methods such as spray coating and the sol-gel method are used for surface modification.[3,5-9] However, considerable quantities of solvent and precursor are consumed in these methods.[12] On the other hand, our group's previous works have successfully demonstrated the application of atomic layer deposition (ALD) with Al_2O_3 on $LiCoO_2$ powder for LIBs employing liquid electrolytes, showing large improvements in cycle performances.[12,13] ALD is a conformal coating method which needs minimal amounts of precursors.[12] Also, ALD can provide uniform coatings on nanosized $LiCoO_2$ particles because of its atomic thickness control.[13] The thickness of 1.1 ~ 1.2 Å is achieved for each ALD Al_2O_3 layer from one ALD sequence.[14,15]

In this work, we prepared SSLBs using a double layer SSE configuration which has previously shown to provide stable interfaces between electrodes and SSE layers.[16] $LiCoO_2$ powders with/without ALD Al_2O_3 layers have been investigated. Galvanostatic charge-discharge

behaviors and electrochemical impedance during cycling were monitored to investigate the effect of ALD Al_2O_3 layer on the cycle stability of the battery using $LiCoO_2$. The interfaces between uncoated/Al_2O_3 ALD-coated $LiCoO_2$ and $Li_{3.15}Ge_{0.15}P_{0.85}S_4$ SSE were investigated using transmission electron microscopy (TEM) and energy dispersive spectroscopy (EDS). Results show that the employment of ALD Al_2O_3 layers on $LiCoO_2$ powders drastically improves cycle stability of SSLBs.

4.1 Experimental

$Li_{3.15}Ge_{0.15}P_{0.85}S_4$ SSE and $77.5Li_2S–22.5P_2S_5$ (mol %) SSE were synthesized by planetary ball milling (PBM) of reagent-grade powders of Li_2S (Alfa Aesar, 99.9%), P_2S_5 (Sigma Aldrich, 99%), and GeS_2 (City Chemical LLC., 99.99%) in appropriate weight ratios in a stainless steel jar with stainless steel balls for grinding. PBM (SFM-1, MTI Corporation) proceeded at 500 rpm for 20 continuous hours to generate well mixed SSE powders. Heat treatment (HT) for as-ball-milled (ABM) $Li_{3.15}Ge_{0.15}P_{0.85}S_4$ SSE powder was performed inside the glove box on a hot plate and heated up to 360℃ at approximately +10 ℃ min^{-1} in a sealed glass container. SSE remained at 360^{o}C on the hot plate for 2 hours before being removed and placed on a cooling rack. All sample preparations and HTs were done in a dry Ar-filled glove box.

ALD Al_2O_3 layers were deposited directly on $LiCoO_2$ powders (LICO Technology Corp.) using a rotary reactor as described in our previous work.[12] $LiCoO_2$ powders with ALD Al_2O_3 layers were put in a Petri dish and placed on a hot plate for HT (+10℃ min^{-1}, 400℃, 14 hours) inside a dry Ar-filled glove box before battery construction. $LiCoO_2$ (uncoated/Al_2O_3 ALD-coated), heat-treated $Li_{3.15}Ge_{0.15}P_{0.85}S_4$ SSE, and acetylene black (AB, Alfa-Aesar, 50%

compressed) were mixed in a weight ratio of 20:30:3 and ground with a mortar and a pestle to prepare the composite cathode material. The double layer SSE was constructed by hand-pressing 100 mg of heat-treated $Li_{3.15}Ge_{0.15}P_{0.85}S_4$ SSE on the top of 100 mg of hand pressed ABM $77.5Li_2S$-$22.5P_2S_5$ (mol %) SSE followed by cold-pressing at 1 metric ton for 3 minutes. 10 mg of the composite cathode material was evenly spread on the top of $Li_{3.15}Ge_{0.15}P_{0.85}S_4$ SSE layer and pelletized by cold-pressing at 5 metric tons for 3 minutes. Lithium foil (Alfa-Aesar, 0.75 mm thick) was then attached to the $77.5Li_2S$-$22.5P_2S_5$ (mol %) SSE side at 2 metric tons. All pressing and experimental operations were done in a polyaryletheretherketone (PEEK) mold (φ = 1.3 cm) with Ti metal cylinders as current collectors for both working and counter electrodes. Figure 4.1 shows the schematic of our $LiCoO_2/Li_{3.15}Ge_{0.15}P_{0.85}S_4/77.5Li_2S$-$22.5P_2S_5$/Li battery. Galvanostatic charge-discharge cycling was carried out between 3.3 ~ 4.3 V (vs. Li/Li^+) at a current of 45 μA cm^{-2} at 30℃ using an Arbin BT2000. All battery fabrication processes and charge-discharge cycling were conducted in a dry Ar filled glove box.

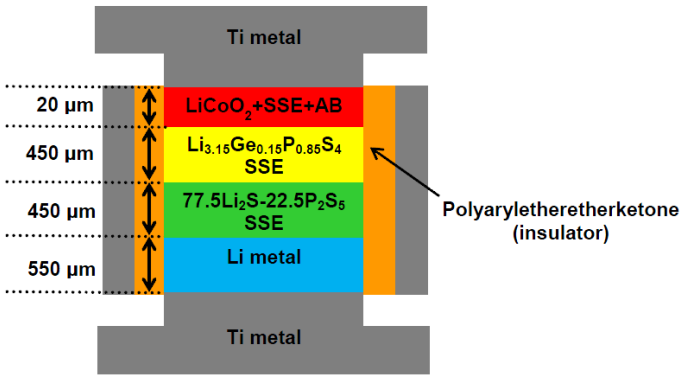

Figure 4.1: The schematic diagram of our double layer SSLB.

Electrochemical impedance spectroscopy (EIS) measurements of SSLBs utilizing uncoated and Al_2O_3 ALD-coated $LiCoO_2$ were collected using a Solartron 1280C. AC impedance profiles were obtained using amplitude of 10 mV and a frequency range from 20 kHz to 1 mHz. Batteries were charged to 4.3 V (vs. Li/Li^+) with a current of 45 μA cm^{-2} and held at 4.3 V (vs. Li/Li^+) for 1 hour before AC impedance profiles were recorded at the open-circuit voltage.

Pellets of our double layer SSLBs were collected from PEEK molds inside the glove box after the 33rd charge process for TEM analysis. A mobile air-lock chamber which keeps the pellets in a vacuum state was used during the loading of a pellet from the glove box to focused ion beam (FIB) machine (FEI NOVA200 dual beam system) to avoid air contact. TEM samples were prepared from cathode layers using FIB from Ga ion source with the same process described in our group's previous paper[17] to investigate interfaces of $LiCoO_2/Li_{3.15}Ge_{0.15}P_{0.85}S_4$ SSE. The interfaces were investigated using the TEM (FEI Tecnai F20) operated at 200 kV to observe interfacial layers. EDS analyses (EDAX Tecnai 136-5) were peformed to verify the thickness of interfacial layers formed at $LiCoO_2/Li_{3.15}Ge_{0.15}P_{0.85}S_4$ SSE interfaces.

4.2 Results and discussion

Figure 4.2 shows the 1st discharge voltage profiles of SSLBs using uncoated and Al_2O_3 ALD-coated $LiCoO_2$ powders. The initial discharge capacity decreases as the number of ALD Al_2O_3 layers increases. The same phenomena were reported in our group's previous work of liquid LIB using Al_2O_3 ALD-coated $LiCoO_2$ powders.[12] The decrease in discharge capacity is attributed to the insulating property of ALD Al_2O_3 layer which compromises electronic conductivity between active $LiCoO_2$ cathode particles.[12, 18]

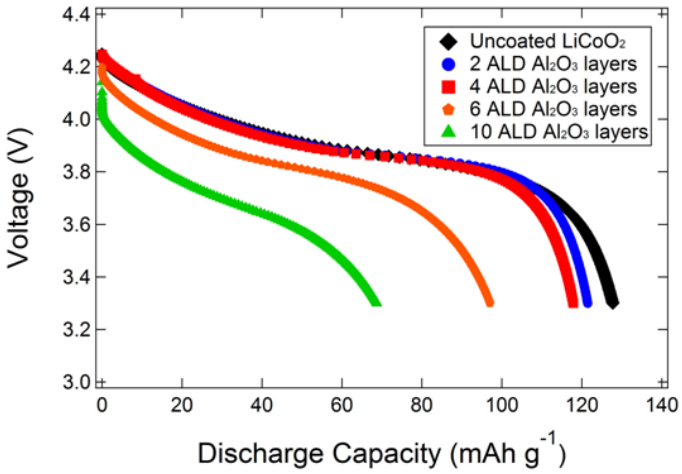

Figure 4.2: The 1st discharge voltage profiles of SSLBs using uncoated and Al_2O_3 ALD-coated $LiCoO_2$ powders.

In order to investigate the effect of ALD Al_2O_3 layer on cycle stability of our SSLBs, galvanostatic charge-discharge cycling was carried out between 3.3 ~ 4.3 V (vs. Li/Li^+). Figure Figure 4.3a displays cycle performances of the SSLBs with uncoated $LiCoO_2$ powders and $LiCoO_2$ powders with ALD Al_2O_3 layers. As shown in Figure 4.2, the initial discharge capacities of batteries using $LiCoO_2$ powders with 2 & 4 ALD Al_2O_3 layers are smaller than that of the battery using uncoated $LiCoO_2$ powders. However, capacity fade is reduced for $LiCoO_2$ powders with 2 & 4 ALD Al_2O_3 layers. As a result, SSLBs using $LiCoO_2$ powders with 2 & 4 ALD layers maintain 90% of their initial discharge capacities after the 25th cycle whereas the battery with uncoated $LiCoO_2$ retains only 70% of the initial discharge capacity. It is clear that ALD Al_2O_3 layers on $LiCoO_2$ powders improve cycle stability significantly.

Charge-discharge voltage profiles of SSLBs using uncoated and Al_2O_3 ALD-coated $LiCoO_2$ powders at the 3rd and the 21st cycle are compared in Figure 4.3b, 4.3c, and 4.3d. All of them exhibit the decrease in both charge and discharge capacities between the 3rd and the 21st

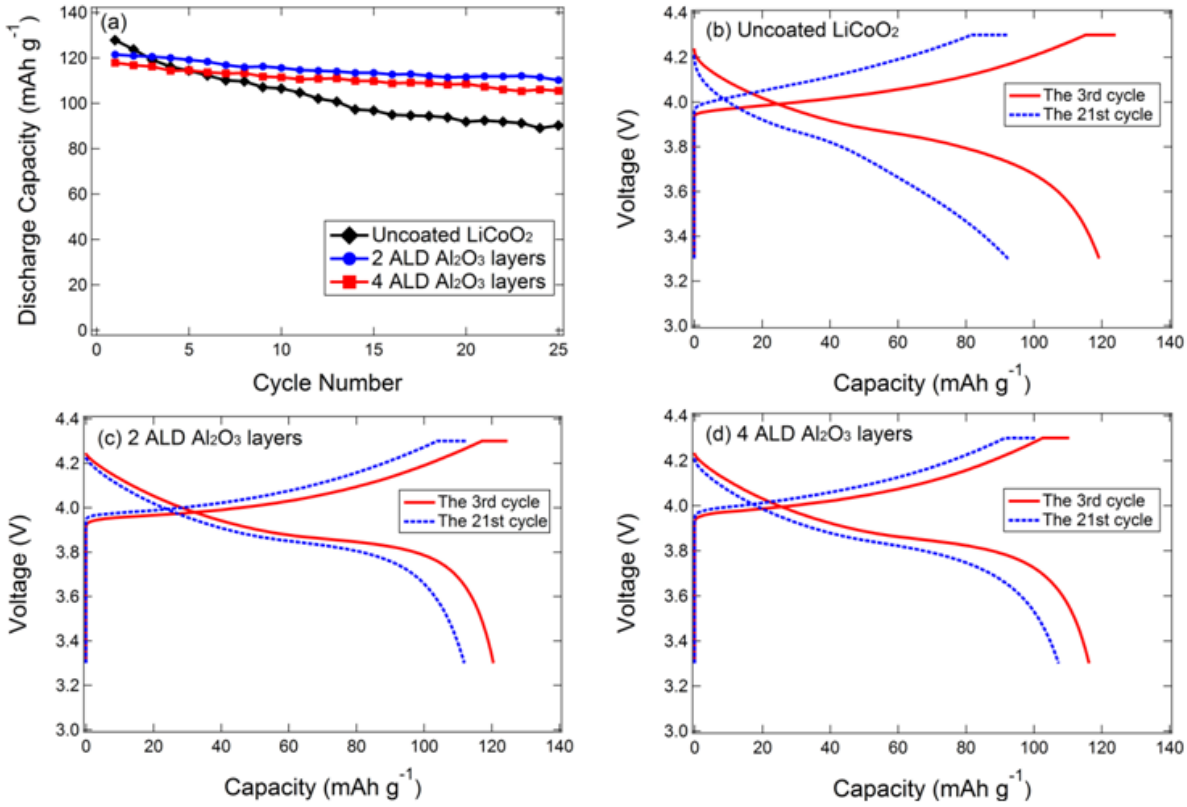

Figure 4.3: (a) Cycle performances of SSLBs using uncoated and Al_2O_3 ALD-coated $LiCoO_2$ powders. Charge-discharge voltage profiles of SSLBs at the 3rd & the 21st cycle using (b) uncoated $LiCoO_2$, (c) $LiCoO_2$ with 2 ALD Al_2O_3 layers, and (d) $LiCoO_2$ with 4 ALD Al_2O_3 layers.

cycle. As the cycle number progresses, however, smaller overpotentials during both charge and discharge processes develop for batteries using $LiCoO_2$ powders with 2 & 4 ALD Al_2O_3 layers. This result indicates that there is smaller increase in interfacial resistance in batteries using Al_2O_3 ALD-coated $LiCoO_2$ powders than that in the battery using uncoated $LiCoO_2$ powders.[7] This improved interfacial stability is corroborated by EIS and TEM analyses in Figure 4.4 and 4.5.

The comparison of the AC impedance profiles of SSLBs at various cycles using uncoated $LiCoO_2$ powders and $LiCoO_2$ powders with 4 ALD Al_2O_3 layers is presented in Figure 4.4. Similar to previous works by Sakuda et al., the bulk resistance of the SSE is shown in the high

frequency region while the charge transfer resistance at the $LiCoO_2/Li_{3.15}Ge_{0.15}P_{0.85}S_4$ interface corresponds to the size of the large semicircle.[6,19] Significant growth in the size of the semicircle during cycling is observed in the SSLB with uncoated $LiCoO_2$ powders as shown in Figure 4.4a. This increase in the resistance is attributed to the increased charge transfer resistance at the interface between uncoated $LiCoO_2$ and $Li_{3.15}Ge_{0.15}P_{0.85}S_4$ SSE in the cathode composite during cycling. Sakuda et al. showed that the formation of an interfacial layer between $LiCoO_2$ and SSE is one of the mechanisms for increased interfacial resistance during charge-discharge cycling.[5] On the other hand, the charge transfer resistance at the interface between $LiCoO_2$ with 4 ALD Al_2O_3 layers and $Li_{3.15}Ge_{0.15}P_{0.85}S_4$ SSE increases in early cycles but exhibits little change after the 12th cycle (Figure 4.4b). This result indicates that the increase of the charge transfer resistance at the interface between $LiCoO_2$ and the SSE can be suppressed by ALD Al_2O_3 layers.

TEM analyses of the interface between $LiCoO_2$ and $Li_{3.15}Ge_{0.15}P_{0.85}S_4$ SSE in composite cathodes were performed to elucidate the mechanism for the increase in the interfacial resistance during cycling. Two SSLBs using uncoated $LiCoO_2$ powders and $LiCoO_2$ powders with 4 ALD

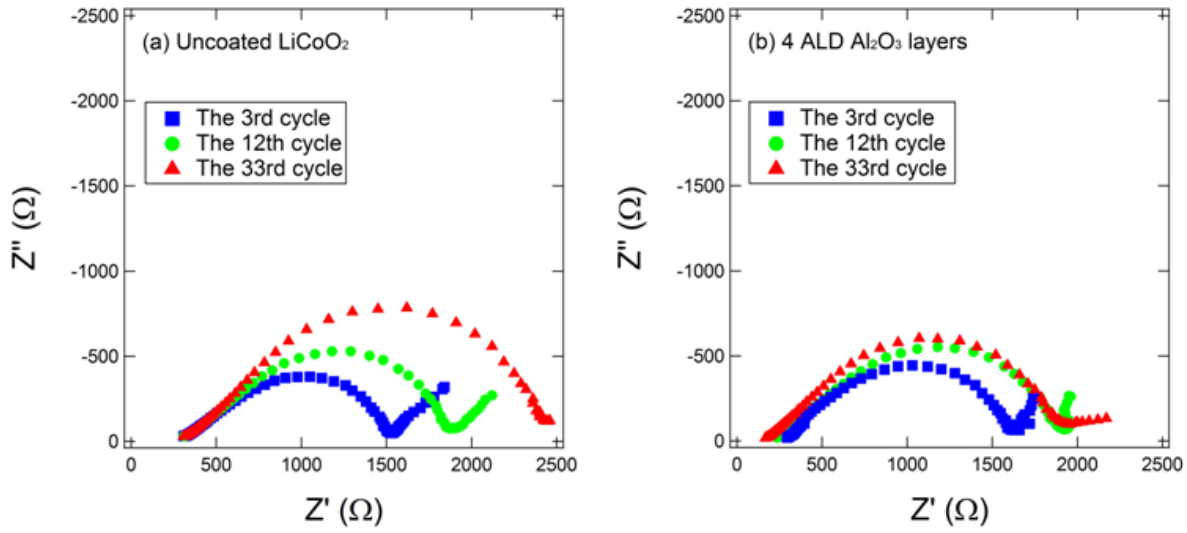

Figure 4.4: AC impedance profiles of SSLBs using (a) uncoated $LiCoO_2$ and (b) $LiCoO_2$ with 4 ALD Al_2O_3 layers at various cycles.

Al_2O_3 layers were charged up to 4.3 V (vs. Li/Li^+) and held at 4.3 V (vs. Li/Li^+) for 1 hour in the 33rd cycle. Pellets of SSLBs were collected from PEEK molds for TEM analyses. Figure 4.5a shows the high-angle annular dark field (HAADF) TEM image of the boundary between uncoated $LiCoO_2$ and $Li_{3.15}Ge_{0.15}P_{0.85}S_4$ SSE. It clearly shows an interfacial layer at the interface between the uncoated $LiCoO_2$ and $Li_{3.15}Ge_{0.15}P_{0.85}S_4$ SSE. Figure 4.5b shows elemental concentration profiles by EDS line scan across the interface which was conducted to obtain the compositional information of the interfacial layer. Co is chosen for the element representing $LiCoO_2$ region while S and P are selected for the elements defining the SSE region. EDS line profiles show the region where Co, S, and P coexist indicating mutual diffusion of these 3 elements which we attribute to the formation of an interfacial layer between $LiCoO_2$ and the SSE during cycling. We chose the Co profile as a criterion to determine the thickness of the interfacial layer since Co is the heaviest elements among three elements and thus least affected by Ga ion milling during FIB process. The diffusion of Co is estimated to be approximately 30 nm as shown in Figure 4.5b. The development of this interfacial layer is believed to contribute to increased interfacial resistance during cycling.[5] In this respect, we propose that a reaction, which causes mutual diffusion of elements in $LiCoO_2$ and $Li_{3.15}Ge_{0.15}P_{0.85}S_4$ SSE occurs at $LiCoO_2$/SSE interface during cycling because of the large difference in chemical potentials between $LiCoO_2$ and sulfide electrolyte. As a result, a highly resistive compound containing the elements of Co, S, and P is formed as an interfacial layer between $LiCoO_2$ and the SSE.

Observation of the HAADF TEM image of the boundary between $LiCoO_2$ with 4 ALD Al_2O_3 layers and $Li_{3.15}Ge_{0.15}P_{0.85}S_4$ SSE is shown in Figure 4.5c. EDS analysis in Figure 4.5d show that the slope of the Co concentration profile in the interfacial layer region is steeper than that in Figure 4.5b. The diffusion distance of Co which corresponds to the thickness of interfacial

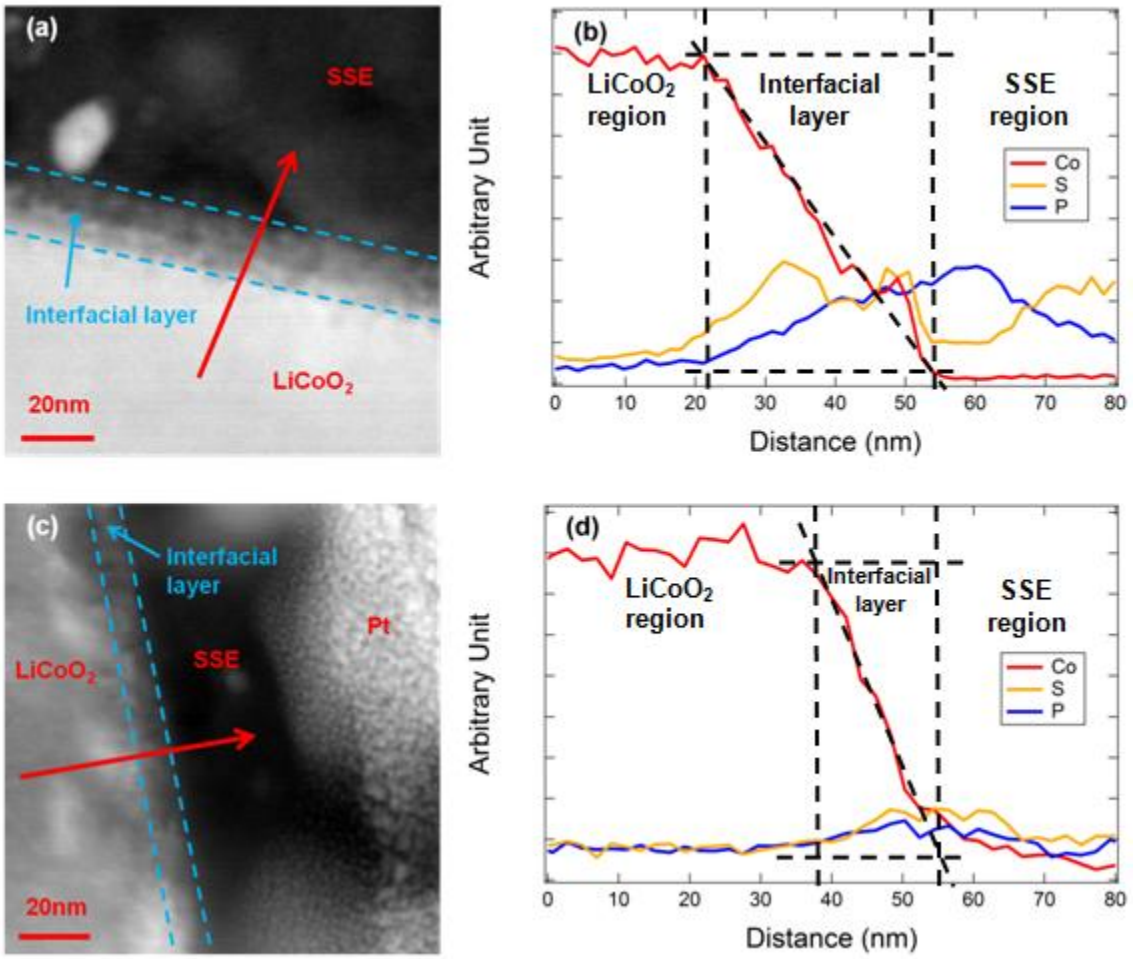

Figure 4.5: (a) HAADF TEM image of uncoated $LiCoO_2/Li_{3.15}Ge_{0.15}P_{0.85}S_4$ SSE interface after the 33rd charging. (b) Elemental concentration profiles of Co, S, and P elements by EDS line scan at uncoated $LiCoO_2/Li_{3.15}Ge_{0.15}P_{0.85}S_4$ SSE interface after the 33rd charging. (c) HAADF TEM image of $LiCoO_2$ with 4 ALD Al_2O_3 layers/$Li_{3.15}Ge_{0.15}P_{0.85}S_4$ SSE interface after the 33rd charging. (d) Elemental concentration profiles of Co, S, and P elements by EDS line scan at $LiCoO_2$ with 4 ALD Al_2O_3 layers/$Li_{3.15}Ge_{0.15}P_{0.85}S_4$ SSE interface after the 33rd charging. Red arrows in (a) and (c) represent the positions and the directions of EDS line scans.

layer is estimated to be approximately 17 nm as shown in Figure 4.5d. This reduced thickness of the interfacial layer is consistent with smaller increase in the charge transfer resistance of the battery using $LiCoO_2$ with 4 ALD Al_2O_3 layers discussed in Figure 4.4. This result also indicates that the diffusion of Co out of $LiCoO_2$ with 4 ALD Al_2O_3 layers is greatly suppressed compared to the diffusion of Co out of uncoated $LiCoO_2$. ALD of Al_2O_3 layers on $LiCoO_2$ prevents direct contact between $LiCoO_2$ and $Li_{3.15}Ge_{0.15}P_{0.85}S_4$ SSE. Similar chemical potentials between the oxide coating material and $LiCoO_2$ powder[3] result in less diffusion of Co from $LiCoO_2$ which leads to a reduced reaction with sulfur compounds in the SSE during charge/discharge processes. Therefore, the formation of interfacial layer with high resistance is repressed at the interface between $LiCoO_2$ with 4 ALD Al_2O_3 layers and the SSE.

4.3 Summary

ALD coating of Al_2O_3 onto $LiCoO_2$ powders was adopted to enhance the cycle performance of SSLBs. The initial discharge capacity decreases with increasing number of ALD Al_2O_3 layers due to the insulating property of ALD Al_2O_3 layer. The batteries using $LiCoO_2$ powders with 2 and 4 ALD layers exhibit improved capacity retention during cycling compared to those using uncoated $LiCoO_2$ powders. Smaller overpotentials during charge/discharge process are observed from the batteries using $LiCoO_2$ powders with 2 and 4 ALD Al_2O_3 layers compared to that from the battery using uncoated $LiCoO_2$ powders. EIS studies reveal that ALD Al_2O_3 layers on $LiCoO_2$ powders suppress the development of interfacial resistance at $LiCoO_2$/$Li_{3.15}Ge_{0.15}P_{0.85}S_4$ SSE interface. Microstructural and elemental analyses of $LiCoO_2$/$Li_{3.15}Ge_{0.15}P_{0.85}S_4$ SSE interfaces in composite cathodes were performed by using high resolution TEM and EDS. The interfacial layer thickness of the SSLB using $LiCoO_2$ with 4 ALD

Al_2O_3 layers was thinner than that of the SSLB using uncoated $LiCoO_2$. We demonstrate that ALD Al_2O_3 layers on active materials effectively reduce the formation of interfacial layer which causes capacity fade during cycling. Therefore, Al_2O_3 ALD is proven to be an effective method for the modification of an interface between $LiCoO_2$ and SSE to improve the cycle performance of SSLBs.

References

1. M. Armand and J.-M. Tarascon, *Nature*, **451**, 652 (2008).

2. F. Mizuno, A. Hayashi, K. Tadanaga, T. Minami, and M. Tatsumisago, *J. Power Sources*, **124**, 170 (2003).

3. N. Ohta, K. Takada, L. Zhang, R. Ma, M. Osada, and T. Sasaki, *Adv. Mater. (Weinheim, Ger.)*, **18**, 2226 (2006).

4. J. W. Fergus, *J. Power Sources*, **195,** 4554 (2010).

5. A. Sakuda, A. Hayashi, and M. Tatsumisago, *Chem. Mater.*, **22**, 949 (2010).

6. A. Sakuda, H. Kitaura, A. Hayashi, K. Tadanaga, and M. Tatsumisago, *J. Power Sources*, **189,** 527 (2009).

7. A. Sakuda, A. Hayashi, and M. Tatsumisago, *J. Power Sources*, **195**, 599 (2010).

8. K. Takada, N. Ohta, L. Zhang, K. Fukuda, I. Sakaguchi, R. Ma, M. Osada, and T. Sasaki, *Solid State Ionics*, **179**, 1333 (2008).

9. S. Oh, J. K. Lee, D. Byun, W. I. Cho, and B. W. Cho, *J. Power Sources*, **132**, 249 (2004).

10. Y. J. Kim, H. Kim, B. Kim, D. Ahn, J.-G. Lee, T.-J. Kim, D. Son, J. Cho, Y.-W. Kim, and B. Park, *Chem. Mater*., **15**, 1505 (2003).

11. Y. J. Kim, T.-J. Kim, J. W. Shin, B. Park, and J. Cho, *J. Electrochem. Soc*., **149**, A1337 (2002).

12. Y. S. Jung, A. S. Cavanagh, A. C. Dillon, M. D. Groner, S. M. George, and S.-H. Lee, *J. Electrochem. Soc*., **157**, A75 (2010).

13. I. D. Scott, Y. S. Jung, A. S. Cavanagh,Y. Yan, A. C. Dillon, S. M. George, and S.-H. Lee, *Nano Lett*., **11,** 414 (2011).

14. M. D. Groner, F. H. Fabreguette, J. W. Elam, and S. M. George, *Chem. Mater*., **16**, 639 (2004).

15. A. W. Ott, J. W. Klaus, J. M. Johnson, and S. M. George, *Thin Solid Films*, **292**, 135 (1997).

16. J. E. Trevey, Y. S. Jung, and S.-H. Lee, *Electrochim. Acta*, **56,** 4243 (2011).

17. S.-B. Son, J. E. Trevey, H. Roh, S.-H. Kim, K.-B. Kim, J. S. Cho, J.-T. Moon, C. M. DeLuca, K. K. Maute, M. L. Dunn, H. N. Han, K. H. Oh, and S.-H. Lee, *Adv. Energy Mater.*, **1**, 1199 (2011).

18. M. D. Groner, J. W. Elam, F. H. Fabreguette, and S. M. George, *Thin Solid Films*, **413**, 186 (2002).

19. A. Sakuda, H. Kitaura, A. Hayashi, K. Tadanaga, and M. Tatsumisago, *Electrochem. Solid-State Lett.*, **11**, A1 (2008).

20. Y. Uchimoto and M. Wakihara, in *Solid State Ionics for Batteries*, T. Minami, Editor, p. 126, Springer-Verlag, Tokyo (2005).

Chapter 5

Utilization of Al_2O_3 Atomic Layer Deposition for Li ion Pathways in Solid State Li Batteries

As mentioned in the previous chapter, solid state Li batteries (SSLBs) which use nonflammable solid state electrolytes (SSEs) are one of the promising solutions to the safety concerns over the flammability of the organic liquid electrolyte normally used in current lithium ion batteries (LIBs).[1-3] Despite their improved safety performance, SSLBs have not been practical subsititutes for conventional LIBs because of their low power densities.[2] Previous works have shown that one of the major causes of relatively poor power performance of SSLBs can be attributed to the interfaces between active material and SSE in working electrodes.[2,4] SSLBs have less interfacial contact area from solid-solid contacts compared to the liquid-solid interfaces in coventional LIBs. The restricted pathways for Li^+ ions and electrons in SSLBs limit ionic and electronic transports which are essential for battery cycling. In addition, many previous works have shown with electrochemical impedance spectroscopy (EIS) and transmission electron microscopy (TEM) that the interfacial resistance at electrode/SSE interfaces ($LiCoO_2$/$80Li_2S{\cdot}20P_2S_5$ SSE, $LiMn_2O_4$/$80Li_2S{\cdot}20P_2S_5$ SSE) increases during charge-discharge processes.[4-8]

There have been many efforts to create better interfaces between active materials and SSEs in solid state batteries such as the employment of oxide coatings on active materials in working electrodes.[2,4-8] It is confirmed in these works that the resistance at the interface is greatly reduced by introduction of a passivating oxide layer. In addition, considerable increases in discharge capacities are observed from solid state batteries which use coatings of various oxide layers on active material pariticles in working electrodes compared to those which use uncoated active material pariticles.[2,4-8] The factors proposed for the role of the oxide layer in the enhancement are (i) the alleviation of resistive layer growth at the interface[4-6] and (ii) the possibility of an increase in the electrochemically active area at the interface.[5,8]

Although these reports about solid state batteries commonly state that the improvement of cycling performance comes from the decrease in the interfacial resistance at the active material/SSE interface, they don't necessarily focus on the way of utilizing oxide coatings to increase capacities of solid state batteries. To illuminate this issue, we focused on the role of the oxide coating not only in (i) but also in (ii) which are mentioned above. Previous works have shown that oxide coating layers on the surface of active materials used in organic liquid electrolyte batteries exhibit desirable properties after heat treatments (HTs).[9-11] Increases in capacities from the batteries using oxide coatings either on active materials or on working electrode also appear in these papers.[10,11] Nevertheless, they didn't clarify the effect of the oxide layers with/without HT either on the active materials or on the working electrodes of Li batteries.

On the other hand, our group demonstrated a novel way of introducing Al_2O_3 coating on the surface of $LiCoO_2$.[12-14] Utilization of atomic layer deposition (ALD) of Al_2O_3 onto the active material resulted in great improvements in cycling performances for both liquid electrolyte Li

battery and SSLB. In addition, Jung *et al.* reported that HT of Al_2O_3 ALD layer on the electrode helped to create a beneficial layer for Li^+ ion transport in liquid electrolyte Li batteries.[15]

In this study, we present a breakthrough in overcoming limited interfaces in SSLBs by the utilization of Al_2O_3 ALD layer on $LiCoO_2$ in the working electrode using HT. SSLBs with the double layer SSE configuration used in our previous work[14] were constructed using $LiCoO_2$ powders coated with Al_2O_3 ALD which were under HT in Ar environment after ALD process. Galvanostatic charge-discharge behaviors, differential capacity (dQ/dV) analysis, EIS profiles, and electrochemical overpotentials obtained from galvanostatic intermittent titration technique (GITT) were studied to determine the effect of HT on Al_2O_3 ALD layer surrounding $LiCoO_2$ particle. Results corroborate our statment of the beneficial Li^+ ion pathway formed from Al_2O_3 ALD layers.

5.1 Experimental

As-ball-milled (ABM) $Li_{3.15}Ge_{0.15}P_{0.85}S_4$ SSE and ABM $77.5Li_2S–22.5P_2S_5$ (mol %) SSE were synthesized by planetary ball milling (PBM) with the same method described in our previous work.[14] Heat treatment (HT) for ABM $Li_{3.15}Ge_{0.15}P_{0.85}S_4$ SSE powder was carried out inside the glove box on a hot plate with the heating rate of +10 ℃ min^{-1} to 460℃ in a sealed glass container. SSE was kept at 460^{o}C on the hot plate for 2 hours before being removed and placed on a cooling rack. All sample preparations and HTs were performed in a dry Ar-filled glove box.

Al_2O_3 ALD layers were coated directly on $LiCoO_2$ powders (LICO Technology Corp.) using a rotary reactor as mentioned in our former report.[12] $LiCoO_2$ powders with Al_2O_3 ALD layers were either put under a constant Ar gas flow using a sealed quartz tube in a furnace for HT

(300℃, 12 hours) or dried using a vacuum oven (120℃, 12 hours). $LiCoO_2$ (uncoated/Al_2O_3 ALD-coated), heat-treated $Li_{3.15}Ge_{0.15}P_{0.85}S_4$ SSE, and acetylene black (AB, Alfa-Aesar, 50% compressed) were mixed at a weight ratio of 20:30:3 using a mortar and a pestle to prepare the working electrode composite for SSLBs. SSLBs with the double layer SSE configuration using Li metal foils as counter electrodes were constructed as described in our previous work.[14] All SSLB fabrications and experimental operations were implemented in galvanostatic charge-discharge processes were performed with SSLBs between 3.3 ~ 4.3 V (vs. Li/Li^+) at a current of 45 μA cm^{-2} at 30℃ using an Arbin BT2000. Charge process and discharge process correspond to the delithiation and the lithiation of $LiCoO_2$. SSLBs were charged to 4.3 V (vs. Li/Li^+) and held at the voltage for 1 hour before discharge processes. All SSLB constructions and experiments were conducted in a dry Ar gas environment.

Electrochemical impedance spectroscopy (EIS) measurements of SSLBs using $LiCoO_2$ particles with different surface conditions were performed by a Solartron 1280C. SSLBs were charged to 4.3 V (vs. Li/Li^+) with a current of 45 μA cm^{-2} and held at the voltage for 1 hour at the 1st cycle before EIS data were obtained at the open-circuit voltage. AC impedance profiles were collected using an amplitude of 10 mV and a frequency range from 20 kHZ to 1 mHz.

A 2032-type coin cell was made for galvanostatic intermittent titration technique (GITT) measurement. A working electrode composite was prepared by spreading a slurry of $LiCoO_2$ powders (LICO Technology Corp.), acetylene black (AB, Alfa-Aesar, 50% compressed), and polyvinylidene fluoride (PVDF) (80:10:10 weight ratio) onto a high grade Al foil and roll-pressed after drying in air at 80°C for 1 h. The electrodes were dried in a vacuum oven at 120°C for 12 hours before battery fabrication. The separator was a glass micro-fiber disk (Whatman GF/F) and the electrolyte was 1 M $LiPF_6$ in ethylene carbonate (EC): diethylene carbonate (DEC)

(1:1 volume ratio). The cell fabrication was done in a dry Ar gas environment using Li metal as a counter electrode. The cell was charged and discharged between 3.3 ~ 4.3 V (vs. Li/Li^+) by applying a constant C/10 rate current and 1 hr voltage hold at 4.3 V (vs. Li/Li^+) for the 1st cycle. For the 2nd cycle, a constant current flux was supplied for 3060 sec (with the current same as C/10 rate) followed by an open circuit stand of the cell for 3600 sec. This GITT procedure was performed at the 2nd charge-discharge process between 3.3 ~ 4.3 V (vs. Li/Li^+).

5.2 Results and discussion

Galvanostatic charge-discharge cycles were performed between 3.3 ~ 4.3 V (vs. Li/Li^+) with SSLBs using $LiCoO_2$ particles coated with different numbers of Al_2O_3 ALD layers and with different HT environments. Figure 5.1 describes voltage profiles of SSLBs using various Al_2O_3 ALD-coated $LiCoO_2$ particles. All of Al_2O_3 ALD-coated $LiCoO_2$ particles used in this figure went through HT in Ar gas flow (300℃, 12 hours) before battery fabrication. What we can see from the figure are relatvely larger 1st charge capacities of SSLBs with Al_2O_3 ALD-coated $LiCoO_2$ particles compared to that of SSLB with uncoated $LiCoO_2$ particles. Since the only difference between them is the existence of Al_2O_3 ALD layer, we attribute additional charge capacities to interactions between the Al_2O_3 ALD layer and $Li_{3.15}Ge_{0.15}P_{0.85}S_4$ SSE which may result in enhanced Li^+ ion transport through the Al_2O_3 ALD layer. Further investigation is needed to clarify the mechanism of the reaction during the 1st charge process in our future work.

In addition, voltage profiles of subsequent cycles from SSLBs using $LiCoO_2$ particles coated with different numbers of Al_2O_3 ALD layers are shown in Figure 5.1. SSLB with uncoated $LiCoO_2$ reveals an increase in the polarization and a decrease in the specific capacity as

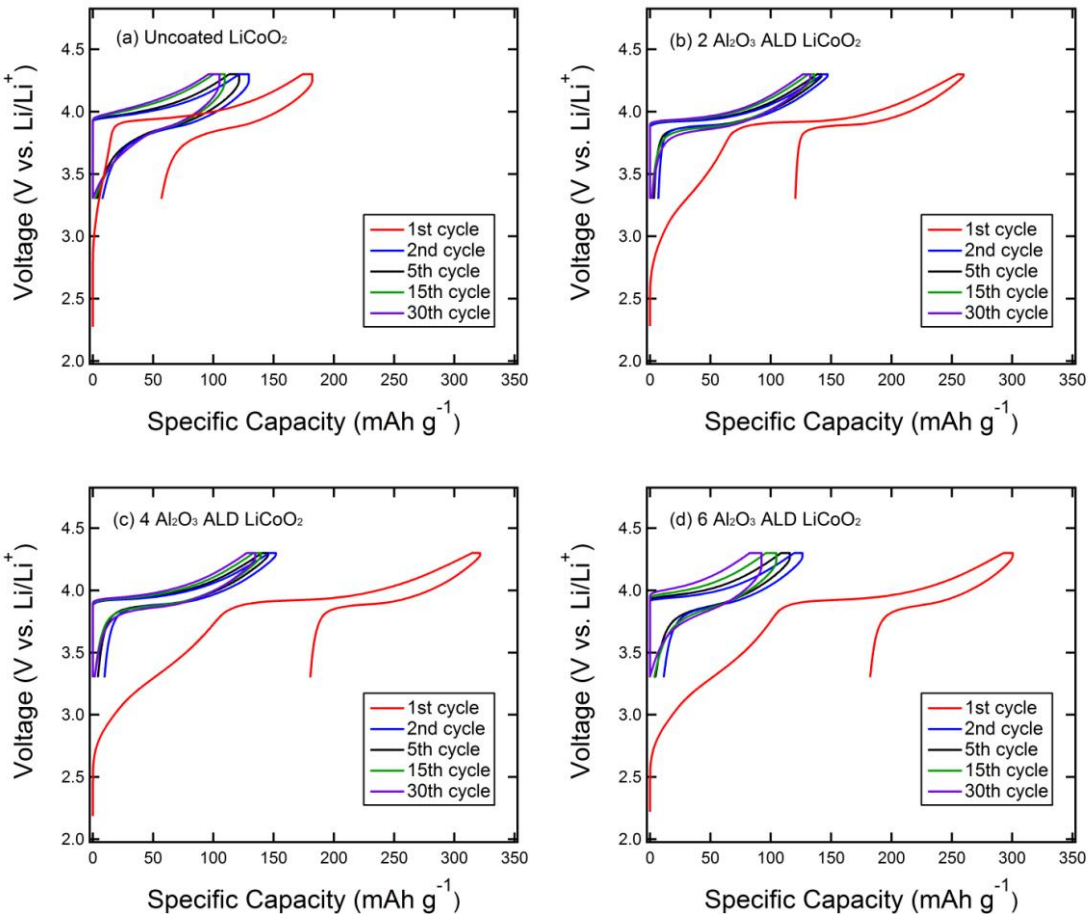

Figure 5.1: Voltage profiles of SSLBs using various Al_2O_3 ALD-coated $LiCoO_2$ particles.

the number of cycles increases (Figure 5.1a). In contrast, SSLBs using $LiCoO_2$ particles with 2 & 4 Al_2O_3 ALD layers shows less polarization and less degradation in the specific capacity during cycling (Figure 5.1b & 5.1c). We attribute this phenomenon to the suppresion of the resistive interfacial layer growth at $LiCoO_2$/SSE interface by Al_2O_3 ALD layer which was shown in our previous work with EIS and TEM.[14] However, SSLB using $LiCoO_2$ particles with 6 Al_2O_3 ALD layers exhibits worse cycling performance even compared with SSLB using uncoated $LiCoO_2$ particles (Figure 5.1d). The electronically insulating properties of thick Al_2O_3 ALD layers is

thought to be the cause.[12,16] Authors speculate that the HT method used in this work is insufficient to resolve the insulating characteristics of Al_2O_3 layers from 6 cycles of ALD.

Galvanostatic cycling performances of different SSLBs between 3.3 ~ 4.3 V (vs. Li/Li^+) are compared in Figure 5.2. $LiCoO_2$ particles coated with Al_2O_3 ALD layers used in Figure 5.2a were heat-treated in Ar gas flow (300℃, 12 hours) prior to battery fabrication. SSLBs using $LiCoO_2$ particles with 2 & 4 Al_2O_3 ALD layers show larger initial discharge capacities (~140 mAh g^{-1}) than that of SSLB using uncoated $LiCoO_2$ particles (125 mAh g^{-1}). This is more than a 10 % increase in capacity which brings the capacity closer to the theoretical available capacity of $LiCoO_2$.[6] Authors attribute this to the participation of Al_2O_3 ALD layers on Li^+ ion transport to $LiCoO_2$ which results in an increase of discharge capacities. On the other hand, SSLB with $LiCoO_2$ particles with 6 Al_2O_3 ALD layers exhibits worse cycling performance than that of SSLB using uncoated $LiCoO_2$ particles. The low discharge capacity and the inferior stability can be attributed to the insulating property of thick Al_2O_3 ALD layer as mentioned in Figure 5.1d.

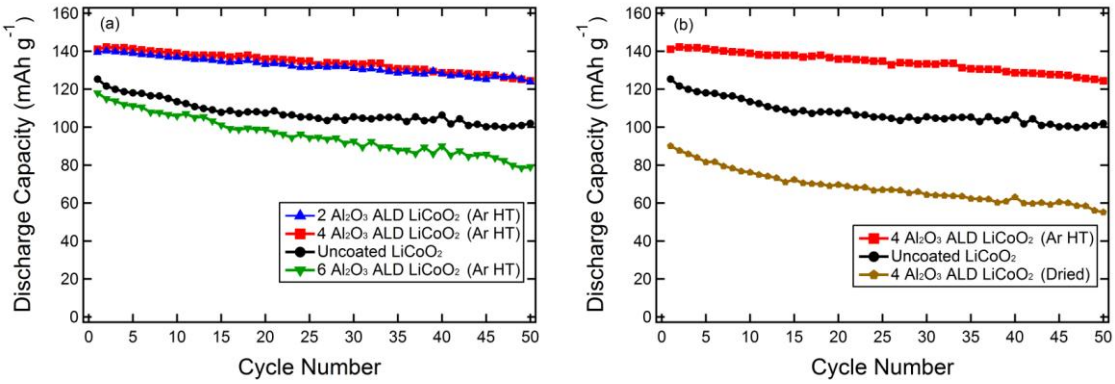

Figure 5.2: Cycling performances of SSLBs with (a) different numbers of Al_2O_3 ALD layers and (b) different HT environments.

The effect of HT in Ar gas flow on the utilization of Al_2O_3 ALD layers on $LiCoO_2$ particles as Li^+ ion pathways is also studied (Figure 5.2b). $LiCoO_2$ particles with 4 Al_2O_3 ALD layers were dried in a vacuum (120℃, 12 hours) and used for SSLB fabrication. The SSLB using dried ALD-coated $LiCoO_2$ particles achieved poor results compared to the SSLB using ALD-coated $LiCoO_2$ particles after HT under Ar gas flow (300℃, 12 hours). This is evidence showing that HT under Ar environment is integral for improvement of Li^+ ion transport in Al_2O_3 ALD layers surrounding $LiCoO_2$. It is believed that ionic diffusion occurs between $LiCoO_2$ and Al_2O_3 ALD layer during the HT process. Oh et al. showed that such ionic diffusion enhances electronic conductivity of Al_2O_3 layer on $LiCoO_2$.[11] More detailed analysis of the change in properties of Al_2O_3 ALD layer after HT will be done in future studies.

In order to understand electrochemical reactions occurred on $LiCoO_2$ particles with various surface conditions, dQ/dV values were calculated (Figure 5.3) from charge-discharge profiles of SSLBs in Figure 5.2b. All 3 SSLBs using different $LiCoO_2$ particles in working electrodes exhibit major redox peaks which correspond to Li^+ intercalation/deintercalation with $LiCoO_2$ at ~ 3.9 V (vs. Li/Li^+).[17] However, significant difference exists in these dQ/dV profiles. Noticeable humps appear at ~ 3.3 V (vs. Li/Li^+) in dQ/dV plots from SSLBs using Al_2O_3 ALD-coated $LiCoO_2$ particles (Ar HT, dried). These humps are expected to correspond to the interaction between Al_2O_3 ALD layer and $Li_{3.15}Ge_{0.15}P_{0.85}S_4$ SSE which is mentioned in Figure 5.1. It seems that additional oxide layers added at $LiCoO_2$/SSE interfaces interact with surroundings to result in higher charge capacities in the 1st charge process. As a result of this interaction, Al_2O_3 ALD-coated $LiCoO_2$ with Ar HT shows sharper and larger major peaks at ~ 3.9 V (vs. Li/Li^+) which can be explained as more effective access to Li^+ ion reaction sites on $LiCoO_2$ particles during charge-discharge cycling, achieving larger capacities. On the contrary,

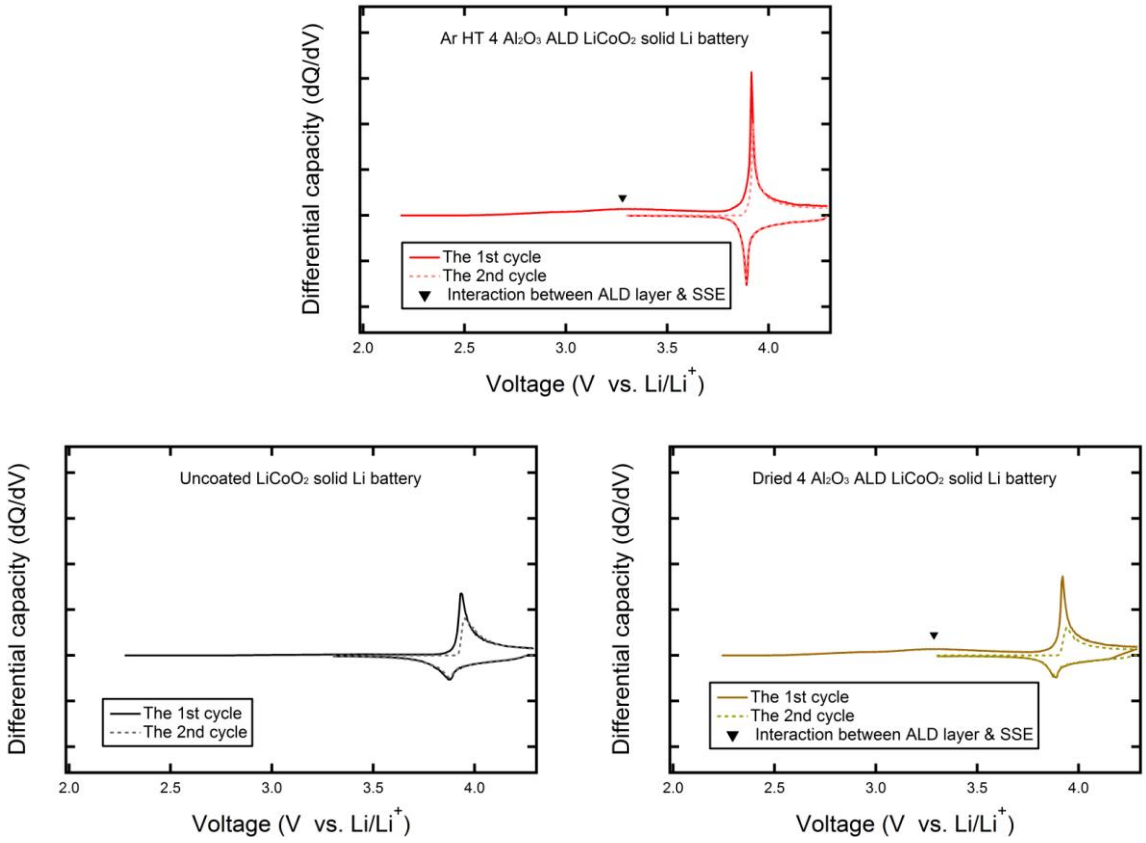

Figure 5.3: dQ/dV profiles of SSLBs with different $LiCoO_2$ particles.

dried Al_2O_3 ALD-coated $LiCoO_2$ exhibits blunt and smaller major peaks at ~ 3.9 V (vs. Li/Li^+) which result in low capacities as shown in Figure 5.2b. Therefore Ar HT process seems to be integral to enhance transport properties of Al_2O_3 ALD layer on $LiCoO_2$.

AC impedance profiles from SSLBs with different active materials (Ar HT 4 Al_2O_3 ALD $LiCoO_2$, uncoated $LiCoO_2$, and dried 4 Al_2O_3 ALD $LiCoO_2$) are shown in Figure 5.4. EIS data were collected after the 1st charge process to exclude the increase in the resistance at $LiCoO_2$/SSE interface during cycling which was shown in our previous report[14] and to focus on the interfacial resistance of $LiCoO_2$/SSE interface at initial stage. All profiles show semicircles

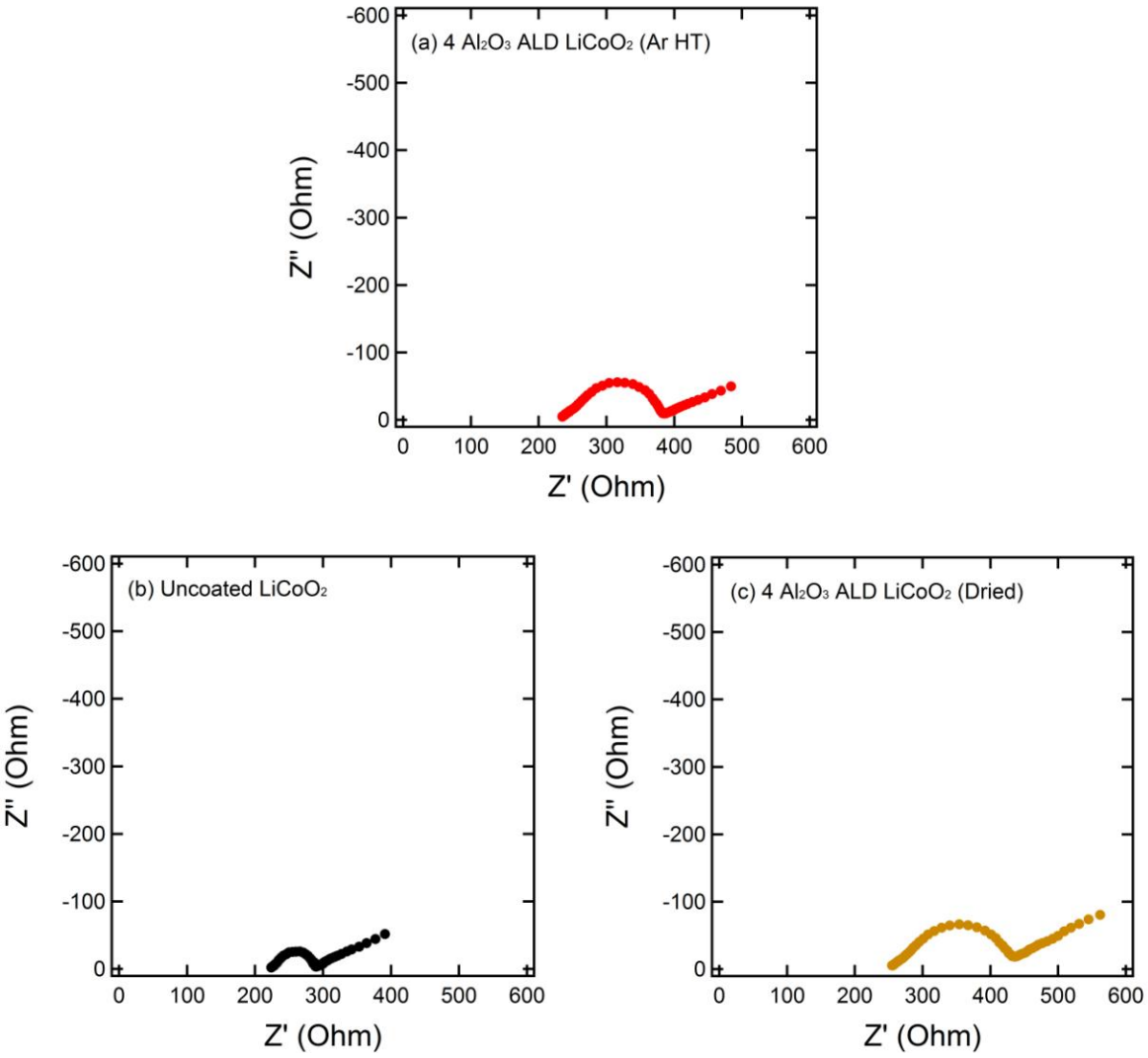

Figure 5.4: AC impedance profiles of SSLBs using $LiCoO_2$ with different surface conditions after the 1st charge process.

which correspond to charge transfer resistance at the interface between $LiCoO_2$ and $Li_{3.15}Ge_{0.15}P_{0.85}S_4$ SSE.[6] SSLB with Ar HT 4 Al_2O_3 ALD $LiCoO_2$ (Figure 5.4a) shows smaller interfacial resistance compared to SSLB with dried 4 Al_2O_3 ALD $LiCoO_2$ (Figure 5.4c). It can be attributed to an enhancement in charge tranfer in Al_2O_3 ALD layer after Ar HT which contributes to better cycling performance as shown in Figure 5.2b. However, Ar HT 4 Al_2O_3 ALD $LiCoO_2$ (Figure 5.4a) does not show improvement in charge transfer resistance compared

to uncoatd $LiCoO_2$ (Figure 5.4b). Based on EIS analysis, it can be thought that superior performance of SSLB using Ar HT 4 Al_2O_3 ALD $LiCoO_2$ to that of SSLB using uncoated $LiCoO_2$ is more related to mass transfer of Li^+ ion than charge transfer.

Along with EIS study, elucidation for the transport properties of $LiCoO_2$ particles with various surface conditions is performed by comparing overpotentials from SSLBs using them. It has been shown that the overpotential of an electrochemical cell can be a way of investigating the transport properties of an active material in a cell.[18] Figure 5.5 assesses varying

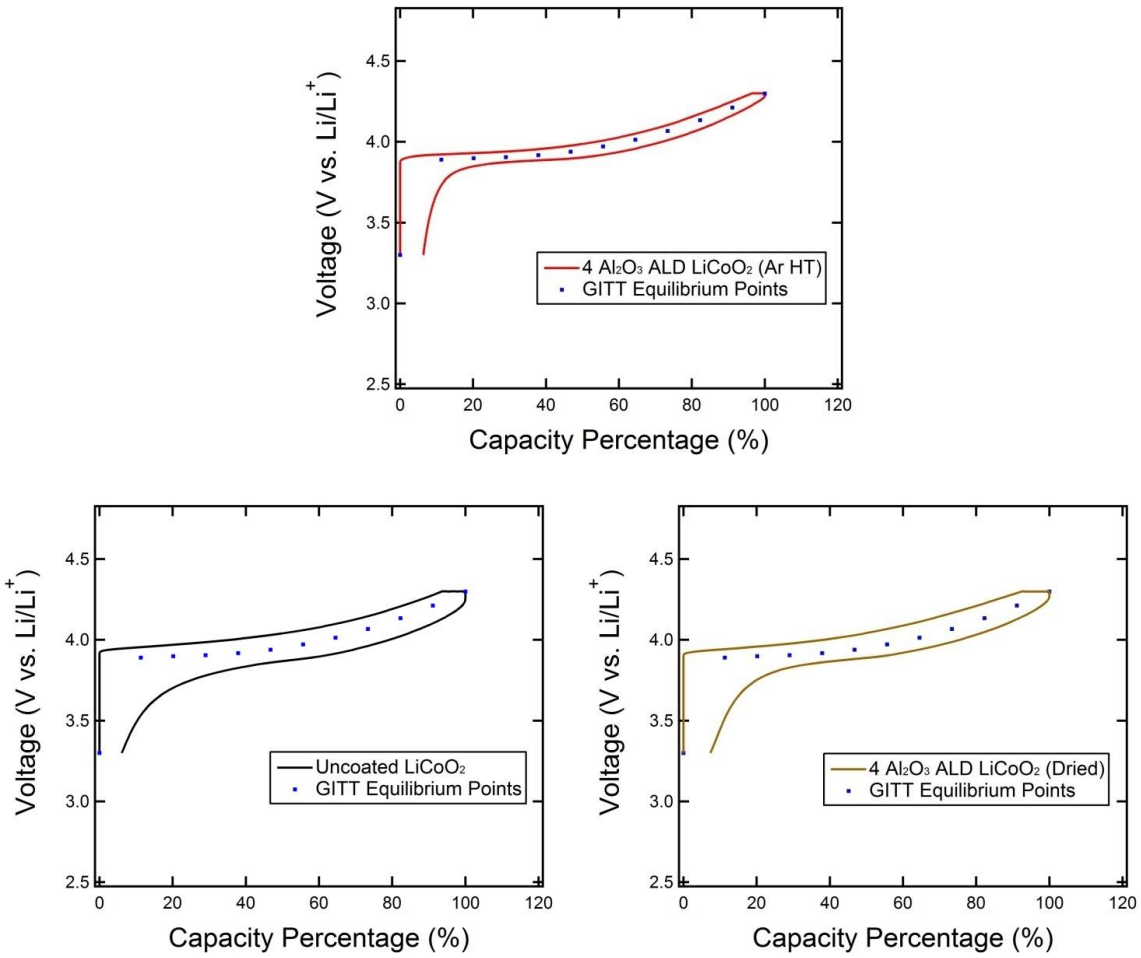

Figure 5.5: Comparison between GITT equilibrium voltage points and 2nd charge-discharge volatage profiles of SSLBs with different $LiCoO_2$ particles. Profiles are normalized to 100% of their charge capacities for the comparison.

overpotentials of different SSLBs by comparing each voltage profile to the thermodynamic equilibrium voltage points of a $LiCoO_2$/Li half cell. Voltage profiles from the 2nd cycles are selected for SSLBs to exclude the effect of the 1st charge reaction which accompanied interaction at Al_2O_3 ALD layer/$Li_{3.15}Ge_{0.15}P_{0.85}S_4$ SSE interface and to minimize the effect of degradation during cycles. Equilibrium points were obtained by applying galvanostatic intermittent titration technique (GITT) to $LiCoO_2$/Li 2032-type coin cell using liquid electrolyte. Average values between voltage points of the coin cell after each open circuit stand during the 2nd charge process and those during the 2nd discharge process are selected as equilibrium points. In addition, all profiles are normalized to 100% of their charge capacities for the comparison. It is obvious that 4 Al_2O_3 ALD $LiCoO_2$ after Ar HT shows the smallest overpotential compared to uncoated $LiCoO_2$ and dried 4 Al_2O_3 ALD $LiCoO_2$. Therefore, it can be concluded that Al_2O_3 ALD layers surrounding $LiCoO_2$ particles have better mass transport property after Ar HT. As a result, it can be expected to provide better Li^+ ion intercalation. On the other hand, 4 Al_2O_3 ALD $LiCoO_2$ without HT showed a large overpotential comparable to the uncoated one. According to EIS analysis and the overpotential study, the relatively poor transport properties of the non-HT ALD layer for both mass and charge transfer resulted in the worst cycling performance in Figure 5.2b.

Based on experimental results shown above, we propose a mechanism of the utilization of Al_2O_3 ALD layer for efficient access to Li^+ ion reaction sites on $LiCoO_2$. It has been widely accepted that reversible Li^+ ion intercalation into $LiCoO_2$ occurs through two-dimensional pathways.[19-21] $LiCoO_2$ has the rhombohedral (space group $R\bar{3}m$) layered structure composed of alternating CoO_2 sheets and sheets of octahedrally coordinated Li^+ ions. Li^+ ions intercalate and deintercalate through gaps between CoO_2 sheets. Therefore, the intercalation is dependent on the

direction of Li^+ ion movement. We can expect that soaking $LiCoO_2$ particles with liquid electrolyte will provide sufficient Li^+ ion pathways within the working electrode.

However, limited interfacial contact area between active material and SSE in working electrodes of SSLBs makes matters worse. Figure 5.6a shows how the number of effective interfaces for Li^+ ion intercalation is limited in a SSLB's working electrode. The number of contacts between $LiCoO_2$ particles and SSE particles in a SSLB is less than that of a liquid electrolyte battery. Among those limited contacts, effective Li^+ ion intercalation only occurs when the Li^+ ion movement direction is along the gap between CoO_2 sheets in a $LiCoO_2$ particle. In addition, a resistive interfacial layer which hinders Li^+ ion transport can develop during cycling of SSLBs.[14] Therefore, we believe that these factors stated above are the reasons for lower capacities and faster degradation of SSLBs compared to those of liquid electrolyte Li batteries.

Figure 5.6b depicts our proposed mechanism of the utilization of Al_2O_3 ALD layer. HT of the Al_2O_3 ALD layer in Ar gas flow allows the ALD layer to serve as a Li^+ ion pathway providing additional access to intercalation sites for Li^+ ions in $LiCoO_2$. This will result in an

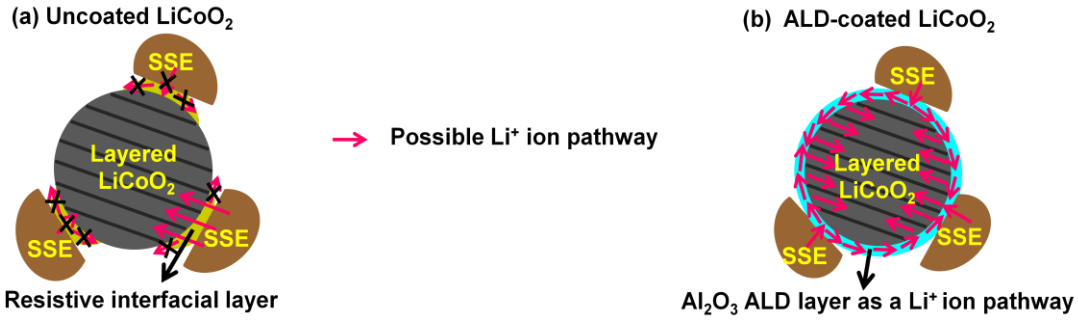

Figure 5.6: Schematic depiction of the interface between (a) uncoated $LiCoO_2$ & SSE, (b) Ar HT Al_2O_3 ALD-coated $LiCoO_2$ & SSE.

increase in battery capacity which is needed for higher energy density. In addition, the Al_2O_3 ALD layer can help to suppress the growth of resistive interfacial layers between $LiCoO_2$ and SSE particles[14] during battery cycling. As a result, $LiCoO_2$ with Ar HT Al_2O_3 ALD layer can achieve high energy density and long-term cycling stability which are essential for the application of Li ion batteries in electric vehicles.

5.3 Summary

Heat treatment in Ar gas flow of Al_2O_3 ALD coated $LiCoO_2$ particles is utilized as a method to improve Li^+ ion transport on the surface of particles. Larger 1st charge capacities are observed from SSLBs with Al_2O_3 ALD-coated $LiCoO_2$ compared to SSLBs with uncoated ones due to the interaction between the heat treated ALD layer and SSE. $LiCoO_2$ particles coated with 2 & 4 cycles of Al_2O_3 ALD and subsequently HT under Ar gas flow achieve smaller polarization increases, relatively larger initial discharge capacities, and better cycling performances compared to those from SSLBs with uncoated $LiCoO_2$ particles. However, $LiCoO_2$ particles coated with 6 cycles of Al_2O_3 ALD and subsequently HT under Ar gas flow show worse performance due to the insulating property of the thicker Al_2O_3 ALD layer. Also, it is shown that HT in Ar gas flow is essential for improving the Al_2O_3 ALD layer's effect on SSLB performance by comparing 4 Al_2O_3 ALD layers with and without HT. Al_2O_3 ALD layer on $LiCoO_2$ seems to exhibit more efficient Li^+ ion transport after HT according to dQ/dV analysis, EIS profiles, and the overpotential study with GITT method. We demonstrate that Al_2O_3 ALD layer coated on $LiCoO_2$ can be utilized as an additional Li^+ ion transport pathway. Therefore, this work proposes an effective strategy to overcome the limited interface issue in SSLBs. More sophiscated studies on

the mechanism of the interaction between $LiCoO_2$, Al_2O_3 ALD layer, and SSE during HT & the 1st charge will be performed in future works.

References

1. F. Mizuno, A. Hayashi, K. Tadanaga, T. Minami, and M. Tatsumisago, *J. Power Sources*, **124**, 170 (2003).

2. N. Ohta,K. Takada, L. Zhang,R.Ma, M. Osada, and T. Sasaki, *Adv. Mater*., **18**, 2226 (2006).

3. J. W. Fergus, *J. Power Sources*, **195**, 4554 (2010).

4. A. Sakuda, A. Hayashi, and M. Tatsumisago, *Chem. Mater.*, **22**, 949 (2010).

5. A. Sakuda, H. Kitaura, A. Hayashi, K. Tadanaga, and M. Tatsumisago, *J. Electrochem. Soc*., **156**, A27 (2009).

6. A. Sakuda, H. Kitaura, A. Hayashi, K. Tadanaga, and M. Tatsumisago, *J. Power Sources*, **189**, 527 (2009).

7. A. Sakuda, A. Hayashi, and M. Tatsumisago, *J. Power Sources*, **195**, 599 (2010).

8. H. Kitaura, A. Hayashi, K. Tadanaga, and M. Tatsumisago, *Solid State Ionics*, **192**, 304 (2011).

9. Y. J. Kim, T.-J. Kim, J. W. Shin, B. Park, and J. Cho, *J. Electrochem. Soc*., **149**, A1337 (2002).

10. Y. J. Kim, H. Kim, B. Kim, D. Ahn, J.-G. Lee, T.-J. Kim, D. Son, J. Cho, Y.-W. Kim, and B. Park, *Chem. Mater*., **15**, 1505 (2003).

11. S. Oh, J. K. Lee, D. Byun, W. I. Cho, and B. W. Cho, *J. Power Sources*, **132**, 249 (2004).

12. Y. S. Jung, A. S. Cavanagh, A. C. Dillon, M. D. Groner, S. M. George, and S.-H. Lee, *J. Electrochem. Soc*., **157**, A75 (2010).

13. I. D. Scott, Y. S. Jung, A. S. Cavanagh,Y. Yan, A. C. Dillon, S. M. George, and S.-H. Lee, *Nano Lett*., **11**, 414 (2011).

14. J. H. Woo, J. E. Trevey, A. S. Cavanagh, Y. S. Choi, S. C. Kim, S. M. George, K. H. Oh,and S.-H. Lee, *J. Electrochem. Soc*., **159**, A1120 (2012).

15. Y. S. Jung, A. S. Cavanagh, Y. Yan, S. M. George, and A. Manthiram, *J. Electrochem. Soc*., **158**, A1298 (2011).

16. M. D. Groner, J. W. Elam, F. H. Fabreguette, and S. M. George, *Thin Solid Films*, **413**, 186 (2002).

17. J. N. Reimers and J. R. Dahn, *J. Electrochem. Soc*., **139**, 2091 (1992).

18. J. Sun, K. Tang, X. Yu, J. Hu, H. Li, and X. Huang, *Solid State Ionics*, **179**, 2390 (2008).

19. K. Mizushima, P. C. Jones, P. J. Wiseman, and J. B. Goodenough, *Mat. Res. Bull.*, **15**, 783 (1980)**.**

20. G. G. Amatucci, J. M. Tarascon, and L. C. Klein, *J. Electrochem. Soc*., **143**, 1114 (1996).

21. P.J. Bouwman, B.A. Boukamp, H. J. M. Bouwmeester, and P. H. L. Notten, *Solid State Ionics*, **152-153**, 181 (2002).

Chapter 6

High Energy Electrodes for Solid State Li-ion Batteries

Lithium ion batteries (LIBs) with superior properties (ex. high energy/power density, stable cycling, safety) are required to replace conventional energy storage systems. Solid state Li-ion batteries (SSLIBs) which use nonflammable inorganic solid state electrolyte (SSE) can address safety concern related with inflammability of organic liquid electrolyte used in conventional LIBs.[1] However, most of studies done for SSLIBs used insufficient amounts of active material and a large portion of SSE in their electrode, resulting in insufficient energy densities (< 100 Wh kg^{-1}) to meet the energy requirement of large scale applications (ex. electric vehicle).[2-15] Therefore, it is reasonable to advance our study to high energy electrode.

Using a larger portion of an active material in electrodes of SSLIBs compared to current laboratory scale testing cells is inevitable to realize commercialized SSLIBs with pratical applications. The transport of Li^+ ions will be the main limiting factor because of more limited numbers of Li^+ ion pathway because of decreased ratio of SSE to an active material in electrodes. Therefore, securing Li^+ ion transport paths in solid state electrodes will be the primary objective to achieve high energy/power density from SSLIBS.

6.1 Solid state Li batteries (SSLBs) with new materials

Among studies on transition metal oxides for electrode materials for Li-ion batteries (LIBs), layered $LiMO_2$ (M= 3d transition metal elements) with α-$NaFeO_2$ structure went through a vast investigation (refer to a review paper).[16] $LiCoO_2$ has been widely implemented as a cathode materieal for commercialized LIBs among those layered metal oxides because of facile synthesis and stable cyclability.[17] Nevertheless, the high cost and the limited attainable capacity of $LiCoO_2$ (~ 140 mAh g^{-1}) arouse the search for alternative cathode materials. $LiNiO_2$ is known to have higher capacity than $LiCoO_2$ (~ 200 mAh g^{-1}) and low cost.[18] Unfortunately, difficulty of synthesis and instability at high voltage make it hard to be used in actual LIBs. Other metal ions have been used to partially substitute Ni in $LiNiO_2$ to improve the electrochemical performance.[19-21] First, $LiNi_{1-x}Co_xO_2$ was proposed as an alternative cathode material to replace $LiNiO_2$ to combine the strong aspects of $LiNiO_2$ (capacity) and $LiCoO_2$ (stability).[22,23] In addition, partial replacement of Ni in lithium nickel cobalt oxide by Mn which is a lower cost material showed enhancement in the initial capacity and the cycle life.[24] Along with previous studies mentioned above, $LiNi_{1/3}Co_{1/3}Mn_{1/3}O_2$ (L333) was proposed to replace $LiCoO_2$ because of its higher capacity (160mAhg^{-1} in the voltage range 2.5 ~ 4.4V) and better thermal stability.[25-27] Furthermore, less content of cobalt helps L333 to be beneficial in the aspect of economy and environmental friendliness. To increase the energy density of our SSLIBs, we employed L333 as the cathode material in our solid state batteries in this chapter.

The role of SSE becomes more critical in electrodes in high energy SSLIBs. Typical electrodes in SSLIBs include passive components (SSE, a conductive additive) which do not participate in electrochemical reactions for battery operation. These passive components provide electronic and ionic pathways which are essential for the Li insertion and extraction with a

reduction and an oxidation (redox). It is important to decrease the portion of these passive compoents in solid state electrodes to increase the energy density of SSLIBs. Since the transport of Li^+ ions occurs through limited number of solid-solid contacts between an active material and SSE as mentioned in Section 5.2, the reduced portion of SSE in solid state elecctrodes will be a limiting factor for achieving a high energy density because of the reduced number of Li^+ ion pathways. Therefore, employment of SSE with high ionic conductivity is inevitable.

In Section 2.3.2, we introduced $Li_{10}SiP_2S_{12}$ SSE which is expected to have similar phase stability, electrochemical stability, and Li^+ ion conductivity as $Li_{10}GeP_2S_{12}$, a novel lithium superionc conductor with the highest ionic conductivity among SSEs. We decided to exploit $Li_{10}SiP_2S_{12}$ as our new SSE system to replace our previous $Li_{3.15}Ge_{0.15}P_{0.85}S_4$, $77.5Li_2S–22.5P_2S_5$ (mol %) SSE systems which were used in Chapter 4 and 5. Our group sucessfully synthesized a Si-based Li superionic conductor, $Li_{10}SiP_2S_{12}$, which exhibited ionic condutivity of 2.3×10^{-3} S cm^{-1}.[28] It showed superior stability versus lithium metal and compatibility with a high voltage cathode material (L333) in SSLBs compared to $Li_{10}GeP_2S_{12}$ under the same condition.

In this section, we present applications of L333 and $Li_{10}SiP_2S_{12}$ SSE to our SSLBs. Atomic layer deposition of Al_2O_3 was performed on L333 in the same way done in Chapter 4 and 5 to validate the benefits of Al_2O_3 ALD coating on L333. SSLBs with L333 powders coated with Al_2O_3 ALD which were under heat treatment (HT) in Ar environment after ALD process were constructed. Galvanostatic charge-discharge cycling displays that Ar HT Al_2O_3 ALD on L333 suppresses the degradation of SSLBs using $Li_{10}SiP_2S_{12}$ SSE during charge-discharge processes as Al_2O_3 ALD did in Chapter 4 and 5.

6.1.1 Experimental

As-ball-milled (ABM) $Li_{10}SiP_2S_{12}$ SSEs were synthesized by planetary ball milling (PBM) using precursors of Li_2S (Alfa Aesar, 99.9%), P_2S_5 (Sigma Aldrich, 99%), and SiS_2 (Alfa Aesar, 95%) in a 5:1:1 molar ratio in a stainless steel jar with stainless steel balls for grinding. PBM (SFM-1, MTI Corporation) proceeded at 500 rpm for 20 continuous hours to generate well mixed SSE powders. Recovered ABM SSE powders were then pressed in to pellets 2 mm thick at 5 metric tons. HT at 550℃ for 8 hours in vacuum borosilicate glass ampoules was performed for these pellets. The resultant pellets were ground using agate mortar and pestle to obtain fine SSE powders. All sample preparations and HTs were performed in a dry Ar environment or vacuum environment.

4 cycles of Al_2O_3 ALD layers were deposited directly on L333 powders (Johnson Controls) using a rotary reactor as described in our previous work.[29] L333 powders with Al_2O_3 ALD layers were put under a constant Ar gas flow using a sealed quartz tube in a furnace for HT (300℃, 12 hours). L333 (uncoated, 4 Al_2O_3 ALD coated), HT $Li_{10}SiP_2S_{12}$ SSE, and acetylene black (AB, Alfa-Aesar, 50% compressed) were mixed at a weight ratio of 70:30:2 using a mortar and a pestle to prepare working electrode composites for SSLBs. SSLBs using lithium foil as a counter electrode were constructed by sequential cold-pressing of powders. 200 mg of HT $Li_{10}SiP_2S_{12}$ SSE was cold-pressed at 1 metric ton. 10 mg of the composite cathode material was evenly spread on the top of $Li_{10}SiP_2S_{12}$ SSE layer and pelletized by cold-pressing at 5 metric tons. Lithium foil (Alfa-Aesar, 0.75 mm thick) was then attached to the $Li_{10}SiP_2S_{12}$ SSE side at 2 metric tons. All pressing and experimental operations were done in a polyaryletheretherketone (PEEK) mold (φ = 1.3 cm) with Ti metal cylinders as current collectors for both working and

counter electrodes. Figure 6.1 shows the schematic of our L333/$Li_{10}SiP_2S_{12}$ SSE/Li battery. Galvanostatic charge-discharge cycling was carried out between 2.5 ~ 4.3 V (vs. Li/Li^+) at a current of 83 μA cm^{-2} at 30℃ and 60℃ using an Arbin BT2000. Charge process and discharge process correspond to the delithiation and the lithiation of L333. SSLBs were charged to 4.3 V (vs. Li/Li^+) and held at the voltage for 1 hour before discharge processes. All battery fabrication processes and charge-discharge cycling were conducted in a dry Ar filled glove box. In addition, morphology of L333 particles and $Li_{10}SiP_2S_{12}$ SSE was observed by using a field emission scanning electron microscope (FE-SEM, JEOL JSM-7401F).

6.1.2 Results and discussion

FE-SEM observation was performed for our L333 and HT $Li_{10}SiP_2S_{12}$ SSE. The FE-SEM images of uncoated L333 powders with different scales are shown in Figure 6.2. The primary particles which are about 0.5 ~ 2 μm in diameter aggregates to constitute secondary particles about 5 ~ 10 μm in diameter. Also, FE-SEM image of HT $Li_{10}SiP_2S_{12}$ SSE are shown in Figure 6.3. SSE particles have irregular shape and 5 ~ 20 μm size. Residual particles about 0.5 ~ 2 μm

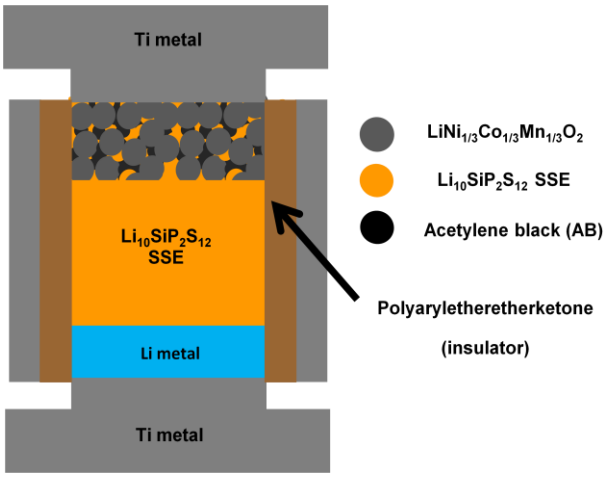

Figure 6.1: The schematic depiction of our SSLB using L333 and $Li_{10}SiP_2S_{12}$.

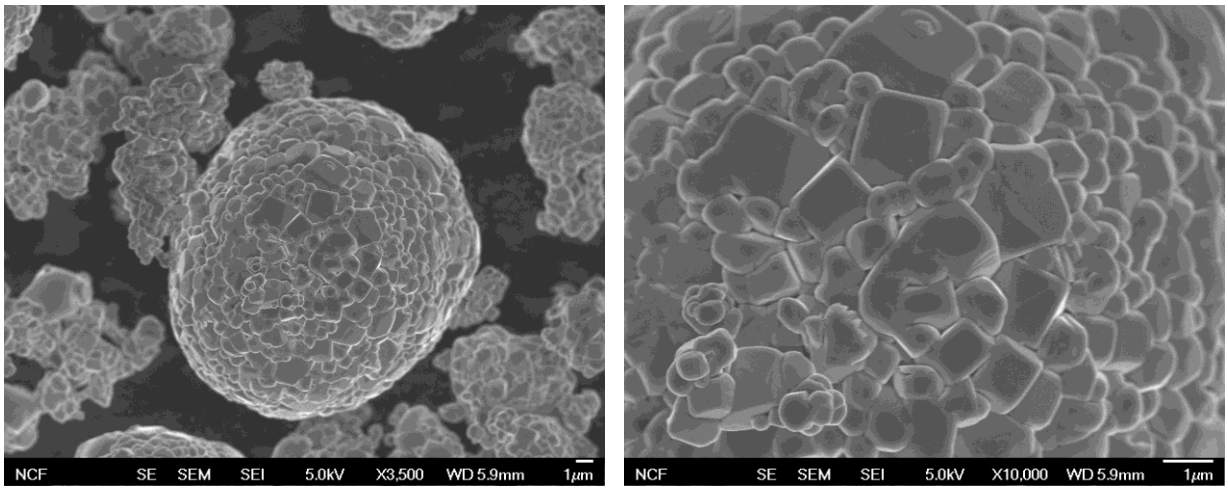

Figure 6.2: FE-SEM images of uncoated L333 with different scales.

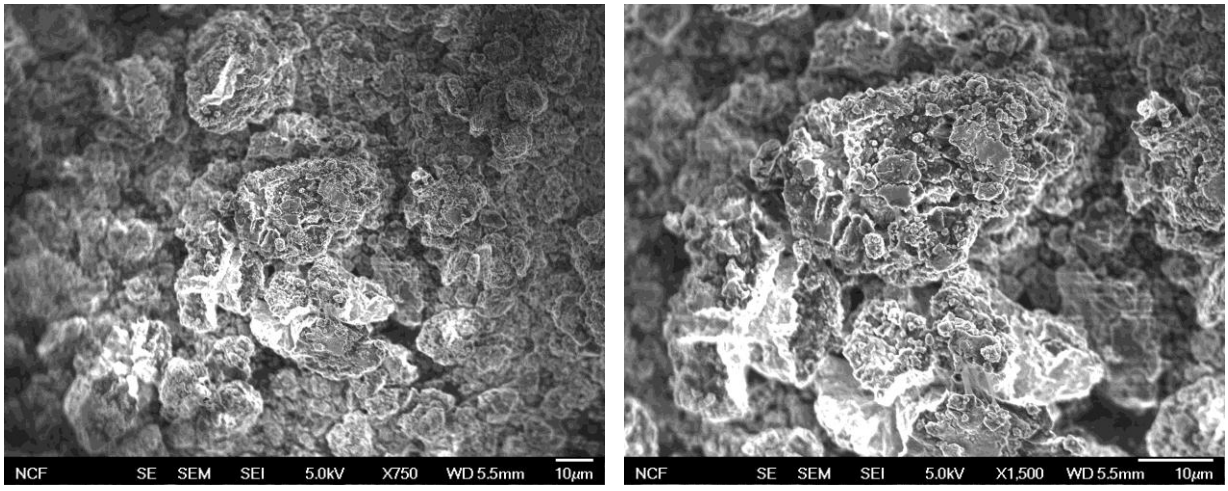

Figure 6.3: FE-SEM images of HT $Li_{10}SiP_2S_{12}$ SSE with different scales.

size exist on the surface of SSE particles.

Galvanostatic charge-discharge cycles were performed between 2.5 ~ 4.3 V (vs. Li/Li^+) with SSLBs using uncoated L333 particles and L333 particles coated with 4 Al_2O_3 ALD cycles with Ar HT. All of SSLBs were cycled at either at 30℃ or at 60℃. Figure 6.4 compares voltage profiles of SSLBs at 30℃ using uncoated/4 Al_2O_3 ALD-coated L333 particles. SSLB at 30℃ with uncoated L333 reveals an polarization and a decrease in the specific capacity as cycle number increases (Figure 6.4a). SSLB at 30℃ using L333 particles with 4 Al_2O_3 ALD layers (Figure 6.4b) shows smaller polarization and less decrease in the specific capacity than those of SSLB with uncoated L333. In addition, voltage profiles of SSLBs at 60℃ with uncoated/4 Al_2O_3 ALD-coated L333 particles are shown (Figure 6.5). Also, smaller polarization and less decrease in specific capacity are observed from SSLB at 60℃ with 4 Al_2O_3 ALD-coated L333 particles than that from SSLB using uncoated L333. We attribute this to the suppression of the degradation at L333/SSE interface during battery cycling. As a result, more stable cycling performances are achieved from SSLBs at 30℃ and 60℃ using 4 Al_2O_3 ALD-coated L333 particles than SSLBs using uncoated L333 particle (Figure 6.6).

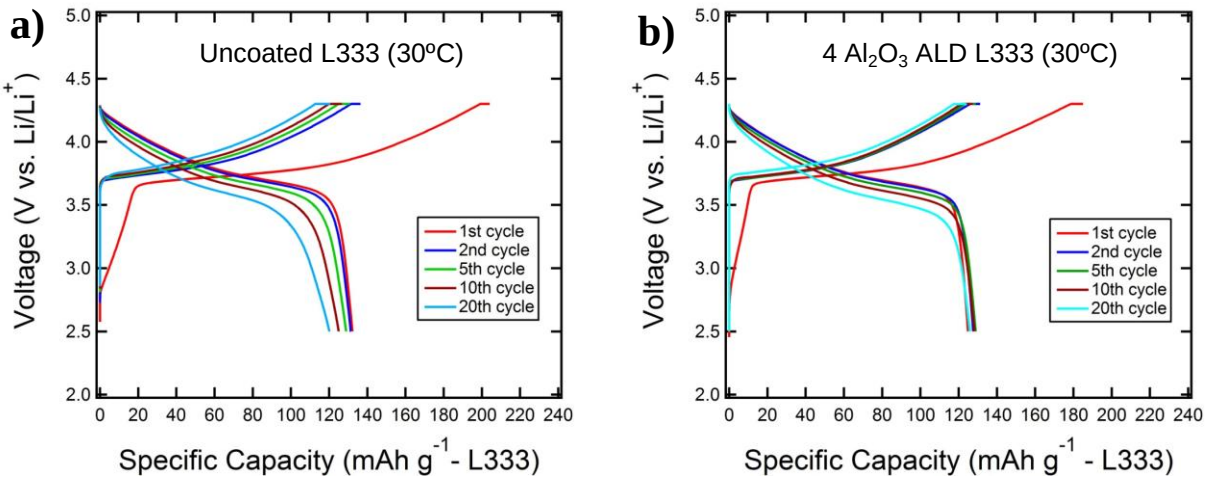

Figure 6.4: Voltage profiles of SSLBs at 30℃ using different L333 particles.

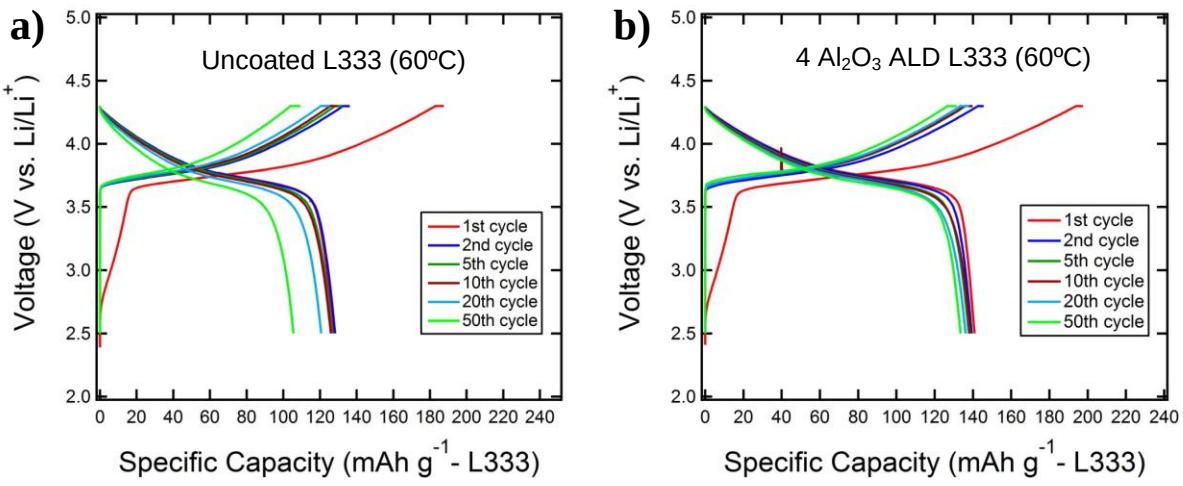

Figure 6.5: Voltage profiles of SSLBs at 60℃ using different L333 particles.

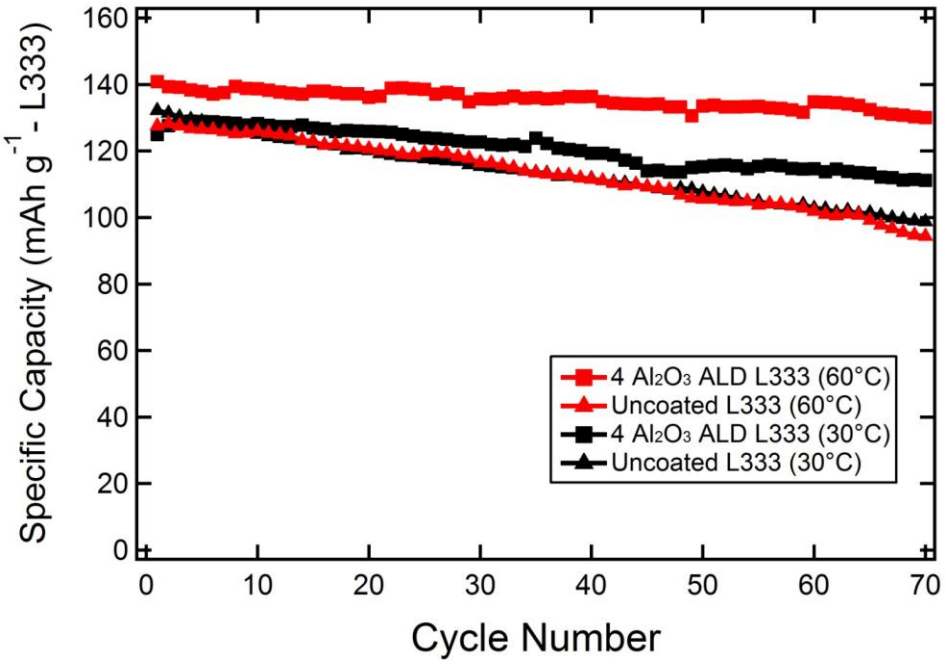

Figure 6.6: Cycling performances of SSLBs at different temperatures using different L333 particles.

A new cathode material (L333) and SSE system ($Li_{10}SiP_2S_{12}$) are employed for our SSLB in this section. Although specific capacities based on the active material (L333 in this case) look similar to that from $LiCoO_2$ SSLBs in previous chapter, total capacity from a working electrode with the same mass increased noticebly. The weight ratio (active material:SSE:conductive additive) of a working electrode composite changed from 20:30:3 to 70:30:2. Therefore, working electrodes used in this section have much larger portion of an active material than Chapter 4 and 5. Total capacity from 10 mg electrode in SSLB increased from ~ 0.5 mAh to ~ 0.85 mAh at 30℃. We were able to obtain higher capacity from SSLB with the same weight compared to SSLBs mentioned in Chapter 4 and 5 by adopting a new electrode material and a new SSE. In other word, higher gravimetric energy density is achieved from our new SSLB configuration.

6.2 Gradients of SSE portion in high energy electrodes

Many efforts were done to enhance Li^+ ion transport in solid state batteries until the previous section, addressing active material/SSE interface issues and battery materials. As mentioned in the early part of Section 6.1, it is beneficial to reduce passive components (SSE, conductive additive) in electrodes of SSLIBs to achieve higher energy density. However, there is a trade-off between the benefits of this strategy and the side effect of it. As portions of SSE and a conductive additive are reduced in electrodes, securing electronic/ionic pathways can be jeopardized. Underutilization of active materials in electrodes can occur to obtain lower energy density than expected value because of limitation on Li^+ ion transport. Therefore, balancing the amount of an active material and that of passive components in electrode is essential for designing high energy electrodes. Investigation into the configuration of components in electrodes was sought. Golmon et al. proposed the optimization of the layout for active material

portion and electrolyte portion in an electrode of a lithium battery to enhance capacity of a battery, using computational multi-scale modeling.[30] Along with this concept, we performed a study for the effect of optimized active material/SSE layout in solid electrodes for our solid state batteries.

6.2.1 Experimental

Planetary ball milling (PBM) was performed to produce as-ball-milled (ABM) $Li_{10}SiP_2S_{12}$ SSEs, using precursors of Li_2S (Alfa Aesar, 99.9%), P_2S_5 (Sigma Aldrich, 99%), and SiS_2 (Alfa Aesar, 95%) in a 5:1:1 molar ratio. The mixture of precursors was ball-milled at 500 rpm for 20 continuous hours in a stainless steel jar with stainless steel balls for grinding. ABM SSE powders were recovered and then pressed in to pellets 2 mm thick at 5 metric tons. ABM SSE pellets were under HT at 550℃ for 8 hours in vacuum borosilicate glass ampoules. The resultant pellets were ground using agate mortar and pestle to obtain fine SSE powders. All sample preparations and HTs were performed in a dry Ar environment or vacuum environment.

4 cycles of Al_2O_3 ALD layers were deposited directly on L333 powders (Johnson Controls) using a rotary reactor as described in our previous work.[29] L333 powders with Al_2O_3 ALD layers were put under a constant Ar gas flow using a sealed quartz tube in a furnace for HT (300℃, 12 hours). 4 Al_2O_3 ALD coated L333, HT $Li_{10}SiP_2S_{12}$ SSE, and acetylene black (AB, Alfa-Aesar, 50% compressed) were mixed at certain weight ratios using a mortar and a pestle to prepare working electrode composites for solid state batteries. Solid state batteries using an LiIn alloy as a counter electrode were constructed by sequential cold-pressing of powders. Since LiIn alloy has a potential of 0.62 V vs. Li/Li^+ within a certain range of composition[31], voltages in figures of this section were converted with repect to Li metal. 200 mg of HT $Li_{10}SiP_2S_{12}$ SSE

was cold-pressed at 1 metric ton. Either three layers of 10 mg electrode composites with certain compositions or a single layer of 30 mg composites with a certain composition were pressed on the top of 200 mg SSE layer. To construct three layers of 10 mg composite, two layers of 10 mg composites were sequentially cold-pressed with 1 metric ton. The third layer of a 10 mg composite was evenly spread on the top of them and cold-pressed with 5 metric tons. To construct a single layers of 30 mg composite electrode, 30 mg of composite material with a certain composition was evenly spread on the top of 200 mg SSE layer and cold-pressed with 5 metric tons. LiIn alloy (FMC Lithium Corp., Lectro Max Powder 100 and Indium powder, Alfa Aesar, Puratronic 99.999%) was then attached to the $Li_{10}SiP_2S_{12}$ SSE side at 2 metric tons. All pressing and experimental operations were done in a polyaryletheretherketone (PEEK) mold (φ = 1.3 cm) with Ti metal cylinders as current collectors for both working and counter electrodes.

Galvanostatic charge-discharge cycling was carried out between 2.5 ~ 4.3 V (vs. Li/Li^+) at various current rates at 30℃ using an Arbin BT2000. Charge process and discharge process correspond to the delithiation and the lithiation of L333. First, solid state batteries were charged to 4.3 V (vs. Li/Li^+) at a current of 172 μA cm^{-1} (C/10 rate) and held at the voltage for 1 hour before the 1st discharge process. Solid state batteries were then discharged at a current of 344 μA cm^{-1} (C/5 rate). At the 2nd charge process, batteries were charged to 4.3 V (vs. Li/Li^+) at the current of 344 μA cm^{-1} (C/5 rate) and held at the voltage for 2 hours. And then a current of 861 μA cm^{-1} (C/2 rate) is applied to solid batteries at the 2nd discharge process. For the 3rd cycle, the current of 861 μA cm^{-1} (C/2 rate) was applied for the charge process and discharged at a current of 1722 μA cm^{-1} (1C rate) after 2 hours of the voltage hold at 4.3 V (vs. Li/Li^+). Finally, the current of 1722 μA cm^{-1} (1C rate) was applied for the 4th charge process. All battery fabrication processes and charge-discharge cycling were conducted in a dry Ar filled glove box.

A 2032-type coin cell was made for galvanostatic intermittent titration technique (GITT) measurement. A working electrode composite was prepared by spreading a slurry of L333 powders (Johnson Controls), acetylene black (AB, Alfa-Aesar, 50% compressed), and polyvinylidene fluoride (PVDF) (90:5:5 weight ratio) onto a high grade Al foil and roll-pressed after drying in air at 80^{o}C for 1 hour. The electrodes were dried in a vacuum oven at 120^{o}C for 12 hours before battery fabrication. The separator was a glass micro-fiber disk (Whatman GF/F) and the electrolyte was 1 M $LiPF_6$ in ethylene carbonate (EC): diethylene carbonate (DEC) (1:1 volume ratio). The cell fabrication was done in a dry Ar gas environment using Li metal as a counter electrode. The cell was charged and discharged between 3.0 ~ 4.5 V (vs. Li/Li^+) by applying a constant C/10 rate current and 1 hr voltage hold at 4.5 V (vs. Li/Li^+) for the 1st cycle. For the 2nd cycle, a constant current flux was supplied for 2250 sec (with the current same as C/10 rate) followed by an open circuit stand of the cell for 3600 sec. This GITT procedure was performed at the 2nd charge-discharge process between 3.0 ~ 4.5 V (vs. Li/Li^+).

6.2.2 Results and discussion

Figure 6.7 depicts configurations of our solid batteries with 30 mg solid-state electrodes. Left two show 3 layers electrodes to exhibit SSE gradients in working electrodes as trials of optimized active material/SSE lay out. SSE gradients are controlled by the weight ratio of L333 and $Li_{10}SiP_2S_{12}$ SSE. Triple electrode is the configuration which has the gradient of decreasing SSE portion at closer sites from a $Li_{10}SiP_2S_{12}$ SSE separator. On the other hand, reverse triple (rev-triple) electrode is the configuration which has the gradient of increasing SSE portion at closer sites from a $Li_{10}SiP_2S_{12}$ SSE separator. Lastly, 50:50:5 electrode is a single layer electrode which has the same amount of L333, $Li_{10}SiP_2S_{12}$ SSE, and AB as aforementioned electrodes.

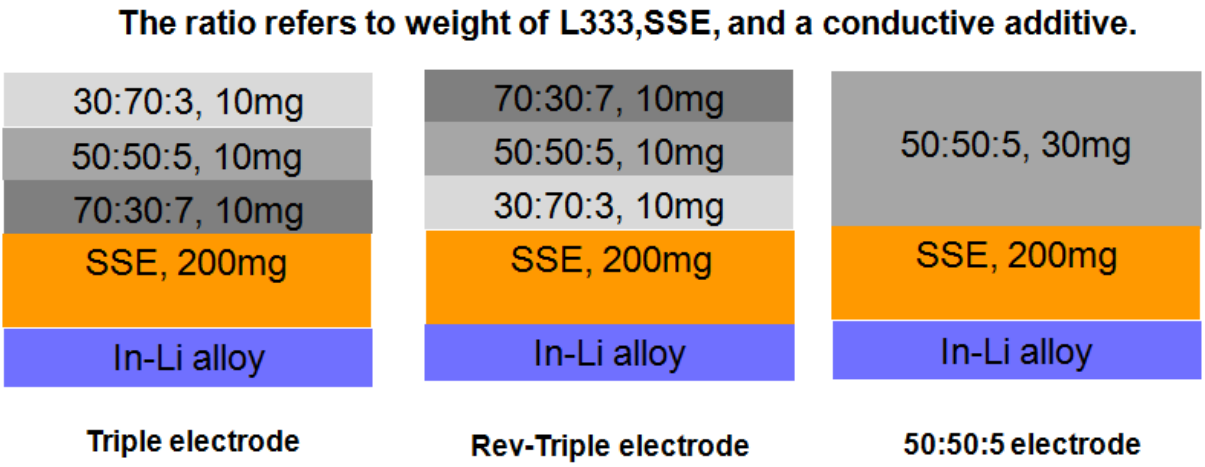

Figure 6.7: Configurations of solid state batteries with 30 mg electrodes with SSE gradients.

Preliminary experimental results regarding electrodes with SSE gradients are shown in this section. Figure 6.8 depicts voltage profiles of solid state batteries using 3 types of 30 mg L333 electrode with different SSE gradients. Voltage profiles of each cell are compared with thermodynamic equilibrium points (red dots). Equilibrium points were obtained by applying galvanostatic intermittent titration technique (GITT) to L333/Li 2032-type coin cell using a liquid electrolyte. Average values between voltage points of the coin cell after each open circuit stand during the 2nd charge process and those during the 2nd discharge process are selected as equilibrium points. The overpotential of an electrochemical cell can be a way of investigating the transport properties in a cell.[32] Largest overpotentials appear for the solid battery using 30 mg triple electrode and the battery was even unable to cycle at 1C rate. Compared to that, the battery with 30 mg rev-triple electrode shows smaller overpotentials than other batteries. Therefore, it seems that SSE gradients in working electrode affect overpotentials at high current rates. In other words, layout of component materials in electrodes affects Li^+ ion transport. Further study will be done in our future work to optimize the layout of component materials in electrodes for high energy SSLIBs.

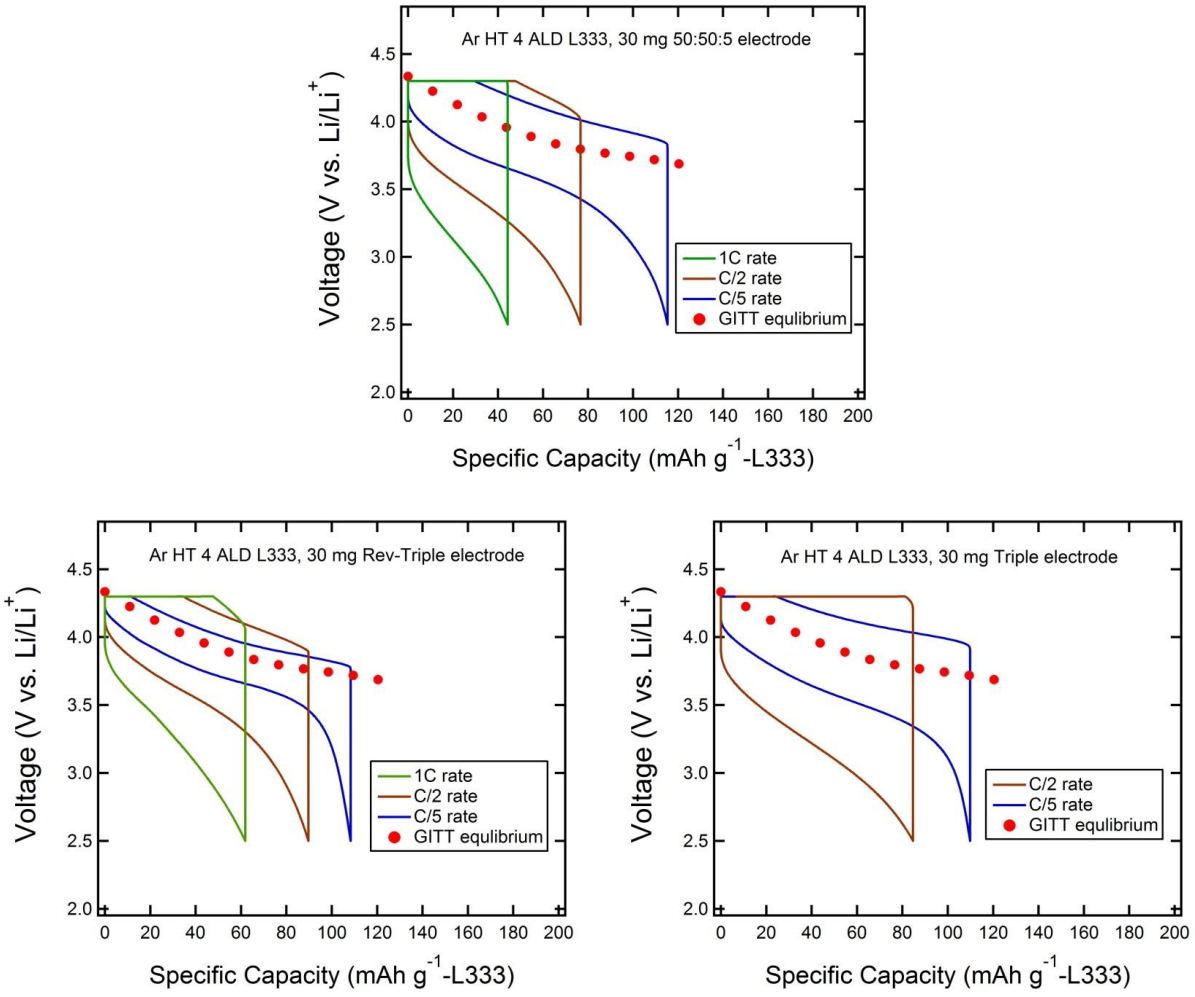

Figure 6.8: Voltage profiles of solid state batteries with different 30mg L333 electrodes.

6.3 Solid state Li-ion batteries with high energy electrodes

The traditional cathode material used for LIBs is $LiCoO_2$ because of its easy production and good cycling performance.[17] However, alternative materials for the cathode of LIB are needed because of high cost and limited capacity (140 mAh g^{-1}) of $LiCoO_2$. These shortcomings make $LiCoO_2$ difficult to be used in large scale batteries. As a result, $LiNi_{1/3}Co_{1/3}Mn_{1/3}O_2$ (L333) was employed to replace $LiCoO_2$ in this chapter because of its higher capacity (160 mAh g^{-1} in the voltage range 2.5~4.4V) and enviromental friendliness.

Recently, our group focused on Sn as an anode material in SSLB because of its high capacity (992 mAh g^{-1}) as mentioned in Section 2.2.2. Using only SSE (30 wt. % of the total composite) as only passive component in a working electrode, we came up with the intergration of Si and Sn which will generate a synergic effect on solid state Li-ion battery (SSLIB) technology. Si-Sn hybrid anode has been fabricated in our group, showing practical capacity (~ 700 mAh g^{-1} (based on the mass of the working electrode) in the case of 70:30 composition (Si-Sn:SSE). It seems like that Sn acts as both electrochemical active material and conductive additive in this Si-Sn anode configuration.

To see our capability of making SSLIBs which use aformentioned electrodes, we constructed SSLIBs using Al_2O_3 atomic layer deposition (ALD) coated L333 cathode, HT $Li_{10}SiP_2S_{12}$ SSE, and hybrid Si-Sn anode (Figure 6.9). SSLIBs went through galvanostatic charge-discharge cycling processes at 60℃. Gravimetric energy densities based on the total mass of eletrodes and SSE separator were calculated with SSLIBs with different amount of battery materials.

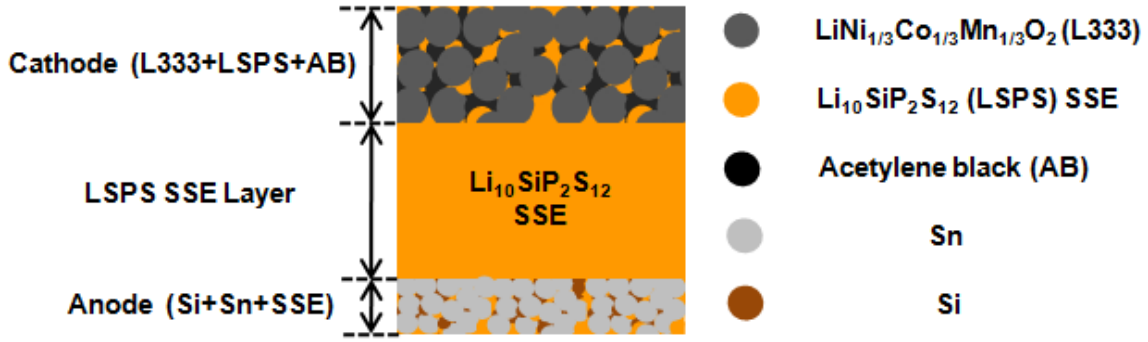

Figure 6.9: Schematic representation of our SSLIB employing $LiNi_{1/3}Co_{1/3}Mn_{1/3}O_2$ cathode and Si-Sn anode.

6.3.1 Experimental

As-ball-milled (ABM) $Li_{10}SiP_2S_{12}$ SSEs were synthesized by planetary ball milling (PBM) using precursors of Li_2S (Alfa Aesar, 99.9%), P_2S_5 (Sigma Aldrich, 99%), and SiS_2 (Alfa Aesar, 95%) in a 5:1:1 molar ratio in a stainless steel jar with stainless steel balls for grinding. PBM (SFM-1, MTI Corporation) proceeded at 500 rpm for 20 continuous hours to generate well mixed SSE powders. Recovered ABM SSE powders were then pressed in to pellets 2 mm thick at 5 metric tons. HT at 550℃ for 8 hours in vacuum borosilicate glass ampoules was performed for these pellets. The resultant pellets were ground using agate mortar and pestle to obtain fine SSE powders. All sample preparations and HTs were performed in a dry Ar environment or vacuum environment.

4 cycles of Al_2O_3 ALD layers were deposited directly on L333 powders (Johnson Controls) using a rotary reactor as described in our previous work.[29] L333 powders with Al_2O_3 ALD layers were put under a constant Ar gas flow using a sealed quartz tube in a furnace for HT (300℃, 12 hours). 4 Al_2O_3 ALD coated L333, HT $Li_{10}SiP_2S_{12}$ SSE, and acetylene black (AB, Alfa-Aesar, 50% compressed) were mixed at a weight ratio of 50:50:5 using a mortar and a pestle to prepare cathode composites for SSLIBs. Si particles (Alfa Aesar, 50 nm), Sn particles

(Sigma Aldrich, 150 nm), and HT $Li_{10}SiP_2S_{12}$ SSE were mixed at a weight ratio of 17.5:52.5:30 by hand-mixing used for cathode composites to prepare anode composites. SSLIBs were constructed by sequential cold-pressing of powders. 200 mg of HT $Li_{10}SiP_2S_{12}$ SSE was cold-pressed at 1 metric ton. The cathode material and the anode material were evenly spread on both sides of $Li_{10}SiP_2S_{12}$ SSE layer and pelletized by cold-pressing at 5 metric tons. The amount of anode material was calculated to match at least 120% capacity of the cathode material. All pressing and experimental operations were done in a polyaryletheretherketone (PEEK) mold (φ = 1.3 cm) with Ti metal cylinders as current collectors for both electrodes. Galvanostatic charge-discharge cyclings were carried out at C/10 current rate based on the amount of L333 in cathodes at 60℃ using an Arbin BT2000. Charge process and discharge process correspond to the delithiation and the lithiation of L333. SSLIBs were charged to 4.295 V and held at the voltage for 1 hour before discharge processes. All battery fabrication processes and charge-discharge cycling were conducted in a dry Ar filled glove box.

6.3.2 Results and discussion

Voltage profiles and cycling performance of a SSLIB at 60℃ using 15 mg of L333 cathode and 2.5 mg of Si-Sn anode are depicted in Figure 6.10. Specific capacities are calculated based on the amount of L333 in the cathode. Plateaus appear in charge and discharge voltage profiles from the contribution of three electrode materials (L333, Si, and Sn). Its cycling performance is not as good as SSLB with 4 Al_2O_3 ALD-coated L333 at 60℃ shown in Section 6.1. We attribute this to the degradation and a low coulombic efficiency from each electrode. However, we were able to cycle the battery until the 150th cycle, preserving more than 50% of its initial capacity.

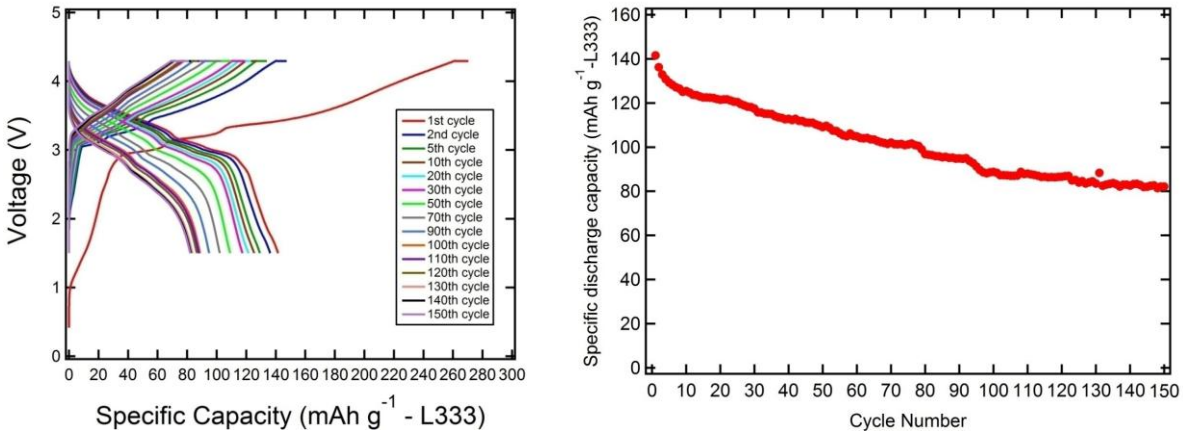

Figure 6.10: Cycling performance of a SSLIB at 60℃ (15 mg L333 cathode, 2.5 mg Si-Sn anode).

A SSLIB using 90 mg of L333 cathode and 10.3 mg of Si-Sn anode was also fabricated to see the scale-up effect. Voltage profiles and cycling performance of the SSLIB at 60℃ until the 15th cycle are described in Figure 6.11. Similar plateaus like Figure 6.10 appear in charge and discharge voltage profiles. Even though the amount of both electrode materials are increased more than 4 times, similar specific capacities based on the amount of L333 are obtained until the 15th cycle.

However, gravimetric energy densities (based on the total mass of electrodes and SSE separator layer) from these SSLIBs which are shown in Table 6.1 are quite different. Calculating from the 1st discharge capacity, the energy density increased from 16.3 mWh g^{-1} to 70.9 mWh g^{-1} by increasing the amount of electrode materials. Table 6.1 also shows energy densities calculated from a different electrode composition and various amounts of battery materials. It clearly shows that the energy density of SSLIB can be greatly increased by reducing the portion of SSE. Gravimetric energy density over 200 mWh g^{-1} can be achieved by increasing the amount of cathode material over 100 mg and decreasing the amount of SSE for a separator to 50 mg with the current SSLIB configuration used in this section.

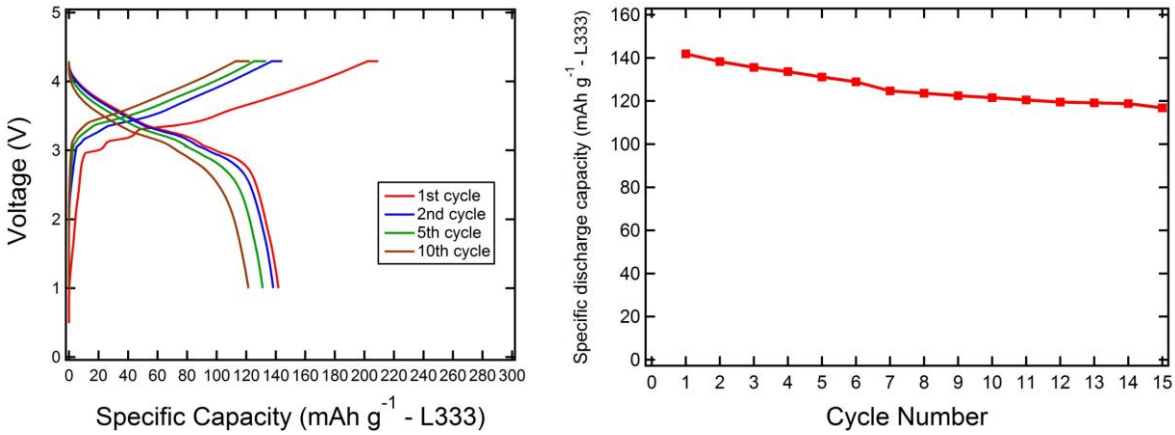

Figure 6.11: Cycling performance of a SSLIB at 60℃ (90 mg L333 cathode, 10.3 mg Si-Sn anode).

Table 6.1: Gravimetric energy densities of our SSLIBs at 60℃ (based on electrodes and SSE layer). The calculations assume a L333 based cathode specific capacity of 140 mAh g^{-1}, a Si-Sn anode specific capacity of 700 mAh g^{-1}, an average cell potential of (3.5V), an anode with a capacity that is 120% that of the cathode, and a variety of SSE layer thicknesses (200, 100, and 50 mg).

L333 loading (wt %)	Si-Sn loading (wt %)	Anode mass (g)	Cathode mass (g)	energy density 200mg SSE (mWh g^{-1})	energy density 100mg SSE (mWh g^{-1})	energy density 50mg SSE (mWh g^{-1})
47.6	70	0.0025	0.015	16.3	<- - - - - Current experimental results	
47.6	70	0.0103	0.09	70.9		
68.6	70	0.00164	0.01	15.9	30.1	54.5
68.6	70	0.0164	0.1	106.2	155.3	201.2
68.6	70	0.0247	0.15	134.6	183.5	224.3

6.4 Summary

This chapter shows our efforts to construct SSLIBs with high energy densities. A new cathode material $LiNi_{1/3}Co_{1/3}Mn_{1/3}O_2$ (L333), and a novel $Li_{10}SiP_2S_{12}$ solid state electrolyte (SSE) were employed in solid state Li batteries (SSLBs) to see the feasibility to increase the energy density. Using Al_2O_3 atomic layer depostion (ALD) on L333, these new battery materials successfully improved the total capacity of 10 mg electrode from ~ 0.5 mAh to ~ 0.85 mAh.

Along with the material study, effective layout of components in solid state electrode was investigated. Gradients of SSE portion in thick electrodes using 30 mg of L333 composites were realized by changing weight ratios between L333, SSE, and a conductive additive. Different overpotentials are observed according to gradients of SSE portion in electrodes. Therefore, it would be meaningful to optimize the layout of components in high energy electrodes in future work.

Finally, actual solid state Li-ion batteries (SSLIBs) were constructed using L333 cathode and Si-Sn anode. SSLIB using 15 mg of L333 cathode and 2.5 mg of Si-Sn anode was cycled up to the 150th cycle at 60℃. It didn't show cycling performance which is as good as SSLB because of degradation and low coulombic efficiency from both electrodes. Along with the scale-up study, it is confirmed that reducing the portion of SSE in SSLIBs greatly increases the gravimetric energy density.

References

1. J. W. Fergus, *J. Power Sources*,**195,** 4554 (2010).

2. N. Ohta,K. Takada, L. Zhang,R.Ma, M. Osada, and T. Sasaki, *Adv. Mater*., **18**, 2226 (2006).

3. A. Sakuda, A. Hayashi, and M. Tatsumisago, *Chem. Mater.*, **22**, 949 (2010).

4. A. Sakuda, H. Kitaura, A. Hayashi, K. Tadanaga, and M. Tatsumisago, *J. Electrochem. Soc*., **156**, A27 (2009).

5. A. Sakuda, H. Kitaura, A. Hayashi, K. Tadanaga, and M. Tatsumisago, *J. Power Sources*, **189,** 527 (2009).

6. A. Sakuda, A. Hayashi, and M. Tatsumisago, *J. Power Sources*, **195**, 599 (2010).

7. H. Kitaura, A. Hayashi, K. Tadanaga, and M. Tatsumisago, *Solid State Ionics*, **192**, 304 (2011).

8. H. Kitaura, A. Hayashi, K. Tadanaga, and M. Tatsumisago, *Electrochimica Acta*, **55**, 8821 (2010).

9. N. Machida, J. Kashiwagi, M. Naito, and T. Shigematsu, *Solid State Ionics*, **225**, 354 (2012).

10. T. Takeuchi, H. Kageyama, K. Nakanishi, M. Tabuchi, H. Sakaebe, T. Ohta, H. Senoh, T. Sakai, and K. Tatsumi, *J. Electrochem. Soc*., **157**, A1196 (2010).

11. M. Nagao, Y. Imade, H. Narisawa, T. Kobayashi, R. Watanabe, T. Yokoi, T. Tatsumi, and R. Kanno, *J. Power Sources*, **222**, 237 (2013).

12. S. Noh, J. Kim, M. Eom, and D. Shin, *Ceramics International*, **39**, 8453 (2013).

13. S. Boulineau, J.-M. Tarascon, J.-B. Leriche, and V. Viallet, *Solid State Ionics*, **242**, 45 (2013).

14. T. Ohtomo, A. Hayashi, M. Tatsumisago, and K. Kawamoto, *J. Solid State Electrochem*, **17**, 2551 (2013).

15. T. Matsuyama, A. Sakuda, A. Hayashi, Y. Togawa, S. Mori, and M. Tatsumisago, *J. Solid State Electrochem.*, **17**, 2697 (2013).

16. R. Koksbang, J. Barker, H. Shi, and M.Y. Saıdi, *Solid State Ionics*, **84**, 1(1996).

17. T. Nagaura and K. Tozawa, *Prog. Batteries Sol. Cells*, **9**, 20 (1990).

18. T. Ohzuku, A. Ueda, and M. Nagayama, *J. Electrochem. Soc*., **140**, 1862 (1993).

19. C. Delmas, I. Saadoune, and A. Rougier, *J. Power Sources*, **43/44**, 595 (1993).

20. D. Caurant, N. Baffier, V. Bianchi,G. Gregoire, and S. Bach, *J.Mater. Chem.* **6**, 1149 (1996).

21. T. Ohzuku, A. Ueda, and M. Kouguchi, *J. Electrochem. Soc*., **142**, 4033 (1995).

22. T. Ohzuku,A. Ueda, M. Nagayama, Y. Iwakoshi, and H. Komori, *Electrochim. Acta*, **38**, 1159 (1993).

23. B. J. Hwang, R. Santhanam, and C. H. Chen, *J. Power Sources*, **114**, 244 (2003).

24. Z. Liu, A. Yu, and J. Y. Lee, *J. Power Sources*, **81-82**, 416 (1999).

25. T. Ohzuku, Y. Makimura, *Chem. Lett*., **1**, 642 (2001).

26. K.M. Shaju, G.V. Subba Rao, and B.V.R. Chowdari, *Electrochim. Acta*, **48**, 145 (2002)

27. I. Belharouak, Y.K. Sun, J. Liu, and K. Amine, *J. Power Sources*,**123**, 247 (2003).

28. J. M. Whiteley, J. H. Woo, E. Hu, K.-W. Nam, and S.-H. Lee, *J. Electrochem. Soc*., **161**, A1812 (2014).

29. Y. S. Jung, A. S. Cavanagh, A. C. Dillon, M. D. Groner, S. M. George, and S.-H. Lee, *J. Electrochem. Soc*., **157**, A75 (2010).

30. S. Golmon, K. Maute, and M. L. Dunn, *Int.J. Numer.Meth. Engng*, **92**, 475 (2012).

31. K. Takada, N. Aotani, K. Iwamoto, and S. Kondo, *Solid State Ionics*, **86-88**(Part 2), 877 (1996).

32. J. Sun, K. Tang, X. Yu, J. Hu, H. Li, and X. Huang, *Solid State Ionics*, **179**, 2390 (2008).

Chapter 7

Hierarchical Framework of Si-Based Electrodes for Minimal Volumetric Expansion

There were many efforts to develop novel electrode materials with high capacity and durable lifetime to meet the high energy needs for the successful application of Li-ion batteries (LIBs) as energy storage systems.[1] Although graphite anode is commercialized for current LIBs, its limited capacity of 372 mAh g^{-1} is not sufficient to be used in future generation LIBs for electric vehicles as mentioned in Section 2.2.2. Silicon (Si) has been drawing attention as an attractive anode material because of its natural abundance and the capability to accommodate a large number of Li atoms providing much more capacity than graphite.[2] However, Si goes through a large volume expansion when it is fully lithiated[3] which induces pulverization inducing a drastic capacity loss.[4]

Various efforts were made to address the capacity fade of Si anode which is from the mechanical failure with Li lithiation. Si nanowire, Si-C nanocomposites, and 3 dimensional (3D) porous Si particles were constructed to resolve the degradation related with the volume expansion during lithiation/delithiation process.[5-7] These approaches were related to construction of Si electrode's nanostructure. However, it was not successful until now to reduce the volume expansion of a Si-based electrode to an acceptable degree which is similar to the volume

expansion of conventional graphite anodes (10 ~ 13%).[8] The smallest electrode expansion of Si anode after full lithiation reported to date was demonstrated by Park et al., showing 18% change of the electrode thickness.[9] Nevertheless, processes to construct such electrodes are complex and expensive, contributing to the difficulty of mass production.

In this chapter, we demonstrate production of a scalable and low price material that goes through even smaller electrode deformation than Park et al.'s study. Si nanoparticles (nSi) embedded in a tunable cyclized-polyacrylonitrile (cPAN) fiber framework bound together by cPAN coating were constructed to realize a scalable, low cost, and highly reversible Si-based electrode. Nano-Si hierarchical framework electrodes which are referred to as nSi@cPAN/cPAN are enabled.

7.1 Experimental

Material Preparation: We used electrospinning for the production of PAN-based fibers with embedded nano-Si particles. Polyacrylonitrile (PAN, Mw=150,000 g mol^{-1}, Sigma Aldrich) and nano-Si particles (Alfa Aesar, 50 nm) were hand mixed using a mortar and pestle with certain weight ratios and then dissolved in N,N-dimethylformamide (DMF, 99%, Alfa Aesar). The solution was mixed via magnetic stirring for 15 hours and then injected into a 10 ml syringe for the electrospinning process. The gauge number of the needle for the electrospinning was 18 and the flows of the solution were injected with several feed rates using a syringe pump. The applied voltage was 27 kV and the needle-to-collector distance was 20 cm. After the solution was electrospun, the nano-Si/PAN fibers were collected and dried at 60˚C for 1hr. The fibers were then heat treated in air at 220˚C to achieve the cyclization of PAN. The nano-Si/cyclized-PAN fibers were mixed with PAN powder at 9:1 weight ratio (fiber:PAN) in DMF via magnetic

stirring for 15 hours to produce a viscous slurry. The slurry was directly bladed onto a copper foil and dried at 60˚C for 2 hours to form an electrode film. The dried electrode was calendared and cut with a 0.5'' diameter punch. Each punch went through a heat treatment under argon in a tube furnace at 300˚C for 12 hours to cyclize the added PAN coating, thus stabilizing the electrodes as a whole. Cells were assembled in an Ar-dry box and tested at room temperature. Electrochemical measurements were all normalized based on the mass of each 0.5" electrode film (typically 1.5-2.0 mg). The morphology of our materials was observed by using a field emission scanning electron microscope (FE-SEM, JEOL JSM-7401F).

Electrochemical Measurement : Electrochemical measurements were carried out using an Arbin BT2000. All cells were assembled using the prepared nSi@cPAN/cPAN coating electrodes as the working electrodes and lithium metal foil as the counter electrode. The electrolyte was 1M $LiPF_6$ dissolved in a 1:1 (volume ratio) mixture of ethylene carbonate (EC) and diethyl carbonate (DEC), the separator was a glass micro-fi ber disk (Whatman GF/F) and the shell was a stainless steel CR2032 coin cell (Pred Materials). We used a constant current constant voltage (CCCV) testing scheme to cycle the cells. The cells were discharged (lithiated) and charged (delithiated) with various cycling currents between 0.05 and 1 V (vs. Li/Li^+). The conducted rate study was carried out with charging rates ranging from C/20 ~ 5C. The discharge rates were started at C/20, increased to C/10 and maintained at this rate for subsequent cycling. Charging and discharging were conducted with constant current (CC) cycling parameters.

7.2 Results and discussion

This study was done by the equal contribution with the author and Daniela Molina Piper.[10] Readers can refer to the reference for more in depth understanding of material characterization. Figure 7.1 describes the detailed process of manufacturing nSi@cPAN/cPAN electrodes.[10] First, PAN powders and nSi powders are hand mixed together using a mortar and a pestle at a certain weight ratio. The resultant composite is dissolved in DMF to make Si-PAN solution for electrospinning process. Si-PAN solution is well mixed using a magnetic stir bar for 15 hours to evenly distribute nSi and PAN particles in DMF. Mixed PAN-Si solution is ejected from a syringe using a syringe pump. High voltage of 27 kV is applied between a syringe needle and a copper foil collector which is grounded. As electrospun nSi@PAN fibers were collected and observed using FE-SEM to see the morphology.

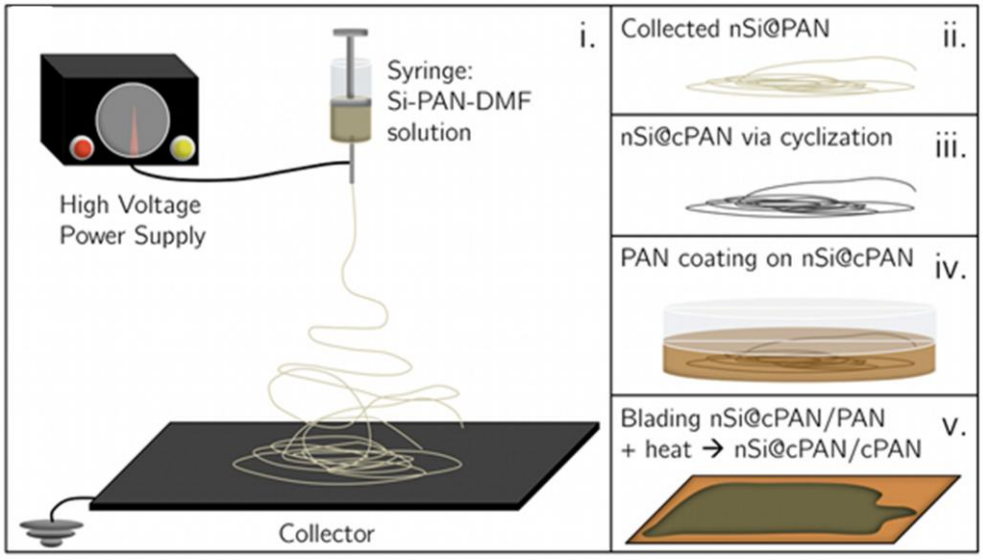

Figure 7.1: The detailed process of manufacturing nSi@cPAN/cPAN.[10]

As mentioned in Section 3.6, the quality of nanofibers produced from electrospinning can be affected by several factors. The feed rate of Si-PAN solution during electrospinning (the speed of Si-PAN solution ejection) is one factor among them. The effect of the feed rate on the geometry of electrospun nSi@PAN fibers was investigated by comparing two different feed rates (0.5 ml hr^{-1}, 2.0 ml hr^{-1}). FE-SEM images of nSi@PAN fibers from different feed rates are shown in Figure 7.2. The weight ratio between Si and PAN was 1:2. nSi@PAN fibers from slower feed rate (0.5 ml hr^{-1}) have the diameter less than 0.5 μm. On the other hand, nSi@PAN fibers from faster feed rate (2.0 ml hr^{-1}) shows the diameter in between 0.5 ~ 1 μm. Therefore, it seems that faster feed rate of Si-PAN solution results in fibers with bigger diameter.

Many sites exposing Si particles on the surface of PAN fibers can be seeen in Figure 7.2b . To minimize the exposure of Si particles on the surface, the weight ratio of PAN in Si-PAN solution for electrospinning was increased. The effect of the weight ratio between Si and PAN in polymer solution on the geometry of electrospun nSi@PAN fibers was also studied by comparing two different weight ratio between Si and PAN. Figure 7.3 describes FE-SEM

a) 0.5 ml hr^{-1} **b) 2.0 ml hr^{-1}**

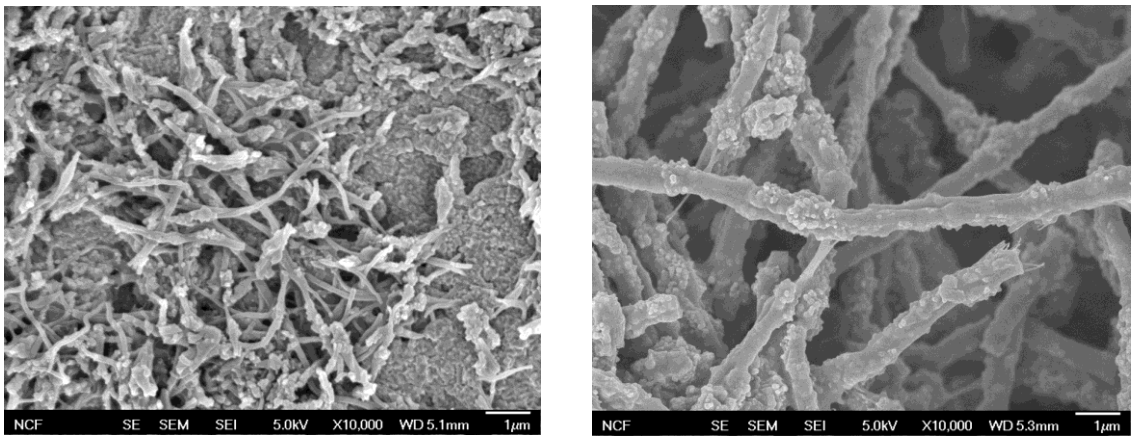

Figure 7.2: FE-SEM images of nSi@PAN fibers from different feed rates.

a) Si:PAN (1:2) **b) Si:PAN (1:2.5)**

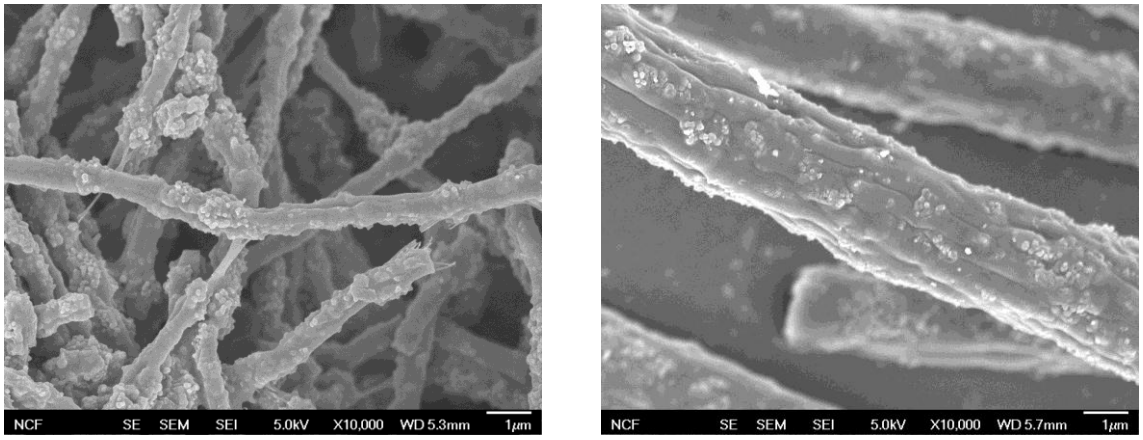

Figure 7.3: FE-SEM images of nSi@PAN fibers from different Si:PAN weight ratios.

images of electrospun nSi@PAN fibers with two different Si:PAN weight ratios (1:2, 1:2.5). The feed rate during electrospinning was fixed at 2.0 ml hr^{-1}. The Si:PAN weight ratio of 1:2.5 shows less exposure of Si particle on the surface of fibers and the fiber diameter larger than 1 μm. As a result, we can confirm that increasing the portion of PAN in Si-PAN solution enlarges the electrospun fiber size, decreasing the exposure of Si particles on the surface.

After fixing parameters of electrospinning based on the investigation in previous paragraphs, actual nSi@cPAN/cPAN electrodes were fabricated. As electrospun nSi@PAN fibers were dried and cyclized in air (220℃) as described in Section 7.1. Cyclized nSi@cPAN fibers were gently mixed with PAN powders and DMF using a magnetic stir bar for 15 hours to make a slurry. The resultant slurry deposited on a copper foil was dried and went through a thermal treatment at 300℃ in Ar environment to cyclize the additional PAN coating on fibers. FE-SEM image of the resultant nSi@cPAN/cPAN electrode is shown in Figure 7.4.

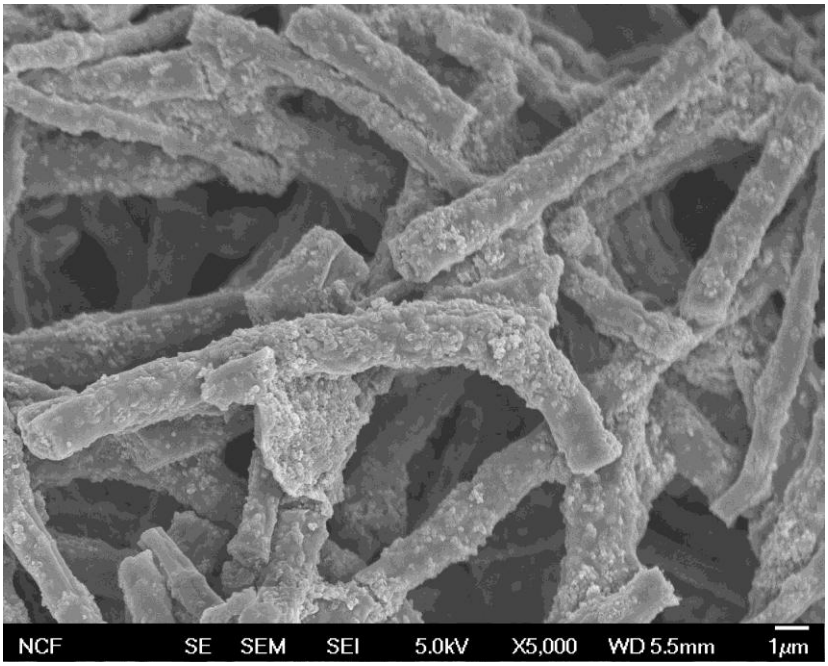

Figure 7.4: FE-SEM images of nSi@cPAN/cPAN electrode.

According to Figure 7.4, our nSi@cPAN/cPAN electrode shows a fibrous, interconnected electrode framwork. Also, it doesn't include auxiliary materials such as a conductive additive and a binder. Microstructural studies with transmission electron microscopy (TEM) and electron energy loss spectroscopy (EELS) in the reference 10 show that Si nanoparticles are fully embedded to cPAN fibers.[10] CR2032 coin cells using liquid electrolyte were made as mentioned in Section 7.1 to see cycling performance of our fiber electrode. Figure 7.5a exhibits the cycling performance and coulombic efficiency (CE) of nSi@cPAN/cPAN electrode in a Li battery.[10] The specific charge capacity (based on the mass of the fiber electrode) of 788 mAh g^{-1} and a CE of 99.5% are achieved after 20 cycles. A rate study was also performed (Figure 7.5b) and an average specific charge capacity of 526 mAh g^{-1} is achieved at 5C current rate.

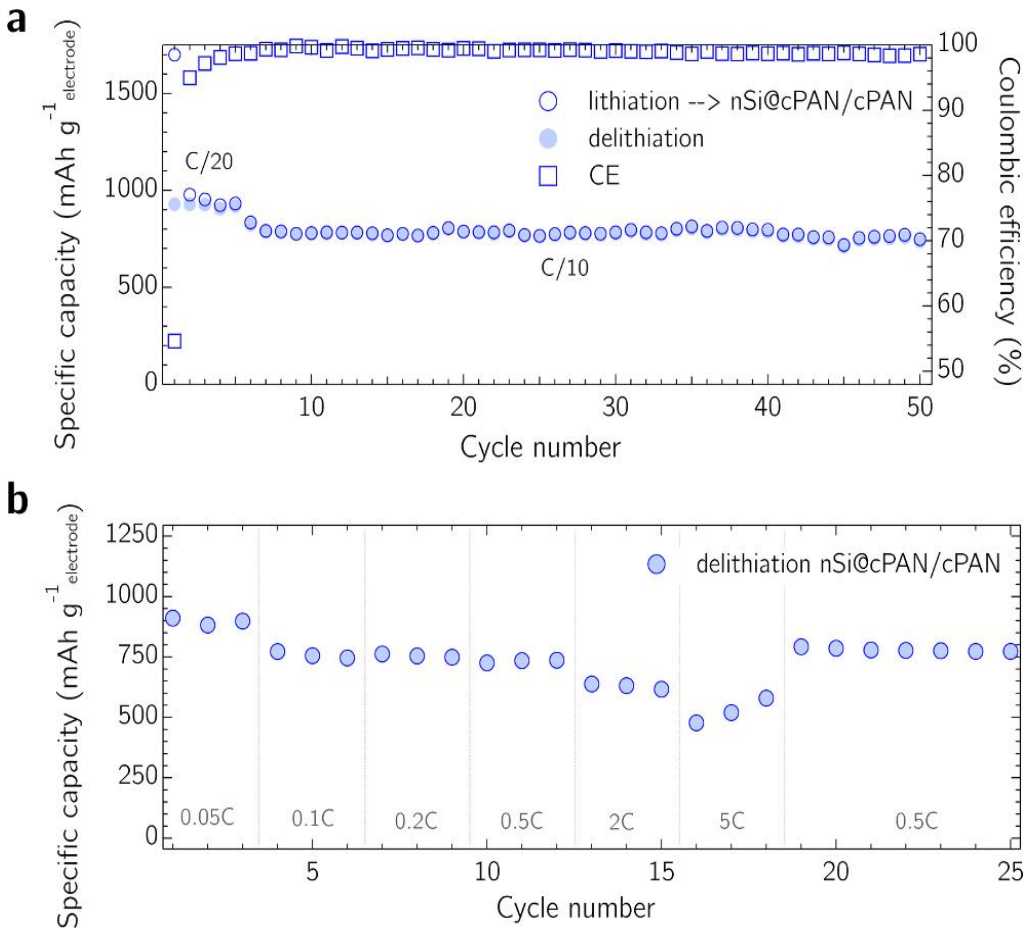

Figure 7.5: (a) Cyclic capacity (circles) and CE (squares) of nSi@cPAN/cPAN electrode. (b) A rate test of nSi@cPAN/cPAN electrode.[10]

Our nSi@cPAN/cPAN electrodes seem to provide an effective accommodation of volumetric expansions of Si nanoparticles and to maintain structural integrity during charge-discharge process, judging from the stable cycling and high CE. Microstructural studies of cycled nSi@cPAN/cPAN electrode confirms the statement.[10] Only 14.3 % of nSi@cPAN/cPAN electrode expansion was observed after the initial lithiation. The value of specific charge capacity at 5C rate tells that our cyclized PAN fiber framework provides adequate Li^+ ion and electron transport.

7.3 Summary

In this chapter, we sucessfully constructed nano-Si hierarchical framework electrodes which provides the desirable mechanical property and electrochemical property. Our fibrous framework effectively accomodates the volume expansion of Si nanoparticles with a minimal electrode deformation which provided stable cycling of liquid electrolyte coin cells. In addition, the scalability which comes from electrospinning process adopted here make this design even attractive for other electrode material which suffers from volume expansion (ex. Sn). Further studies to improve CE will be performed in our future work through surface treatment of electrodes and electrolyte modification.

References

1. T. Song, J. Xia, J.-H. Lee, D. H. Lee, M.-S. Kwon , J.-M. Choi, J. Wu, S. K. Doo, H. Chang, W. I. Park, D. S. Zang, H. Kim, Y. Huang, K.-C. Hwang, J. A. Rogers, U. Paik, *Nano Lett.*, **10**, 1710 (2010) .

2. U. Kasavajjula, C. S. Wang, and A. J. Appleby, *J. of Power Sources*, **163** , 1003 (2007).

3. J. L. Goldman, B. R. Long, A. A. Gewirth, and R. G. Nuzzo, *Adv.Funct. Mater*. **21**, 2412 (2011).

4. a) J. O. Besenhard, J. Yang, and M. Winter, *J. Power Sources*, **68** , 87 (1997); b) W. J. Weydanz, M. Wohlfahrt-Mehrens, and R. A. Huggins, *J. Power Sources*, **81** , 237 (1999); c) X. W. Zhang, P. K. Patil , C. S. Wang, A. J. Appleby, F. E. Little, and D. L. Cocke, *J. Power Source*, **125**, 206 (2004).

5. C. K. Chan, R. Ruffo, S. S. Hong, R. A. Huggins, and Y. Cui, *Nat. Nanotechnology.*, **3** , 31 (2007).

6. A. Magasinski, P. Dixon, B. Hertzberg, A. Kvit, J. Ayala, and G. Yushin, *Nat. Mater.*, **9**, 353(2010) .

7. J. Cho, *J. Mater. Chem.*, **20**, 4009 (2010).

8. a) Y. Koyama, T. E. Chin, U. Rhyner, R. K. Holman, S. R. Hall, and Y.-M. Chiang , *Adv. Funct. Mater.*, **16**, 492 (2006); b) J. H. Lee, H. M. Lee, and S. Ahn, *J. Power Sources*, **113** , 833(2003) ; c) M. Winter, G. H. Wrodnigg, J. O. Besenhard, W. Biberacher, P. Novak, *J. Electrochem. Soc.*, **147 ,** 2427 (2000).

9. Y. Park, N.-S. Choi, S. Park, S. H. Woo, S. Sim, B. Y. Jang, S. M. Oh, S. Park, J. Cho, and K. T. Lee, *Adv. Energy Mater.*, **3**, 206 (2013).

10. D. M. Piper, J. H. Woo, S.-B. Son, S. C. Kim, K. H. Oh, and S.-H Lee, *Adv. Mater*., **26**, 3520 (2014).

Chapter 8

Conclusion

This dissertation demonstrates our efforts to enhance Li^+ ion transport in solid state Li-ion batteries (SSLIBs). One of the major factors which limits Li^+ ion transport in SSLIBs is interfaces between active material and solid state electrolyte (SSE) in electrodes. Issues related to active material/SSE interfaces are (1) highly resistive layers which are formed at the interfaces during battery cycling and (2) less number of Li^+ ion transport paths which comes from limited numbers of solid-solid contacts compared to that of conventional Li-ion batteries (LIBs) which use liquid electrolytes. Various approaches to overcome these two issues are shown throughout chapters in this dissertation.

Atomic layer deposition (ALD) of Al_2O_3 onto $LiCoO_2$ powders was employed to improve the cycling performance of solid Li batteries (SSLBs) in Chapter 4. SSLBs using $LiCoO_2$ powders with adequate numbers of Al_2O_3 ALD cycles show improved capacity retention compared to batteries using uncoated $LiCoO_2$ powders. Electrochemical impedance spectroscopy (EIS) and transmission electron microscopy (TEM) analysis show that Al_2O_3 ALD layers successfully suppress a resistive layer growth at $LiCoO_2$/SSE interface, alleviating interfacial resistance increase.

In addition, Chapter 5 describes a way to utilize Al_2O_3 ALD layers on $LiCoO_2$ powders as Li^+ ion pathways through heat treatment (HT). Al_2O_3 ALD coated $LiCoO_2$ powders went through HT in Ar gas flow before SSLB fabrication. $LiCoO_2$ particles coated with 2 & 4 cycles of Al_2O_3 ALD and subsequently HT under Ar environment exhibit relatively larger initial discharge capacities, smaller polarization increases, and better cycling stability compared to those from uncoated $LiCoO_2$ particles. It is shown that HT in Ar gas flow is integral to improve SSLB performance with Al_2O_3 ALD layers. Better Li^+ ion transport from Ar HT Al_2O_3 ALD layers is corroborated by dQ/dV analysis, EIS profiles, and the overpotential study.

Al_2O_3 ALD coated $LiNi_{1/3}Co_{1/3}Mn_{1/3}O_2$ (L333) and $Li_{10}SiP_2S_{12}$ SSE are adopted in Chapter 6 to construct high energy SSLIBs. SSLBs with these new battery materials improved the total capacity of 10 mg solid electrode from ~ 0.5 mAh to ~ 0.85 mAh. Along with new battery materials, an effective layout of components in solid state electrode was studied. Gradients of SSE portion in thick electrodes using 30 mg of L333 composites show different overpotentials at high current rates. Furthermore, actual SSLIBs were constructed using L333 cathode and Si-Sn anode. SSLIBs with different amounts of electrode materials were cycled at 60℃. It is shown that reducing the portion of SSE in SSLIBs increases the gravimetric energy density.

Finally, nano-Si hierarchical frameworks were constructed by electrospinning as an anode material to provide desirable mechanical/electrochemical properties in Chapter 7. Different feed rates and the material ratio of Si-PAN solution affected the geometry of electrospun fibers. With resultant electrodes from an adequate condition, the volume expansion of Si nanoparticles was effectively accommodated, resulting in a minimal electrode deformation which provided stable cycling in liquid electrolyte coin cells.

The author believes that aforementioned approaches provide effective strategies to enhance the performance of SSLIBs. Nevertheless, further studies are required for SSLIBs to outperform current LIBs. Alternative materials for coatings on active materials, optimized mass ratio of components in electrodes, thinner SSE separator layer, and high rate performance of SSLIBs are examples of remaining tasks for future study. In addition, understanding fundamental mechanisms for phenomena at active material/SSE interfaces is beneficial to fully resolve the degradation of interfaces in SSLIBS during cycling.

Bibliography

Chapter 1

1. M. Armand and J.-M. Tarascon, *Nature*, **451**, 652 (2008).

2. J.-M. Tarascon and M. Armand, *Nature*, **414**, 359 (2001).

3. F. Mizuno, A. Hayashi, K. Tadanaga, T. Minami, and M. Tatsumisago, *J. Power Sources*, **124**, 170 (2003).

4. N. Ohta, K. Takada, L. Zhang,R.Ma, M. Osada, and T. Sasaki, *Adv. Mater*., **18**, 2226 (2006).

5. J. W. Fergus, *J. Power Sources*, **195,** 4554 (2010).

6. A. Sakuda, A. Hayashi, and M. Tatsumisago, *Chem. Mater.*, **22**, 949 (2010).

7. A. Sakuda, H. Kitaura, A. Hayashi, K. Tadanaga, and M. Tatsumisago, *J. Electrochem. Soc*., **156**, A27 (2009).

8. A. Sakuda, H. Kitaura, A. Hayashi, K. Tadanaga, and M. Tatsumisago, *J. Power Sources*, **189,** 527 (2009).

9. A. Sakuda, A. Hayashi, and M. Tatsumisago, *J. Power Sources*, **195**, 599 (2010).

10. H. Kitaura, A. Hayashi, K. Tadanaga, and M. Tatsumisago, *Solid State Ionics*, **192**, 304 (2011).

11. H. Kitaura, A. Hayashi, K. Tadanaga, and M. Tatsumisago, *Electrochimica Acta*, **55**, 8821 (2010).

12. N. Machida, J. Kashiwagi, M. Naito, and T. Shigematsu, *Solid State Ionics*, **225**, 354 (2012).

13. T. Takeuchi, H. Kageyama, K. Nakanishi, M. Tabuchi, H. Sakaebe, T. Ohta, H. Senoh, T. Sakai, and K. Tatsumi, *J. Electrochem. Soc*., **157**, A1196 (2010).

14. M. Nagao, Y. Imade, H. Narisawa, T. Kobayashi, R. Watanabe, T. Yokoi, T. Tatsumi, and R. Kanno, *J. Power Sources*, **222**, 237 (2013).

15. S. Noh, J. Kim, M. Eom, and D. Shin, *Ceramics International*, **39**, 8453 (2013).

16. S. Boulineau, J.-M. Tarascon, J.-B. Leriche, and V. Viallet, *Solid State Ionics*, **242**, 45 (2013).

17. T. Ohtomo, A. Hayashi, M. Tatsumisago,and K. Kawamoto, *J. Solid State Electrochem*, **17**, 2551 (2013).

18. T. Matsuyama, A. Sakuda, A. Hayashi, Y. Togawa, S. Mori, and M. Tatsumisago, *J. Solid State Electrochem.*, **17**, 2697 (2013).

19. I. D. Scott, Y. S. Jung, A. S. Cavanagh,Y. Yan, A. C. Dillon, S. M. George, and S.-H. Lee, *Nano Lett*., **11**, 414 (2011).

20. T. Minami, A. Hayashi, and M. Tatsumisago, *Solid State Ionics***, 177,** 2715 (2006).

21. K. Takada, T. Inada, A. Kajiyama, H. Sasaki, S. Kondo, M. Watanabe, M. Murayama, and Ryoji Kanno, *Solid State Ionics*, **158**, 269 (2003).

22. R. Kanno and M. Maruyama, *J. Electrochem. Soc*., **148**, A742 (2001).

23. J. Trevey, J. S. Jang, Y. S. Jung, C. R. Stoldt, and S.-H. Lee, *Electrochem. Commun.*, **11,** 1830 (2009).

24. N. Kamaya, K. Homma, Y. Yamakawa, M. Hirayama, R. Kanno, M. Yonemura, T. Kamiyama, Y. Kato, S. Hama, K. Kawamoto, and A. Mitsui, *Nat. mater*., **10,** 682 (2011).

25. S.P. Ong, Y. Mo, W.D. Richards, L. Miara, H.S. Lee, and G. Ceder, *Energy Environ. Sci.*,**6,** 148 (2012).

26. T. Ohzuku and Y. Makimura, *Chem. Lett*., **1**, 642 (2001).

27. K.M. Shaju, G.V. Subba Rao, and B.V.R. Chowdari, *Electrochim. Acta*, **48**, 145 (2002).

28. I. Belharouak, Y.K. Sun, J. Liu, and K. Amine, *J. Power Sources*, **123**, 247 (2003).

29. U. Kasavajjula , C. S. Wang , and A. J. Appleby, *J. Power Sources*, **163** , 1003 (2007).

30. D. M. Piper, J. H. Woo, S.-B. Son, S. C. Kim, K. H. Oh, and S.-H. Lee, *Adv. Mater*., **26**, 3520 (2014).

Chapter 2

1. M. Armand and J.-M. Tarascon, *Nature*, **451**, 652 (2008).

2. M. M. Thackeray, C. Wolverton, and E. D. Isaacs, *Energy Environ.Sci.*, **5**, 7854 (2012).

3. T. Nagaura and K. Tozawa, Lithium ion rechargeable battery. *Prog. Batteries Solar Cells* **9,** 209 (1990).

4. B. Dunn, H. Kamath, and J.-M. Tarascon, *Science*, **334**, 928 (2011).

5. A. Sakuda, H. Kitaura, A. Hayashi, K. Tadanaga, and M. Tatsumisago, *J. Power Sources*, **189**, 527 (2009).

6. H. Kitaura, A. Hayashi, K. Tadanaga, and M. Tatsumisago, *Electrochim. Acta*, **55,** 8821 (2010).

7. Y. Liu, S. Gorgutsa, C. Santato, and M. Skorobogatiy, *J. Electrochem. Soc*., **159**, A349 (2012).

8. J. R. Dahn , T. Zheng , Y. Liu , and J. S. Xue , *Science*, ***270*** , 590 (1995) .

9. J.-M. Tarascon and M. Armand, *Nature*, **414**, 359 (2001).

10. J. N. Reimers and J. R. Dahn, *J. Electrochem. Soc*. **139**, 2091 (1992).

11. K. Mizushima, P. C. Jones, P. J. Wiseman, and J. B. Goodenough, *Mat. Res. Bull.,* **15**, 783 (1980)**.**

12. T. Ohzuku and A. Ueda, *J. Electrochem. Soc*. **141**, 2972 (1994).

13. G. G. Amatucci, J. M. Tarascon, and L. C. Klein, *J. Electrochem. Soc*., **143**, 1114 (1996).

14. W. J. Weydanz, M. Wohlfahrt-Mehrens, and R. A. Huggins, *J. Power Sources*, **81**, 237 (1999).

15. Y. Wang and J. Dahn , *J. Electrochem. Soc*., **153** , A2314 (2006).

16. T. D. Hatchard and, J. R. Dahn , *J. Electrochem. Soc.*, **151**, A838 (2004).

17. Y. M. Kang, S. B. Suh, and Y. S. Kim, *Inorg. Chem.*, **48** , 11631 (2009).

18. Y. Idota, T. Kubota, A. Matsufuji, Y. Maekawa, and T. Miyasaka, *Science*, **276**, 1395 (1997).

19. M. Winter and J. O. Besenhard, *Electrochim. Acta*, **45**, 31 (1999).

20. J. L. Goldman, B. R. Long, A. A. Gewirth, and R. G. Nuzzo, *Adv.Funct. Mater*. **21**, 2412 (2011).

21. S. Grugeon, S. Laruelle, R. Herrera-Urbina, L. Dupont, P. Poizot, and J.M. Tarascon, *J. Electrochem. Soc*., **148**, A285 (2001).

22. E. Shembel, R. Apostolova, V. Nagirny, I. Kirsanova, Ph. Grebenkin, and P. Lytvyn, *J. Solid State Electrochem.*, **9**, 96 (2005).

23. F. Mizuno, A. Hayashi, K. Tadanaga, T. Minami, and M. Tatsumisago, *J. Power Sources*, **124**, 170 (2003).

24. J. W. Fergus, *J. Power Sources*, **195,** 4554 (2010).

25. G. Adachi, N. Imanaka, and H. Aono, *Adv. Mater.*, **8**, 127 (1996).

26. H. Hong, *Mat. Res. Bull.,* **13**, 117 (1978)**.**

27. R. Kanno and M. Murayama, *J. Electrochem. Soc.*, **148**, A742 (2001).

28. A. Hayashi, S. Hama, T. Minami, and M. Tatsumisago, *Electrochem. Commun.*, **5**, 111 (2003).

29. N. Kamaya, K. Homma, Y. Yamakawa, M. Hirayama, R. Kanno, M. Yonemura, T. Kamiyama, Y. Kato, S. Hama, K. Kawamoto, and A. Mitsui, *Nat. mater*., **10,** 682 (2011).

30. Y. Mo, S. P. Ong, and G. Ceder, *Chem. Mater.*, **24**, 15 (2012).

31. S.P. Ong, Y. Mo, W.D. Richards, L. Miara, H.S. Lee, and G. Ceder, *Energy Environ. Sci.*,**6,** 148 (2012).

Chapter 3

1. A. Hayashi, S. Hama, H. Morimoto, M. Tatusmisago, and T. Minami, *J. Am. Ceram. Soc*., **84**, 477 (2001).

2. A. Hayashi, S. Hama, F. Mizuno, K. Tadanaga, T. Minami, and M. Tatsumisago, *Solid State Ionics*, **175**, 683 (2004).

3. A. Hayashi, S. Hama, T. Minami, and M. Tatsumisago, *Electrochem. Commun.*, **5**, 111 (2003).

4. C. C. Koch, *J. Non-Cryst. Solids*, **117**, 670 (1990).

5. E. H. Zhou, C. Suryanarayana,and F. H. Fores, *Mater. Lett*., **23**, 27 (1995).

6. Y. Chen, C. P. Li, H. Chen, and Y. J. Chen, *Science and Technology of Advanced Materials*, **7**, 839 (2006).

7. G. Adachi, N. Imanaka, H. Aono, *Adv. Mater*., **8**, 127 (1996).

8. T. Minami, A. Hayashi, and M. Tatsumisago, *Solid State Ionics***, 177,** 2715 (2006).

9. K. Takada, T. Inada, A. Kajiyama, H. Sasaki, S. Kondo, M. Watanabe, M. Murayama, and Ryoji Kanno, *Solid State Ionics*, **158**, 269 (2003).

10. A. J. Bard and L. R. Faulkner, *ELECTROCHEMICAL METHODS: Fundamentals and Applications, 2nd ed.*, p. 370, John Wiley & Sons, New York (2001).

11. A. J. Bard and L. R. Faulkner, *ELECTROCHEMICAL METHODS: Fundamentals and Applications, 2nd ed.*, p. 305, John Wiley & Sons, New York (2001).

12. A. J. Bard and L. R. Faulkner, *ELECTROCHEMICAL METHODS: Fundamentals and Applications, 2nd ed.*, p. 632, John Wiley & Sons, New York (2001).

13. S. M. George, *Chem. Rev.*, **110**, 111 (2010).

14. A. C. Dillon, A. W. Ott, J. D. Way, and S. M. George, *Surf. Sci.*, **322**, 230 (1995).

15. M. D. Groner, F. H. Fabreguette, J. W. Elam, and S. M. George, *Chem. Mater*., **16**, 639 (2004).

16. A. W. Ott, J. W. Klaus, J. M. Johnson, and S. M. George, *Thin Solid Films*, **292**, 135 (1997).

17. Y. S. Jung, A. S. Cavanagh, A. C. Dillon, M. D. Groner, S. M. George, and S.-H. Lee, *J. Electrochem. Soc*., **157**, A75 (2010).

18. A. L. Andrady, *Science and Technology of Polymer Nanofibers*, John Wiley & Sons, New York (2008).

Chapter 4

1. M. Armand and J.-M. Tarascon, *Nature*, **451**, 652 (2008).

2. F. Mizuno, A. Hayashi, K. Tadanaga, T. Minami, and M. Tatsumisago, *J. Power Sources*, **124**, 170 (2003).

3. N. Ohta, K. Takada, L. Zhang, R. Ma, M. Osada, and T. Sasaki, *Adv. Mater. (Weinheim, Ger.)*, **18**, 2226 (2006).

4. J. W. Fergus, *J. Power Sources*, **195,** 4554 (2010).

5. A. Sakuda, A. Hayashi, and M. Tatsumisago, *Chem. Mater.*, **22**, 949 (2010).

6. A. Sakuda, H. Kitaura, A. Hayashi, K. Tadanaga, and M. Tatsumisago, *J. Power Sources*, **189,** 527 (2009).

7. A. Sakuda, A. Hayashi, and M. Tatsumisago, *J. Power Sources*, **195**, 599 (2010).

8. K. Takada, N. Ohta, L. Zhang, K. Fukuda, I. Sakaguchi, R. Ma, M. Osada, and T. Sasaki, *Solid State Ionics*, **179**, 1333 (2008).

9. S. Oh, J. K. Lee, D. Byun, W. I. Cho, and B. W. Cho, *J. Power Sources*, **132**, 249 (2004).

10. Y. J. Kim, H. Kim, B. Kim, D. Ahn, J.-G. Lee, T.-J. Kim, D. Son, J. Cho, Y.-W. Kim, and B. Park, *Chem. Mater*., **15**, 1505 (2003).

11. Y. J. Kim, T.-J. Kim, J. W. Shin, B. Park, and J. Cho, *J. Electrochem. Soc*., **149**, A1337 (2002).

12. Y. S. Jung, A. S. Cavanagh, A. C. Dillon, M. D. Groner, S. M. George, and S.-H. Lee, *J. Electrochem. Soc*., **157**, A75 (2010).

13. I. D. Scott, Y. S. Jung, A. S. Cavanagh,Y. Yan, A. C. Dillon, S. M. George, and S.-H. Lee, *Nano Lett*., **11,** 414 (2011).

14. M. D. Groner, F. H. Fabreguette, J. W. Elam, and S. M. George, *Chem. Mater*., **16**, 639 (2004).

15. A. W. Ott, J. W. Klaus, J. M. Johnson, and S. M. George, *Thin Solid Films*, **292**, 135 (1997).

16. J. E. Trevey, Y. S. Jung, and S.-H. Lee, *Electrochim. Acta*, **56,** 4243 (2011).

17. S.-B. Son, J. E. Trevey, H. Roh, S.-H. Kim, K.-B. Kim, J. S. Cho, J.-T. Moon, C. M. DeLuca, K. K. Maute, M. L. Dunn, H. N. Han, K. H. Oh, and S.-H. Lee, *Adv. Energy Mater.*, **1**, 1199 (2011).

18. M. D. Groner, J. W. Elam, F. H. Fabreguette, and S. M. George, *Thin Solid Films*, **413**, 186 (2002).

19. A. Sakuda, H. Kitaura, A. Hayashi, K. Tadanaga, and M. Tatsumisago, *Electrochem. Solid-State Lett.*, **11**, A1 (2008).

20. Y. Uchimoto and M. Wakihara, in *Solid State Ionics for Batteries*, T. Minami, Editor, p. 126, Springer-Verlag, Tokyo (2005).

Chapter 5

1. F. Mizuno, A. Hayashi, K. Tadanaga, T. Minami, and M. Tatsumisago, *J. Power Sources*, **124**, 170 (2003).

2. N. Ohta,K. Takada, L. Zhang,R.Ma, M. Osada, and T. Sasaki, *Adv. Mater*., **18**, 2226 (2006).

3. J. W. Fergus, *J. Power Sources*, **195**, 4554 (2010).

4. A. Sakuda, A. Hayashi, and M. Tatsumisago, *Chem. Mater.*, **22**, 949 (2010).

5. A. Sakuda, H. Kitaura, A. Hayashi, K. Tadanaga, and M. Tatsumisago, *J. Electrochem. Soc*., **156**, A27 (2009).

6. A. Sakuda, H. Kitaura, A. Hayashi, K. Tadanaga, and M. Tatsumisago, *J. Power Sources*, **189**, 527 (2009).

7. A. Sakuda, A. Hayashi, and M. Tatsumisago, *J. Power Sources*, **195**, 599 (2010).

8. H. Kitaura, A. Hayashi, K. Tadanaga, and M. Tatsumisago, *Solid State Ionics*, **192**, 304 (2011).

9. Y. J. Kim, T.-J. Kim, J. W. Shin, B. Park, and J. Cho, *J. Electrochem. Soc*., **149**, A1337 (2002).

10. Y. J. Kim, H. Kim, B. Kim, D. Ahn, J.-G. Lee, T.-J. Kim, D. Son, J. Cho, Y.-W. Kim, and B. Park, *Chem. Mater*., **15**, 1505 (2003).

11. S. Oh, J. K. Lee, D. Byun, W. I. Cho, and B. W. Cho, *J. Power Sources*, **132**, 249 (2004).

12. Y. S. Jung, A. S. Cavanagh, A. C. Dillon, M. D. Groner, S. M. George, and S.-H. Lee, *J. Electrochem. Soc*., **157**, A75 (2010).

13. I. D. Scott, Y. S. Jung, A. S. Cavanagh,Y. Yan, A. C. Dillon, S. M. George, and S.-H. Lee, *Nano Lett*., **11**, 414 (2011).

14. J. H. Woo, J. E. Trevey, A. S. Cavanagh, Y. S. Choi, S. C. Kim, S. M. George, K. H. Oh,and S.-H. Lee, *J. Electrochem. Soc*., **159**, A1120 (2012).

15. Y. S. Jung, A. S. Cavanagh, Y. Yan, S. M. George, and A. Manthiram, *J. Electrochem. Soc*., **158**, A1298 (2011).

16. M. D. Groner, J. W. Elam, F. H. Fabreguette, and S. M. George, *Thin Solid Films*, **413**, 186 (2002).

17. J. N. Reimers and J. R. Dahn, *J. Electrochem. Soc*., **139**, 2091 (1992).

18. J. Sun, K. Tang, X. Yu, J. Hu, H. Li, and X. Huang, *Solid State Ionics*, **179**, 2390 (2008).

19. K. Mizushima, P. C. Jones, P. J. Wiseman, and J. B. Goodenough, *Mat. Res. Bull.*, **15**, 783 (1980)**.**

20. G. G. Amatucci, J. M. Tarascon, and L. C. Klein, *J. Electrochem. Soc*., **143**, 1114 (1996).

21. P.J. Bouwman, B.A. Boukamp, H. J. M. Bouwmeester, and P. H. L. Notten, *Solid State Ionics*, **152-153**, 181 (2002).

Chapter 6

1. J. W. Fergus, *J. Power Sources*,**195,** 4554 (2010).

2. N. Ohta, K. Takada, L. Zhang,R.Ma, M. Osada, and T. Sasaki, *Adv. Mater*., **18**, 2226 (2006).

3. A. Sakuda, A. Hayashi, and M. Tatsumisago, *Chem. Mater.*, **22**, 949 (2010).

4. A. Sakuda, H. Kitaura, A. Hayashi, K. Tadanaga, and M. Tatsumisago, *J. Electrochem. Soc*., **156**, A27 (2009).

5. A. Sakuda, H. Kitaura, A. Hayashi, K. Tadanaga, and M. Tatsumisago, *J. Power Sources*, **189,** 527 (2009).

6. A. Sakuda, A. Hayashi, and M. Tatsumisago, *J. Power Sources*, **195**, 599 (2010).

7. H. Kitaura, A. Hayashi, K. Tadanaga, and M. Tatsumisago, *Solid State Ionics*, **192**, 304 (2011).

8. H. Kitaura, A. Hayashi, K. Tadanaga, and M. Tatsumisago, *Electrochimica Acta*, **55**, 8821 (2010).

9. N. Machida, J. Kashiwagi, M. Naito, and T. Shigematsu, *Solid State Ionics*, **225**, 354 (2012).

10. T. Takeuchi, H. Kageyama, K. Nakanishi, M. Tabuchi, H. Sakaebe, T. Ohta, H. Senoh, T. Sakai, and K. Tatsumi, *J. Electrochem. Soc*., **157**, A1196 (2010).

11. M. Nagao, Y. Imade, H. Narisawa, T. Kobayashi, R. Watanabe, T. Yokoi, T. Tatsumi, and R. Kanno, *J. Power Sources*, **222**, 237 (2013).

12. S. Noh, J. Kim, M. Eom, and D. Shin, *Ceramics International*, **39**, 8453 (2013).

13. S. Boulineau, J.-M. Tarascon, J.-B. Leriche, and V. Viallet, *Solid State Ionics*, **242**, 45 (2013).

14. T. Ohtomo, A. Hayashi, M. Tatsumisago, and K. Kawamoto, *J. Solid State Electrochem*, **17**, 2551 (2013).

15. T. Matsuyama, A. Sakuda, A. Hayashi, Y. Togawa, S. Mori, and M. Tatsumisago, *J. Solid State Electrochem.*, **17**, 2697 (2013).

16. R. Koksbang, J. Barker, H. Shi, and M.Y. Saı¨di, *Solid State Ionics*, **84**, 1(1996).

17. T. Nagaura and K. Tozawa, *Prog. Batteries Sol. Cells*, **9**, 20 (1990).

18. T. Ohzuku, A. Ueda, and M. Nagayama, *J. Electrochem. Soc*., **140**, 1862 (1993).

19. C. Delmas, I. Saadoune, and A. Rougier, *J. Power Sources*, **43/44**, 595 (1993).

20. D. Caurant, N. Baffier, V. Bianchi,G. Gregoire, and S. Bach, *J.Mater. Chem.* **6**, 1149 (1996).

21. T. Ohzuku, A. Ueda, and M. Kouguchi, *J. Electrochem. Soc*., **142**, 4033 (1995).

22. T. Ohzuku,A. Ueda, M. Nagayama, Y. Iwakoshi, and H. Komori, *Electrochim. Acta*, **38**, 1159 (1993).

23. B. J. Hwang, R. Santhanam, and C. H. Chen, *J. Power Sources*, **114**, 244 (2003).

24. Z. Liu, A. Yu, and J. Y. Lee, *J. Power Sources*, **81-82**, 416 (1999).

25. T. Ohzuku, Y. Makimura, *Chem. Lett*., **1**, 642 (2001).

26. K.M. Shaju, G.V. Subba Rao, and B.V.R. Chowdari, *Electrochim. Acta*, **48**, 145 (2002)

27. I. Belharouak, Y.K. Sun, J. Liu, and K. Amine, *J. Power Sources*,**123**, 247 (2003).

28. J. M. Whiteley, J. H. Woo, E. Hu, K.-W. Nam, and S.-H. Lee, *J. Electrochem. Soc*., **161**, A1812 (2014).

29. Y. S. Jung, A. S. Cavanagh, A. C. Dillon, M. D. Groner, S. M. George, and S.-H. Lee, *J. Electrochem. Soc*., **157**, A75 (2010).

30. S. Golmon, K. Maute, and M. L. Dunn, *Int.J. Numer.Meth. Engng*, **92**, 475 (2012).

31. K. Takada, N. Aotani, K. Iwamoto, and S. Kondo, *Solid State Ionics*, **86-88**(Part 2), 877 (1996).

32. J. Sun, K. Tang, X. Yu, J. Hu, H. Li, and X. Huang, *Solid State Ionics*, **179**, 2390 (2008).

Chapter 7

1. T. Song, J. Xia, J.-H. Lee, D. H. Lee, M.-S. Kwon , J.-M. Choi, J. Wu, S. K. Doo, H. Chang, W. I. Park, D. S. Zang, H. Kim, Y. Huang, K.-C. Hwang, J. A. Rogers, U. Paik, *Nano Lett.*, **10**, 1710 (2010) .

2. U. Kasavajjula, C. S. Wang, and A. J. Appleby, *J. of Power Sources*, **163** , 1003 (2007).

3. J. L. Goldman, B. R. Long, A. A. Gewirth, and R. G. Nuzzo, *Adv.Funct. Mater*. **21**, 2412 (2011).

4. a) J. O. Besenhard, J. Yang, and M. Winter, *J. Power Sources*, **68** , 87 (1997); b) W. J. Weydanz, M. Wohlfahrt-Mehrens, and R. A. Huggins, *J. Power Sources*, **81** , 237 (1999); c) X. W. Zhang, P. K. Patil , C. S. Wang, A. J. Appleby, F. E. Little, and D. L. Cocke, *J. Power Source*, **125**, 206 (2004).

5. C. K. Chan, R. Ruffo, S. S. Hong, R. A. Huggins, and Y. Cui, *Nat. Nanotechnology.*, **3** , 31 (2007).

6. A. Magasinski, P. Dixon, B. Hertzberg, A. Kvit, J. Ayala, and G. Yushin, *Nat. Mater.*, **9**, 353(2010) .

7. J. Cho, *J. Mater. Chem.*, **20**, 4009 (2010).

8. a) Y. Koyama, T. E. Chin, U. Rhyner, R. K. Holman, S. R. Hall, and Y.-M. Chiang , *Adv. Funct. Mater.*, **16**, 492 (2006); b) J. H. Lee, H. M. Lee, and S. Ahn, *J. Power Sources*, **113** , 833(2003) ; c) M. Winter, G. H. Wrodnigg, J. O. Besenhard, W. Biberacher, P. Novak, *J. Electrochem. Soc.*, **147 ,** 2427 (2000).

9. Y. Park, N.-S. Choi, S. Park, S. H. Woo, S. Sim, B. Y. Jang, S. M. Oh, S. Park, J. Cho, and K. T. Lee, *Adv. Energy Mater.*, **3**, 206 (2013).

10. D. M. Piper, J. H. Woo, S.-B. Son, S. C. Kim, K. H. Oh, and S.-H Lee, *Adv. Mater*., **26**, 3520 (2014).